

Tuomas Alatarvas

EVOLUTION OF INCLUSION POPULATION IN CALCIUM TREATED ULTRA-HIGH STRENGTH STEELS

NOVEL APPLICATIONS OF SAMPLE DATA
TREATMENT

UNIVERSITY OF OULU GRADUATE SCHOOL;
UNIVERSITY OF OULU,
FACULTY OF TECHNOLOGY



ACTA UNIVERSITATIS OULUENSIS
C Technica 682

TUOMAS ALATARVAS

**EVOLUTION OF INCLUSION
POPULATION IN CALCIUM
TREATED ULTRA-HIGH STRENGTH
STEELS**

Novel applications of sample data treatment

Academic dissertation to be presented with the assent of the Doctoral Training Committee of Technology and Natural Sciences of the University of Oulu for public defence in Kaljusensali (KTK112), Linnanmaa, on 30 November 2018, at 12 noon

UNIVERSITY OF OULU, OULU 2018

Copyright © 2018
Acta Univ. Oul. C 682, 2018

Supervised by
Professor Timo Fabritius
Professor Seppo Louhenkilpi
Docent Eetu-Pekka Heikkinen

Reviewed by
Assistant Professor Silvia Barella
Docent Andrey Karasev

Opponent
Professor Joohyun Park

ISBN 978-952-62-2097-0 (Paperback)
ISBN 978-952-62-2098-7 (PDF)

ISSN 0355-3213 (Printed)
ISSN 1796-2226 (Online)

Cover Design
Raimo Ahonen

JUVENES PRINT
TAMPERE 2018

Alatarvas, Tuomas, Evolution of inclusion population in calcium treated ultra-high strength steels. Novel applications of sample data treatment

University of Oulu Graduate School; University of Oulu, Faculty of Technology

Acta Univ. Oul. C 682, 2018

University of Oulu, P.O. Box 8000, FI-90014 University of Oulu, Finland

Abstract

Non-metallic inclusions are unavoidable particles in steel and are often detrimental to the steelmaking process and the mechanical properties of the steel. While it is not feasible to remove all inclusions, in the well-established calcium treatment of aluminium-killed steel, solid aluminium oxides are transformed into less harmful liquid calcium aluminates.

The main objective of this work was to develop a new inclusion identification and classification method. The presented method offers valuable information on phases of the inclusions. This data is often buried within simple inclusion classification criteria. The method offers the best approximation of the phases in each inclusion detected with minimal time, if no time-consuming elemental map analyses are available. In this work, applications for the inclusion phase identification method are presented. Utilising the method, the dispersion and evolution of inclusions during the sampling of liquid steel in lollipop samples is investigated, as well as the evolution of inclusions during continuous casting. New information is obtained on the elongation of inclusions and formation of oxide–sulphide stringers during hot rolling.

The results for the investigated steels show that with sulphur contents higher than 10 ppm, calcium aluminates were back-modified to alumina and spinel inclusions during casting. However, with decreasing sulphur contents, and adequate simultaneous calcium treatment of oxides, Al_2O_3 and spinel formation is hindered or even avoided.

The most elongated inclusions are often also found in stringers. According to the results of this study, low melting calcium aluminate inclusions are not the most elongated oxide inclusions in the hot rolled product. With moderate calcium treatment, an optimal oxide composition can be obtained, found within the C12A7–CA–MgO composition. These liquid inclusions ensure good castability, while they do not easily elongate or fragment into detrimental stringers after continuous casting.

Keywords: calcium treatment, hot rolling, liquid steel sampling, non-metallic inclusions, steel

Alatarvas, Tuomas, Sulkeumakuvan kehittyminen kalsiumkäsittelyissä ultra-lujuusteräksissä. Uusia näytedatankäsittelyn soveltamistapoja

Oulun yliopiston tutkijakoulu; Oulun yliopisto, Teknillinen tiedekunta

Acta Univ. Oul. C 682, 2018

Oulun yliopisto, PL 8000, 90014 Oulun yliopisto

Tiivistelmä

Epämetalliset sulkeumat ovat väistämättä osa terästä, ja ne aiheuttavat ongelmia prosessille ja teräksen mekaanisille ominaisuuksille. Sulkeumien poiston sijaan niiden koostumusta muokataan kalsiumkäsittelyllä. Tällöin kiinteät alumiinioksidit muuttuvat vähemmän ongelmallisiksi suliksi kalsiumalumiinaateiksi.

Tämän työn päätavoitteena oli kehittää uusi sulkeumien tunnistus- ja luokittelumenetelmä. Sulkeuma-analyysien data voi jäädä hyödyntämättä, jos luokitteluun käytetään yksinkertaisia kriteerejä. Työssä esitetty menetelmä antaa parhaan arvion sulkeumissa olevista faaseista, mikäli sulkeumista ei ole alkuainekarttoja, joiden muodostaminen vie huomattavasti aikaa. Väitöskirjassa esitetään sulkeumien tunnistus- ja luokittelumenetelmän soveltamiskohteita. Menetelmän avulla tutkitaan sulkeumien muutosta ja jakaantumista sulan teräksen näytteenotossa ja sulkeumakuvan muutosta jatkuvavalun aikana. Uutta tietoa esitetään oksidi-sulfidiketjujen muodostumisesta kuumavalssauksen aikana.

Tutkituilla teräksillä rikkipitoisuuden noustessa yli 10 ppm:n sulat kalsiumalumiinaatit takaisinmuokkautuvat kiinteiksi alumiinioksideiksi tai spinelleiksi jatkuvavalun aikana. Riittävän matalalla rikkipitoisuudella ja kohtuullisella kalsiumkäsittelyllä alumiinioksidien ja spinellien muodostumista voidaan hillitä tai jopa estää se.

Tutkimuksessa esitetään, että kuumavalssauksessa venyvimmät sulkeumat muodostavat myös lukuisten sulkeumien oksidi-sulfidiketjuja, jotka ovat tuotteen ominaisuuksien kannalta haitallisia. Tulosten mukaan kalsiumalumiinaatit, jotka sulavat matalimmissa lämpötiloissa, eivät kuitenkaan ole taipuvaisimpia venymään valssauksessa. Maltillisella kalsiumkäsittelyllä saavutetaan optimaalinen oksidikoostumus C12A7–CA–MgO-faasiseurueesta. Nämä sulkeumat ovat sulia jatkuvavalussa varmistaen teräksen valettavuuden. Toisaalta ne eivät helposti veny tai rikoonnu ketjuiksi valssauksessa jatkuvavalun jälkeen.

Asiasanat: kalsiumkäsittely, kuumavalssaus, näytteenotto, sulkeumat, teräs

Acknowledgements

This research was carried out at the Process Metallurgy Research Unit, University of Oulu from 2012 to 2018. The research was carried out in various projects, most notably the Energy and Lifecycle-efficient Metal Processes (ELEMET) and System Integrated Metals Processing (SIMP) research projects coordinated by DIMECC Oy and funded by Business Finland, formerly the Finnish Funding Agency for Technology and Innovation. SSAB Europe Oy is acknowledged for participating in the projects, funding research, and allowing the use of data. Parts of this research were also carried out under the University of Oulu profiling area Genome of Steel.

Scholarships awarded for the years 2014–2016 by the Steel and Metal Producers' Fund of the Technology Industries of Finland Centennial Foundation are highly appreciated. The Finnish Foundation for Technology Promotion is acknowledged for a personal grant. University of Oulu Graduate school is acknowledged for a travel grant to the 9th International Conference on Clean Steel in Budapest.

Most importantly, I would like to express my gratitude towards my supervisors Professor Timo Fabritius, Professor Seppo Louhenkilpi and Docent Eetu-Pekka Heikkinen for the guidance and support during my doctoral studies. In addition, I would like to thank my follow-up group – Professor David Porter, Dr. Jyrki Heino and Dr. Pasi Suikkanen – for the interest in the topic and for the encouraging comments.

I would like to thank Assistant Professor Silvia Barella and Docent Andrey Karasev for acting as pre-examiners and providing valuable comments and feedback on the dissertation.

Warm thanks belong to Dr. Matti Aula, Matias Hultgren, Dr. Mikko Iljana, Olli Peltosaari, and Dr. Ville-Valtteri Visuri for the great discussions while having lunch and coffee. In addition, I want to thank my colleagues in the Process Metallurgy Research Unit for the great atmosphere to work. Many thanks to Tommi Kokkonen and Riku Mattila for technical support.

Personnel of SSAB Europe Oy are acknowledged for sampling, inclusion analyses, and providing the data. In particular, I want to thank Leena Määttä and Tuomas Antola for the co-operation and valuable feedback during the projects.

I would like to thank Anssi Mäkelä for the practical introduction to the electrolytic extraction technique in inclusion analysis. I am grateful to Teija Sipola, for giving a boost in the research field in our group and for the development of the analysis procedures. I want to thank Elvi Hiltula and Pasi Juntunen with the Center

of Microscopy and Nanotechnology for the help in sample preparation and scanning electron microscope operation. Many thanks to Toni Malila for the fruitful discussions on a wide variety of topics.

Warmest thanks belong to my parents Ahti and Kaisa for always encouraging me in my studies. Thanks to my brother Antti, engineering was the way to go.

Dearest Anette, thank you for your support during these years. Aatos and Tobias, there is nothing as important as you.

Oulu, October 17th 2018

Tuomas Alatarvas

Abbreviations

| | |
|-----------|---------------------------------------------------------------------------|
| ω | Constant $\frac{2}{3}$ for square bloom or billet, $\frac{1}{2}$ for slab |
| λ | Ratio of length to thickness of inclusion after hot rolling |
| (i) | Compound i as inclusion |
| [i] | Element i dissolved in steel |
| A | Area |
| Ar | Argon-protected lollipop sample |
| a | Activity |
| AR | Aspect ratio |
| ASTM | The American Society for Testing and Materials |
| B | Breadth |
| BCC | Body-Centred Cubic |
| BOF | Basic Oxygen Furnace |
| C | Centre |
| CAS-OB | Composition Adjustment by Sealed argon bubbling with Oxygen Blowing |
| CET | Columnar-to-equiaxed transition zone |
| D | Diameter |
| D_{eq} | Diameter, equivalent to a sphere |
| EDS | Energy-Dispersive X-Ray Spectroscopy |
| EPMA | Electron Probe Micro Analyser |
| h | ratio of observed inclusion area before and after hot rolling |
| IF | Interstitial Free |
| FCC | Face-Centred Cubic |
| FESEM | Field emission scanning electron microscope |
| IPIM | Inclusion Phase Identification and classification Method |
| K | Equilibrium constant |
| K-S | Kolmogorov-Smirnov test |
| kV | Kilovolt |
| L | Length |
| L | Lower third |
| LCAK | Low Carbon Aluminium Killed steel |
| M | Molar mass |
| M | Middle third |
| M-WU | Mann-Whitney U test |
| m_i | Mass of element or compound i |

| | |
|------------|---------------------------------------------------------------|
| $m_{i,OX}$ | Mass of element or compound i in oxide phases |
| MC | Metal Cap protected lollipop sample |
| mol.% | Molar percent |
| N | Number of inclusions in the sample |
| n | Molar amount |
| n_i | Molar amount of component i |
| O_{tot} | Total oxygen content |
| OES | Optical Emission Spectroscopy |
| OES-PDA | Optical Emission Spectroscopy – Pulse Discrimination Analysis |
| OX | Oxide, denotes Al_2O_3 , CaO, and MgO combined |
| p | Probability value in statistical tests |
| ppm | Parts per million |
| RD | Relative deformation |
| RFCS | Research Fund for Coal and Steel |
| RH | Ruhrstahl Heraeus vacuum treatment |
| S | Surface |
| SEM | Scanning electron microscope |
| T | Thickness |
| U | Upper third |
| V | Volume |
| W | Width |
| w | Mass fraction |
| wt.% | Weight percent |

Chemical compounds

| | |
|-----------|-------------------------------------------------------------------------|
| Al_2O_3 | Aluminium oxide |
| C_xA_y | Calcium aluminate $(CaO)_x(Al_2O_3)_y$, in the following compositions: |
| CA | |
| CA2 | |
| CA6 | |
| C3A | |
| C12A7 | |
| CaO | Calcium oxide |
| CaS | Calcium sulphide |
| MA | Spinel ($MgO \cdot Al_2O_3$) |
| MgO | Magnesium oxide |

| | |
|----------------------------------------|--------------------|
| $\text{MgO}\cdot\text{Al}_2\text{O}_3$ | Spinel |
| MnO | Manganese oxide |
| MnS | Manganese sulphide |
| SiO_2 | Silicon dioxide |
| TiN | Titanium nitride |
| ZrO_2 | Zirconium dioxide |

Table of Contents

| | |
|-----------------------------------------------------------------------------|-----------|
| Abstract | |
| Tiivistelmä | |
| Acknowledgements | 7 |
| Abbreviations | 9 |
| Table of Contents | 13 |
| 1 Introduction | 17 |
| 1.1 Background and research environment | 17 |
| 1.2 Objectives and scope | 18 |
| 2 Non-metallic inclusions in the steelmaking processes | 21 |
| 2.1 Non-metallic inclusions | 21 |
| 2.2 Calcium treatment | 22 |
| 2.2.1 Modification of aluminium oxide inclusions | 24 |
| 2.2.2 Modification of spinel inclusions | 26 |
| 2.2.3 Formation of calcium sulphides | 28 |
| 2.3 Continuous casting | 29 |
| 2.3.1 Formation of calcium aluminate–CaS or alumina–CaS inclusions | 31 |
| 2.3.2 Factors affecting the location of inclusions in the slab | 33 |
| 2.4 Hot rolling | 35 |
| 2.4.1 Deformation and elongation of inclusions | 35 |
| 2.4.2 Oxide–sulphide stringers | 39 |
| 3 Steel sampling and inclusion analyses | 45 |
| 3.1 Total oxygen | 45 |
| 3.2 Cross section analyses | 46 |
| 3.2.1 Lollipop samples | 47 |
| 3.2.2 Rolled product samples | 48 |
| 3.3 Thermodynamic calculations | 48 |
| 3.4 Methods used in this study | 50 |
| 4 Classification of inclusions and data treatment | 53 |
| 4.1 Composition-based classification | 53 |
| 4.2 Standards | 55 |
| 5 Proposed method | 57 |
| 5.1 Component calculation | 57 |
| 5.2 Phase identification | 59 |
| 5.3 Inclusion classification | 62 |

| | | |
|----------|------------------------------------------------------------------------------------|------------|
| 6 | Classification validation | 65 |
| 6.1 | Sample sets..... | 65 |
| 6.2 | Methods..... | 67 |
| 6.3 | Oxygen and nitrogen contents of inclusions | 68 |
| 6.4 | Elemental maps of inclusions..... | 69 |
| 6.4.1 | Ladle furnace samples | 71 |
| 6.4.2 | Mould samples..... | 77 |
| 6.4.3 | Product samples..... | 80 |
| 7 | Practical applications of the new classification method | 87 |
| 7.1 | Dispersion of inclusions in a lollipop sample | 87 |
| 7.1.1 | Size distributions | 89 |
| 7.1.2 | MgO content..... | 92 |
| 7.1.3 | Summary..... | 95 |
| 7.2 | Evolution of inclusions during sampling..... | 96 |
| 7.2.1 | Slightly modified heat 76325 | 97 |
| 7.2.2 | Medium modified heat 68852..... | 98 |
| 7.2.3 | Overmodified with calcium, heat 62078 | 100 |
| 7.2.4 | Discussion..... | 102 |
| 7.3 | Evolution of inclusions during continuous casting | 107 |
| 7.3.1 | Slightly modified heat 76325 | 108 |
| 7.3.2 | Medium modified heat 68852..... | 109 |
| 7.3.3 | Overmodified with calcium, heat 62078 | 110 |
| 7.3.4 | Discussion..... | 112 |
| 7.4 | Elongation of inclusions during hot rolling..... | 116 |
| 7.4.1 | Fraction of elongated inclusions..... | 116 |
| 7.4.2 | The effect of CaS and MgO on the tendency to elongate | 118 |
| 7.4.3 | Ternary contours | 125 |
| 7.4.4 | The effect of thickness location..... | 128 |
| 7.5 | Oxide–sulphide stringers..... | 131 |
| 7.5.1 | Parameters | 131 |
| 7.5.2 | Assessing the characteristics of an unfragmented inclusion..... | 132 |
| 7.5.3 | Results | 133 |
| 8 | Summary | 157 |
| 8.1 | Development of a new inclusion classification method..... | 157 |
| 8.2 | New information obtained with the inclusion classification and data treatment..... | 157 |
| 8.3 | Dispersion of inclusions in lollipop samples..... | 158 |

| | | |
|-------------------|-----------------------------------------------------------------------------------------------------|------------|
| 8.4 | Assessment of inclusion evolution during steel melt shop processing with the developed method | 158 |
| 8.5 | Assessment of inclusion evolution during liquid steel sampling with the developed method | 159 |
| 8.6 | Elongation of inclusions during hot rolling..... | 159 |
| 8.7 | Oxide–sulphide stringers..... | 160 |
| 8.8 | Theoretical implications..... | 161 |
| 8.9 | Practical implications | 161 |
| 8.10 | Reliability and validity | 162 |
| 8.11 | Recommendations for further research | 162 |
| References | | 163 |

1 Introduction

1.1 Background and research environment

Liquid steel is sampled with so-called lollipop samples. After rapid solidification, these are primarily used to analyse the chemical composition of the steel melt during the steelmaking processes. The analysis is obtained using optical emission spectroscopy (OES) and is of the bulk concentration, not separating non-soluble phases, i.e., non-metallic inclusions. In addition, the samples can be used to analyse inclusions in the steel melt. While it is relatively easy to assess the inclusions from a solidified steel sample, the results do not depict the inclusion characteristics in the liquid steel. Instead, thermodynamic calculations should be performed in order to assess the situation in the hot steel melt. For instance, it has been shown that despite the fast cooling rate, inclusion phases precipitate during the solidification of the sample. On top of this, the inclusion analyses differ within regions in lollipop samples because of the turbulent flow of the liquid steel into the sampler, and differences between the cooling rates in the surface and centre parts of the sample.

Inclusion analyses, depending on the method applied, demand time and resources. Furthermore, the obtained results must be interpreted properly. The chemical composition of the inclusions alone does not provide adequate information on the inclusions – not even necessarily if thermodynamic calculations are performed. It is shown that further data processing is needed in order to properly analyse the results, and to understand the structure and the phases in the inclusions. In-depth inclusion classification is usually not provided by the analysis software, and on the other hand, it is laborious to perform using conventional spreadsheet calculations. As an example of a laborious analysis, the investigation of oxide–sulphide stringers found on hot rolled steel products can be mentioned.

In the literature, calcium treatment is often considered successful if nozzle clogging is avoided by modifying solid aluminium oxide inclusions into liquid calcium aluminates. However, the inclusion composition may radically alter during the solidification of the steel as the solubilities of various elements in the liquid steel decrease. Consequently, inclusions in the liquid steel, e.g. in the continuous casting mould, do not depict the inclusions found in the final product of the very same heat. Furthermore, non-metallic inclusions act differently during hot rolling, mainly depending on the inclusion phase composition. In this study, inclusions have been investigated both from the lollipop samples, taken from the liquid steel, as

well as the hot rolled final product. The samples were taken from the SSAB Europe steel mill at Raahe in Finland. In addition, the target inclusion composition from the casting point of view of might be different from the optimal inclusion composition during the hot rolling process. For example, in this dissertation, some low-melting calcium aluminates are shown to form detrimental stringers during hot rolling.

1.2 Objectives and scope

The objectives of this thesis are as follows:

1. To develop a new inclusion identification and classification method
2. To assess the inclusion evolution during steel melt shop processing with the developed method
3. To assess the inclusion evolution during liquid steel sampling with the developed method
4. To provide new information on industrial samples via the developed inclusion classification and data treatment method

All aspects are considered in the context of aluminium-killed, calcium treated steels. In Figure 1, the layout of the SSAB Europe Raahe steel melt shop is illustrated. In the basic oxygen furnace (BOF) converter, the carbon concentration is reduced by oxygen blowing. Upon tapping, the steel is killed with aluminium additions, effectively lowering of oxygen content. Before continuous casting, the steel melt composition and temperature are carefully controlled in ladle treatments. In the SSAB Raahe melt shop, a ladle furnace or CAS-OB station can be used. In addition, an option for vacuum treatment for demanding steel grades exists at the plant.

In the figure, the sampling locations are denoted with the numbering 1–3. The ladle and mould samples were taken from the liquid steel: after the ladle treatments, and during continuous casting, respectively. The product samples were obtained from the hot rolled steel. While the ladle samples were obtained before the continuous casting, the research in this dissertation is focused on the evolution of the inclusion characteristics from the continuous casting mould to the hot rolled product. The samples have been used for analysing the chemical composition of the steel, and for the characterisation of non-metallic inclusions.

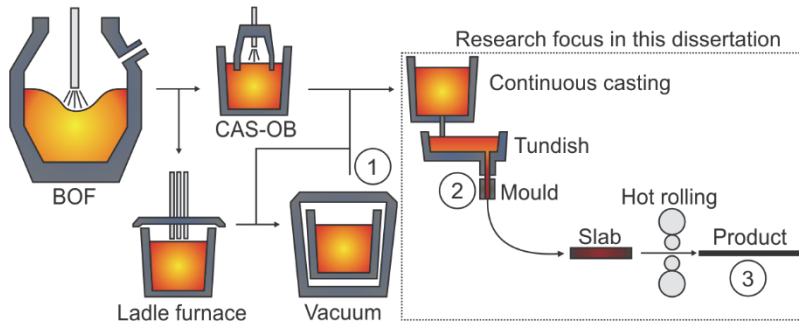


Fig. 1. Overview of the steel melt shop. Sampling locations: 1) Ladle after treatments; 2) Mould; 3) Hot rolled product. Modified from SSAB Europe presentation material (2012).

The experimental part of this dissertation is divided into the following subsections:

- Development of the inclusion phase identification and classification method (IPIM)
- Validation of the IPIM
- Dispersion of inclusions in lollipop samples
- Evolution of inclusions during liquid steel sampling
- Evolution of inclusions during continuous casting
- Elongation of inclusions during hot rolling
- Investigation of oxide–sulphide stringers

2 Non-metallic inclusions in the steelmaking processes

2.1 Non-metallic inclusions

Inclusions are non-metallic compounds, typically oxides, sulphides, and nitrides found in the steel. They are always present in the steel, and producing inclusion-free steel – in large quantities – is not feasible by any means. For the most part, thermodynamics constrain the level of impurities in the steel. For example, with aluminium deoxidation, around 3–5 ppm oxygen will always remain dissolved in the liquid steel (Holappa, 2010). When the steel solidifies during casting, the dissolved oxygen content will inevitably form oxides.

Abundant inclusion content in steel affect both the process control and product quality. Kaushik, Pielet, and Yin (2009) list the process control effects as nozzle clogging, poor castability, slab downgrades and rejections. In addition, the authors noted the increased costs in recycling of steel and refractory use. Inclusions are detrimental to mechanical properties of steel, leading to shortened service life of steel parts and leading to complaints.

Traditionally, non-metallic inclusions have been classified into endogeneous and exogeneous, depending on their origin (Way, 2001). Endogeneous inclusions form in the steel melt by chemical reactions, such as deoxidation or reoxidation. Exogeneous inclusions, on the other hand, originate from outside the liquid steel melt, e.g. from covering slags or refractories. Usually endogeneous inclusions are small and less harmful, whereas exogeneous inclusions may be very large and markedly worsen the steel cleanliness because of their large size. Because exogeneous inclusions originate quite randomly, typically from slags or refractories, the prediction of their occurrence is a challenging task, where thermodynamics play no role.

Further, endogeneous inclusions may be categorised into primary, secondary, and tertiary inclusions (Sahai & Emi, 2007). Deoxidation products are typically considered primary inclusions. However, some researchers consider any inclusions in the steel melt to be primary, and any inclusions forming during solidification secondary inclusions (Janis et al., 2013). For example, Ericsson (2010) regarded inclusions smaller than 0.6 μm to be secondary inclusions, formed during solidification. During casting, the solubility of oxygen and nitrogen decrease and sulphur is enriched in the remaining melt. According to Sahai and Emi (2007),

secondary inclusions precipitate on the surface of primary inclusions, and tertiary inclusions form on the secondary inclusions. In aluminium-killed and calcium-treated steels, it is quite common to observe such complex inclusions in the product samples.

While it is not realistic to remove all inclusions, their chemical composition can be adjusted in the steelmaking processes. A typical example is calcium treatment, where aluminium oxides are converted into liquid calcium aluminates. Aluminium oxides are easily agglomerated and floated into the slag, but they are more harmful if left in the steel compared to liquid calcium aluminates. Small and liquid inclusions are more difficult to remove to the slag, but they are not that harmful to the steel properties or process control. Besides chemical modification, the physical modification of inclusions is also possible (Choudhary & Ghosh, 2009; Wang, Valdez, & Sridhar, 2002). The aim of physical modification is to coat hard and nondeformable inclusions with a softer phase. During hot rolling, the softer phase is deformed, while the nondeformable inclusion does not affect the deformation of the steel matrix.

2.2 Calcium treatment

One of the most important ladle operations is calcium treatment. Calcium is added to steel in the form of wire or powder to meet three primary goals: to modify oxide inclusions, to desulphurise steel, and to control the shape of sulphide inclusions (Choudhary & Ghosh, 2008). The target of calcium treatment is to liquefy all the oxides and to avoid the formation of solid sulphides (Abdelaziz, Megahed, El-Mahallawi, & Ahmed, 2009). The exact amount of calcium needed depends on the total sulphur and oxygen contents in the steel.

A proper calcium addition modifies aluminium oxides or spinel inclusions and transforms them into liquid calcium aluminate inclusions, which do not adhere to refractory materials, and secondly are capable to absorb sulphur from the melt (Ahlborg, Fruehan, Potter, Badger, & Casuccio, 2003). Solid Al_2O_3 , spinel and CaS inclusions cause harm during the steelmaking processes: the most notable effect is nozzle clogging. Ahlborg et al. (2003) state that theoretically all solid inclusions, including solid calcium aluminates CA_6 , CA_2 , and CA can cause clogging. In addition, solid inclusions at steelmaking temperatures are typically hard and nondeformable in the solidified steel, and detrimental to the mechanical properties of the steel.

With proper calcium addition, during continuous casting CaS is formed either on the surfaces of existing oxide inclusions or as singular, small, and evenly distributed inclusions in the continuously cast slab, when their detrimental effects are minimised. In the worst case, sulphur, not bound by calcium during ladle treatments, is enriched in the remaining melt during solidification, resulting in the formation of manganese sulphides, which are prone to severely elongate during hot rolling, markedly worsening the steel quality.

However, excess calcium treatment leads to the abundant formation of CaS or CaO in the liquid steel. According to Geldenhuis & Pistorius (2000), reactions with the alumina in the slag or with alumina containing refractories can occur with excess calcium additions. However, inadequate calcium treatment leads to unsatisfactory modification of alumina or spinel inclusions.

There are two main factors, which complicate successful calcium treatment. Firstly, usually no accurate information on the amount of alumina inclusions, or even the oxygen content in the steel melt is available at the time of calcium addition. Therefore, the exact amount of calcium needed in order to modify all the alumina inclusions is not known specifically for each heat (Holappa, Hämäläinen, Liukkonen, & Lind, 2003).

Secondly, the yield of the calcium fed into the ladle is often quite poor. Calcium has a low boiling point, high volatility and chemical activity (Janke, Ma, Valentin, & Heinen, 2000; Lu, Irons, & Lu, 1994). Therefore, the estimation of the yield is problematic. It has been estimated that more than half of the added calcium is lost due to vaporisation (Abdelaziz et al., 2009; Geldenhuis & Pistorius, 2000; Pistorius, Presoly, & Tshilombo, 2006; Pistorius, Roy, & Verma, 2013; Tiekink et al., 2006).

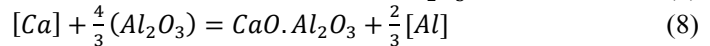
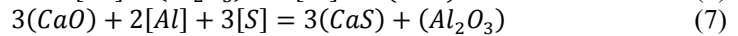
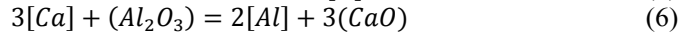
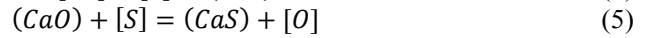
Martinez (1995) points out that the degree of calcium modification depends not only the total calcium content, but also on the sulphur concentration. With the same calcium contents, a higher Ca/Al ratio in inclusions is expected with lower sulphur levels.

The full modification of aluminium oxide inclusions requires 43–58 wt.% Al_2O_3 , i.e. a mixture of CA–C12A7 or C3A–C12A7 in the inclusion at 1550°C (Choudhary & Ghosh, 2008). However, some researchers have suggested that a partial liquefaction of inclusions would ensure satisfactory castability. For example, Fuhr, Cicutti, Walter, and Torga, (2003) observed good castability performance when the liquid fraction of inclusions was more than 50%. According to Geldenhuis & Pistorius (2000) and Choudhary & Ghosh (2008), partial liquefaction with oxide composition between CA and C12A7 would ensure good castability.

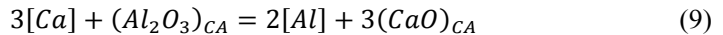
Added calcium reacts in various ways in the steel melt. It can modify aluminium oxides and spinels, and form calcium sulphides. These modifications take place through immediate reactions with oxygen and sulphur, forming CaO and CaS, respectively. In the following sections, the reactions proposed in the literature are reviewed.

2.2.1 Modification of aluminium oxide inclusions

After aluminium deoxidation, aluminium oxides are the prevailing inclusions in the steel melt. After calcium addition, the following reactions take place (Abdelaziz et al., 2009; Holappa & Wijk, 2014). In these reactions, the modification reaction of alumina takes place due to dissolved calcium.



Janke et al. (2000) present the simultaneous reactions:



when the overall reaction can be written as:



Further, the competition of oxide and sulphide modification is presented by:



Ye, Jönsson, & Lund (1996) reported that the modification of alumina inclusions follows the linear path of Al_2O_3 –CA6–CA2–CA into liquid calcium aluminates, i.e., increasing the CaO content in the oxides. At steelmaking temperatures (1550°C), pure CA appears solid, while calcium aluminate with a composition corresponding to C12A7 is fully liquid. Further, the authors concluded that the activity of Al_2O_3 decreases with the progressing modification of alumina inclusions with calcium, ultimately resulting in the precipitation of CaS, instead of CaO in calcium aluminate. The Al_2O_3 –CaO binary phase diagram, calculated by FactSage 7.1, is

presented in Figure 2. The databases used here did not include the calcium aluminate C12A7, which is located near the eutectic composition between CA and C3A.

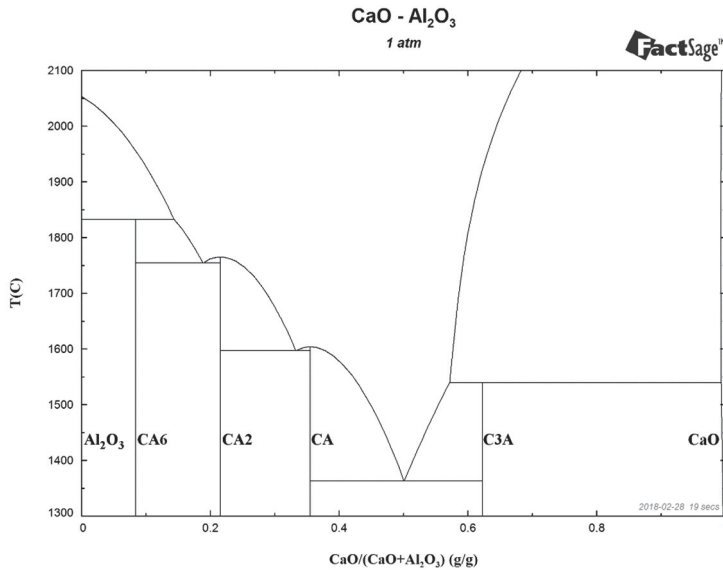


Fig. 2. Al₂O₃–CaO phase diagram, calculated by FactSage 7.1.

Overmodification and higher CaO contents result in solid calcium aluminates with a C3A composition. It is evident that the modification of alumina oxides with calcium involves several steps, and hitting the liquid area is challenging, especially with high sulphur contents when the liquid window is narrower (Choudhary & Ghosh, 2008).

Many researchers have proposed that the modification of Al₂O₃ takes place according to the unreacted core model (Ito, Suda, Kato, Nakato, & Sorimachi, 1996; Ye et al., 1996). According to Wang et al. (2014), CaO diffuses towards the centre of the inclusion, while Al₂O₃ diffuses outwards. The portion of the calcium aluminate layer increases, while the Al₂O₃ core diminishes. Wang et al. (2014) consider the diffusion of Al₂O₃ or CaO in the reacted layer as the rate controlling step in the modification.

In liquid steel, transient CaO and CaS compounds are formed instantly after the addition of Ca. Lind & Holappa (2010) and Tiekink et al. (2006) observed that right after calcium treatment, both CaO and CaS component fractions in inclusions

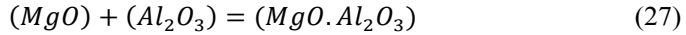
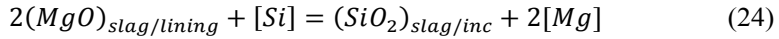
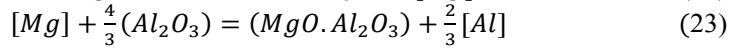
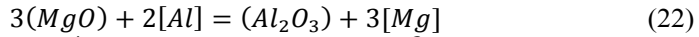
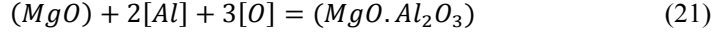
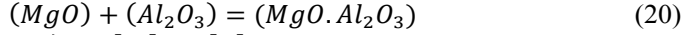
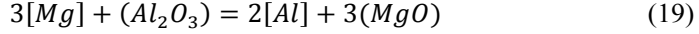
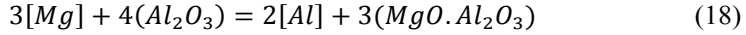
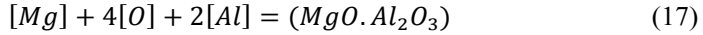
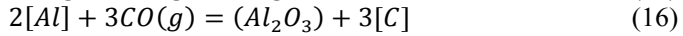
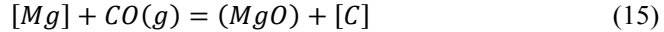
increased. The results obtained by Verma, Pistorius, Fruehan, Potter, Lind, & Story (2011b) have similar trends. In low-sulphur laboratory heats with 7 ppm sulphur, small CaO inclusions formed right after calcium treatment, followed by the formation of CaS. In the experiments, CaO and CaS were observed as transient phases, modifying alumina inclusions.

Similarly, Ren, Zhang, & Li (2014) reported in their laboratory experiments with 30 ppm sulphur, that transient $\text{Al}_2\text{O}_3\text{--CaS--CaO}$ inclusions were immediately formed after calcium addition. With increasing time, the CaS content of the inclusions notably decreased. In their later investigation, Ren, Zhang, & Zhang (2017) showed that upon calcium injection, a Ca-rich plume zone is formed. In the plume zone, calcium immediately reacts with [S] and [O] becoming CaS and CaO inclusions. After stirring, calcium-rich inclusions react with slightly modified calcium aluminates in the steel bulk. As a consequence, liquid calcium aluminates are generated. It is plausible that the modification of alumina takes place via instantly formed CaS–CaO phases instead of dissolved calcium.

2.2.2 Modification of spinel inclusions

Besides the modification made by calcium leading to liquid calcium aluminates, Al_2O_3 can also react with MgO, forming $\text{MgO}\cdot\text{Al}_2\text{O}_3$ spinels. Various origins have been proposed for MgO in the steel melt. Geldenhuis & Pistorius (2000) assumed that most MgO originates from magnesium impurities in the aluminium deoxidiser. On the other hand, MgO has been said to originate from the reactions between steel melt, inclusion and refractories (Janke et al., 2000). On top of this, (Holappa, 2001) points out that reactions between Al-killed steel and MgO in refractories are emphasised under elongated treatment times and in vacuum treatment.

Yang, Wang, Zhang, Li, & Peaslee (2012) list a number of reactions explaining the formation of spinel inclusions. The reactions are divided into four categories: reduction by carbon, direct reaction, reduction by aluminium, and reduction by silicon, presented in Equations 13–19, 20–21, 22–23, and 24–27, respectively.



In the work by Pistorius et al. (2006), all oxide inclusions after the deoxidation, but before the calcium treatment were found to be spinels. According to the authors, the reduction of MgO from the refractory resulted in soluble magnesium in the steel, finally reacting with alumina inclusions to form spinels. The authors note that although spinels are known to cause clogging, the MgO content in the oxide inclusion widens the liquid window, enhancing the liquefaction of inclusions. This can also be verified in Figure 3, where the fully liquid area at 1550°C is plotted on an Al₂O₃–CaO–MgO ternary diagram. Verma, Lind, Pistorius, & Fruehan (2010) point out that MgO is not soluble in Al₂O₃, resulting in spinel formation when any MgO is present. Later, Verma et al. (2012) proposed that the modification of spinels takes place via a transient CaS phase. However, the overall reaction was considered identical to the modification of alumina, with no role of MgO.

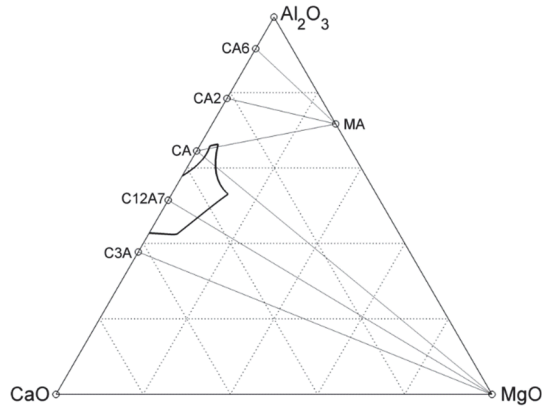


Fig. 3. Al_2O_3 –CaO–MgO ternary diagram with a liquid window at 1550°C, calculated by FactSage.

If spinels are treated with calcium, a liquid phase is reported to form immediately. In addition, the modification of alumina demands more CaO in order to form the first liquid phase (Yang, Li, Wang, Li, & Lin, 2011). Large spinel inclusions have a layered structure and are difficultly modified with Ca, as reported by Yang et al. (2012). However, they also claimed that $\text{MgO}\cdot\text{Al}_2\text{O}_3$ inclusions smaller than 2 μm are easily modified and transformed into calcium aluminates.

Janke et al. (2000) deduced that very low oxygen levels would lead to the formation of spinel inclusions. In the thermodynamic calculations by Yang et al. (2013), spinels could be fully modified to become calcium aluminates with dissolved calcium contents as low as 2 ppm.

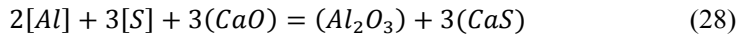
2.2.3 Formation of calcium sulphides

CaS formation should be avoided in the ladle for a number of reasons. Firstly, it hinders the alumina modification. Secondly, it may cause clogging and refractory wear. Finally, calcium sulphides are harmful to the mechanical properties of the steel. (Story, 2001)

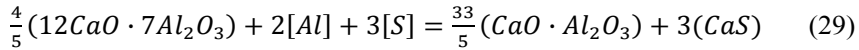
If CaS is formed in the ladle processes, it is an indication of calcium overmodification (Geldenhuis & Pistorius, 2000). According to researchers, singular CaS inclusions are rare (Verma, Pistorius, Fruehan, Potter, Lind, & Story, 2011a; Zhao, Li, Bao, & Yang, 2015). That is, CaS is usually attached to solid or liquid oxide inclusions. Geldenhuis & Pistorius (2000) assume that CaS inclusions associated with liquid inclusions do not cause clogging. However, Nurmi,

Louhenkilpi, & Holappa (2009) stated that during the casting and solidification of steel, CaS formation starts readily as the sulphur is enriched in the remaining melt. Yang, Wang, Yang, Wei, & He (2014) note that with lower total oxygen contents, less calcium is adequate for alumina modification and the formation of CaS.

As stated in the previous sections, calcium sulphide is a transient phase in alumina and spinel modification. The reaction leading to CaS formation is presented in Equation 28, which is essentially the same as Equation 11.



Another reaction where liquid calcium aluminate reacts to solid CA is presented in Equation 29 (Choudhary & Ghosh, 2008). Reaction constants for both of these reactions depend only on [Al] and [S] contents, rather than the [Ca] content. The equilibrium constant for both reactions can be expressed as $1/([S]^3[Al]^2)$, if the activities of the compounds are assumed to be unity.



After calcium treatment, the CaS phase distribution can be classified into three types, according to Yang et al. (2013). These types are collision with oxide, surrounding oxide, and uniformly distributed within oxide. Evidently, the CaS shape in the steel melt also affects the CaS precipitation mechanism during the solidification.

The samples taken from a continuous casting mould typically contain oxide-sulphide inclusions. Verma et al. (2010) observed sulphide rings around partially modified oxide inclusions. The authors assumed that the ring had formed during the solidification of the sample.

2.3 Continuous casting

After ladle treatments, steel is cast into slabs by continuous casting. In Figure 4, a caster with auxiliary equipment is illustrated. During continuous casting, the steel melt is teemed into a water-cooled copper mould. In the mould, the solidification of the steel starts, continuing towards the lower sections of the caster, where further solidification takes place usually by water spray cooling.

The tundish can be considered the last vessel in the steelmaking process. The tundish is used to transfer the steel melt from the ladle into the continuous casting mould. The tundish may be installed with accessories such as weirs, dams and baffles in order to lengthen the residence time and to promote the flotation of

inclusions (De Santis et al., 2010). The revolving turret and the tundish, acting as a reservoir, enable sequential casting of numerous ladles. During the ladle changes, the liquid steel may be exposed to air, resulting in harmful reoxidation.

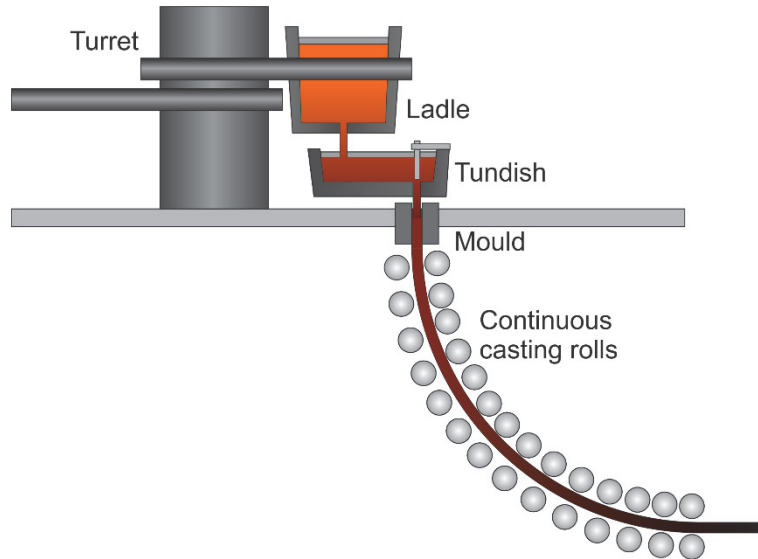


Fig. 4. Schematic view of continuous casting equipment.

For the most part, steel cleanliness is achieved in the ladle furnace process. Nowadays the tundish is seen as an intermediate vessel, rather than a refiner (Sahai & Emi, 2007). That is, the primary aim of using the tundish is to prevent further reoxidation, and slag entrapment – in other words to maintain the achieved steel cleanliness. The main objectives of tundish operation are to achieve a controlled flow rate and even temperature. According to Sahai & Emi (2007), calcium additions or other adjustments in the tundish are only acceptable if nozzle clogging is otherwise unavoidable.

However, efforts have been made to enhance the inclusion absorption capability of tundish slags, especially for steels with high cleanliness requirements (Holappa et al., 2013).

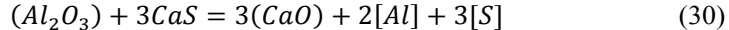
Reoxidation in a tundish may result in the formation of spinels. Li, Jiang, He, Sun, & Wang (2016) observed large $\text{CaO-MgO-Al}_2\text{O}_3$ clusters in continuous cast blooms, which were possibly aggregated by smaller inclusions during continuous casting.

It is essential to remove the largest inclusions from the steel melt into the slag in the tundish. Any macro-inclusions existing in the tundish have three alternative paths. Either they will be floated into the tundish slag, or they will pass through the nozzle and flow into the mould. There they end up in the slab and in the steel product, if they are not absorbed by the mould slag.

During cooling of the steel, the solubilities of oxygen, sulphur and nitrogen decrease, resulting in inclusions and precipitates forming as oxides, sulphides and nitrides, respectively. During solidification, segregation also occurs, when the solidifying steel rejects some elements such as sulphur into the remaining melt. The inclusions in the solidified steel cannot be predicted thermodynamically, and they are heterogeneous in composition (Holappa et al., 2003).

2.3.1 Formation of calcium aluminate–CaS or alumina–CaS inclusions

During the solidification of steel, sulphur is rejected into the remaining liquid, accelerating the formation of CaS (Choudhary & Ghosh, 2008; Wang et al., 2002). The increase in sulphur in the steel melt and the decrease in temperature causes the reaction in Equation 30 to shift from right to the left, forming Al₂O₃-rich inclusions and CaS (Ahlborg et al., 2003).



Tiekink et al. (2006) noted that the occurrence of CaS–Al₂O₃ inclusions cannot be explained by thermodynamics alone. In their opinion, calcium sulphides are formed only after the aluminium oxides have been fully modified by calcium and have become calcium aluminates. Further, they assume that Al₂O₃ occurs randomly in oxygen-depleted zones in the steel melt, and these inclusions act as reaction sites for calcium sulphides. The formation of CaS happens readily, with adequate calcium and sulphur activities in the melt, along with sufficiently low oxygen activity.

As in the CaS formation caused by calcium treatment, oxide–sulphide inclusions formed during steel casting appear in a variety of forms. Guo, Cheng, Cheng, & Xin (2013) list two types of oxide-sulphide inclusions. According to the researchers, a CaS ring can be formed on the surface of a solid inclusion core, or CaS can form on liquid calcium aluminate in a chemical reaction. It is reported that the former is easily broken into small fragments, whereas the latter elongates with the steel matrix. The view by Zhao et al. (2015) differs slightly. In their opinion, an

oval-shaped CaS layer is formed as a result of collision of the inclusions, and breaks easily during hot rolling. On the other hand, CaS is likely to be formed by diffusion, if it takes the form of a crescent.

CaS can also precipitate from the liquid inclusion when its sulphide capacity decreases with temperature (Zhao et al., 2015). According to Martinez (1995), the solubility of CaS in a CaO–Al₂O₃ system is around 4–5 wt.%, depending on the temperature. He reported small CaS precipitates within a calcium aluminate inclusion, suggesting CaS was found in the liquid inclusion solution in the steel melt, before the solidification of the sample. Verma et al. (2011a) reported the solubility of sulphur in liquid calcium aluminate to be around 2 atomic percent, which is in accordance with the estimation by Wang et al. (2002).

It is not clear where the CaS phase tends to form during the solidification of steel. Wang et al. (2002) reported that upon solidification, CaS starts to form on liquid calcium aluminates. After the precipitation of CaS, inclusions agglomerated easily, unlike the liquid inclusions. According to Wang et al. (2002), the transformation of liquid inclusions into CaS-containing inclusions may cause clogging and worsen the steel quality. However, Verma et al. (2011b) considered the alumina–steel interface the most probable nucleation site for CaS.

Yang, Guo, Li, & Zhang (2017) observed liquid calcium aluminates in the tundish, but the transformation into Al₂O₃–CaO–MgO–CaS inclusions occurred during the cooling and solidification of the steel. Typically, they found that spinel phases formed inside the calcium aluminate inclusion, whereas the CaS phase precipitated on the surface of the existing inclusion. The total oxygen content remained on the same level in tundish and slab samples, indicating reoxidation was not the reason for the transformation.

Some researchers regard the increase in the Al₂O₃ content in inclusions as an indicator of reoxidation. For instance, Yang et al. (2014) reported reoxidation in the tundish during the casting of the first heat in the sequence. They observed a decreasing CaO to Al₂O₃ ratio in the inclusions along the process, indicating an increase in the Al₂O₃ content. The samples were taken after the RH vacuum treatment, from the tundish, and from the slab. Similarly, Li et al. (2016) observed reoxidation in the tundish, resulting in the transformation of liquid calcium aluminates into solid calcium aluminates, spinels, or Al₂O₃–CaO–MgO inclusions. However, the investigators offered no information on the role of CaS.

While the prevention of CaS formation in the tundish is essential to avoid nozzle clogging, it should be well noted that in practice, all sulphur soluble in the steel melt will finally be found as sulphides in the solidified steel. That is, the

formation of calcium sulphides, singularly or on calcium aluminates, is inevitable, if the formation of manganese sulphides has to be prevented.

2.3.2 Factors affecting the location of inclusions in the slab

Especially with bow casters, some investigators (Cappel, Flender, Hoffken, Kemper, & Wunnenberg, 2005; Fuchs, Wagner, Jacobi, & Wunnenberg, 1993; Pandey, Choubey, & Raj, 2008) have reported inclusion bands, where non-metallic inclusions concentrate at a certain thickness location on continuously cast slabs during casting. The band is formed in the curved zone of the caster, when inclusions in the narrowing liquid cone are floated upwards. A schematic view is illustrated in Figure 5, where inclusion trajectories in the remaining melt are demonstrated. The inclusion band effect is reduced with vertical bending casters, where the vertical liquid steel section is longer, and inclusions have more time to flow upwards.

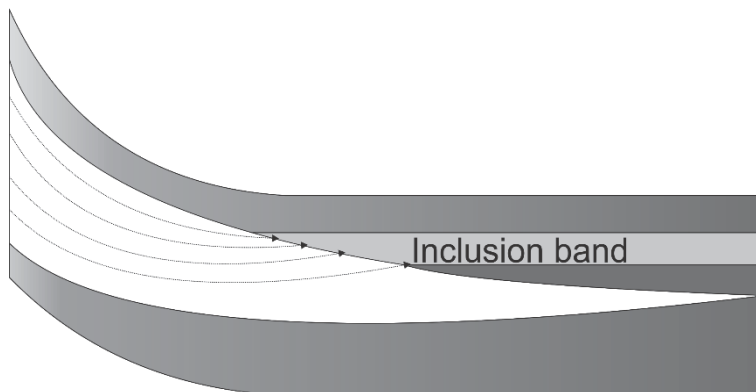


Fig. 5. Formation of an inclusion band on a solidifying slab during casting. Modified from Javurek (2012).

Besides the inclusion flotation in the remaining liquid during continuous casting, the inclusion path is affected by the solidifying steel fronts. Juretzko, Dhindaw, Stefanescu, Sen, & Curreri (1998) have listed the interactions of inclusions and the solidification front as pushing, engulfment and entrapment, see Figure 6. Whether the inclusion is pushed, engulfed or entrapped, depends on the following factors: the solidification front type (planar, cellular, dendritic or equiaxed) and speed, the inclusion size, and the surface energies, which are affected by the chemical

composition of the steel and inclusions. Ohta & Suito (2006) found that solid MgO, ZrO₂, and Al₂O₃ inclusions were more easily pushed by the solidifying Fe–10%Ni front, compared to liquid MnO–SiO₂ or CaO–Al₂O₃ inclusions.

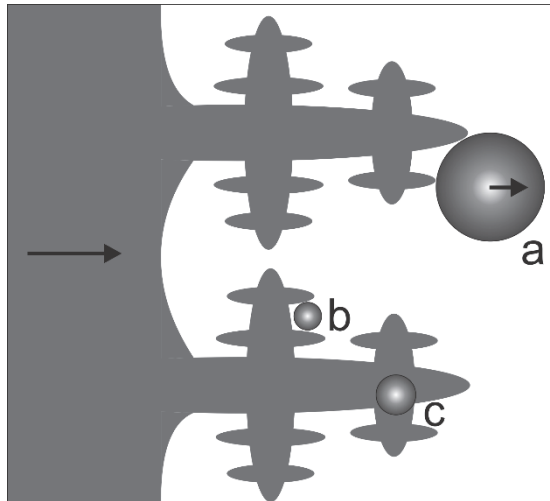


Fig. 6. Inclusion interaction with a dendritic solidification front: a) pushed, b) entrapment, c) engulfment by the solidification front. Modified from Juretzko et al. (1998).

In the conference publication by Castro et al. (2005), the distribution of Al₂O₃–CaO–MgO+CaS inclusions in continuously cast slabs was investigated. The samples were taken from the middle width of the slabs, for three thicknesses: the upper surface, the centreline, and approximately ¼ thickness from the lower side. On average, inclusions were less abundant in the lower part. However, no significant difference was found between the centreline and upper parts. According to the researchers, the fraction of the CaS phase was higher in the centreline inclusions.

Zhang et al. (2006) reported the distribution of inclusions in IF and LCAK steels. The researchers stated that the mass fraction of inclusions decreased by 22% from the tundish sample to the slab sample. The inclusions were concentrated at the 20 mm depth from the upper side of the 250 mm thick slabs, but also between quarter depth and the centreline.

Kaushik & Yin (2012) investigated the distribution of oxides, sulphides and nitrides in continuously cast slabs. The samples were taken at the quarter width, at

three thicknesses: the upper and lower surfaces, as well as the centreline. The researchers noted that the area fractions of sulphides and titanium nitrides were larger in the centreline due to the tendency of sulphur and nitrogen to segregate. However, this was not observed with oxides such as calcium aluminates or spinels.

2.4 Hot rolling

2.4.1 Deformation and elongation of inclusions

During hot rolling, inclusions may deform with the steel matrix, mainly depending on the inclusion size and phase composition. Malkiewicz & Rudnik (1963) determine the relative deformation (RD) of non-metallic inclusions as

$$RD = \omega \ln \lambda / \ln h \quad (31)$$

where

ω is a constant $\frac{2}{3}$ for a square bloom or billet, and $\frac{1}{2}$ for a slab,

λ is the ratio of length to thickness of the inclusion after hot rolling,

h is the ratio of the observed inclusion area before and after hot rolling.

Elongated inclusions and stringer formation of the inclusions in the rolling direction has been shown to reduce transverse toughness and in general create anisotropic toughness properties (Maiti & Hawbolt, 1985). Earlier, Saxena (1982) noted a steel plate splitting tendency during bending, low transverse notch toughness, lamellar tearing during welding, and low through-thickness ductility.

The inclusion microhardness, melting temperature, and thermal expansion coefficients have been used to quickly assess the deformation behaviour of inclusions. As Kawahara, Tanabe, Banno, & Yoshida (1992) have pointed out, a strong correlation exists between the melting or softening temperature and the hardness of the inclusion. Thus, a high hardness of inclusions often leads to lower deformability during hot rolling. In Table 2, some properties for typical inclusion phases are presented. It can be seen that the microhardness of aluminium oxides and spinels is markedly high, whereas sulphides exhibit lower values. On the other hand, the hardness of calcium aluminates can vary greatly, depending on the phase composition.

Table 2. Properties of typical inclusion phases, as reported by Cicutti et al. (1997), if not stated otherwise.

| Phase | Melting temperature (°C) | Vickers hardness | Thermal expansion coefficient (°C ⁻¹) |
|------------------------------------|--------------------------|-------------------------|---------------------------------------------------|
| Al ₂ O ₃ | 2050 | 3750 | 8×10 ⁻⁶ |
| CA6 | 1850 | 2200 | 9×10 ⁻⁶ |
| CA2 | 1750 | 1100 | 5×10 ⁻⁶ ¹⁾ |
| CA | 1605 | 930 | 7×10 ⁻⁶ |
| C12A7 | 1455 | – | 8×10 ⁻⁶ |
| C3A | 1535 | – | 1.0×10 ⁻⁵ |
| CaO | 2570 | 400 | 1.4×10 ⁻⁵ ¹⁾ |
| MgO·Al ₂ O ₃ | 2108 ⁴⁾ | 2100–2400 ²⁾ | 8×10 ⁻⁶ ¹⁾ |
| MgO | 2825 ⁴⁾ | – | 1.4×10 ⁻⁵ ¹⁾ |
| CaS | 2450 | > 300 ³⁾ | 1.5×10 ⁻⁵ |
| MnS | 1610 | 170 | 1.8×10 ⁻⁵ |

1) From Ånmark et al. (2015), 2) From Yang et al. (2012), 3) From Jiang et al. (1997), 4) From FactSage FactPS database

As Choudhary (2011) states, the deformability of an inclusions depends mainly on its chemical composition. When assessing the elongation and deformability of inclusions, the phase composition is an essential factor. It has been reported that during the rolling process, calcium aluminates do not deform at all (Kiessling & Lange, 1978). Instead, they tend to get crushed during hot deformation. Further, Kiessling & Lange (1978) report that the temperature hardly affects the plastic behaviour of calcium aluminates during deformation. The authors also assumed that calcium aluminates are not usually crystallised in steel, leaving the CaO and Al₂O₃ components often in glassy inclusions. However, based on research by Sugimura et al. (2011), inclusions in the Al₂O₃–CaO–MgO system observed in continuously cast steel and which has undergone hot rolling are expected to contain crystalline structures.

In the review article by Ånmark, Karasev, & Jönsson (2015) it is listed that calcium-treated oxides are not deformable in temperatures below 1200°C, whereas their deformability is high when the temperature exceeds 1300°C. For calcium-treated sulphides, it is proposed that no deformation occurs in temperatures under 1200°C, but there is some deformability at temperatures over 1300°C. Keeping in mind the main purpose of hot rolling or thermomechanical treatments is to obtain a desired phase structure of the steel, it is clear that the rolling temperature cannot be determined by the inclusion behaviour alone.

According to Zhang (2006), spinels, calcium aluminates, and alumina are considered non-deformable inclusions. The non-deformability of an inclusion in hot rolled steel is defined as the ratio of the length to the width, i.e., the aspect ratio, is smaller than three. Faulring (1999) applies the same length to width ratio in determining non-deformable inclusions, and quite similarly, lists calcium aluminates as non-deformable along with spinels and alumina. While some calcium aluminates may exhibit non-deformable behaviour during hot rolling, in the Al_2O_3 – CaO – MgO oxide system, calcium aluminates have the lowest melting point, and thus would be considered the most deformable. However, when examining an Al_2O_3 – CaO – SiO_2 system, inclusions with even lower melting points are found with relatively high SiO_2 concentrations. In the steels investigated in the experimental section, however, high SiO_2 bearing inclusions are extremely rare, and SiO_2 contents of the inclusions in general are usually negligible.

Choudhary & Ghosh (2008) have stated that sulphides, not counting MnS , are virtually non-deformable during rolling. Similarly, Cicutti, Madías, & González, (1997) and Zhang et al. (2017) considered calcium sulphides to be non-deformable.

Bernard, Riboud, & Urbain (1981) presented typical inclusion compositions exhibiting the following behaviours during hot rolling: firstly, those that are too viscous to be deformed and which form voids on the head and tail during rolling; secondly inclusions that are likely to recrystallise and become non-deformable; and finally inclusions that are more deformable than steel, resulting in elongated inclusions. However, the inclusion compositions investigated encompassed low-melting Al_2O_3 – CaO – SiO_2 and Al_2O_3 – MnO – SiO_2 systems. The researchers hypothesised that a vitreous shell around the core would prevent the deformation and breakage of the inclusion. In addition, according to them, a fully crystallised complex cluster would result in an irregular stringer in the hot rolled product.

It has been postulated that globular non-deformable inclusion acts as crack initiation sites during deformation. Gagné & Thibault (1998) refer to multiple articles summarising the relationship between the composition of inclusions and their deformability. Again, in these studies, Al_2O_3 – CaO – SiO_2 system was investigated rather than an Al_2O_3 – CaO – MgO system. Further, the notable presence of a SiO_2 component in inclusions causes amorphous phases to exist. Understandably, glassy phases behave very differently to crystalline inclusions during hot rolling. Even though Gagné & Thibault also investigated the effect of added MgO on the deformation behaviour of inclusions, the concentration of SiO_2 component were in the range of tens of percent. As expected, amorphous structures were often observed.

Traditionally, inclusions have been classified into categories, depending on their deformation behaviour during hot rolling. In Figure 7a) a hard non-deformable inclusion has caused cavities in the hot rolling direction. In Figure 7b) brittle inclusions have broken into smaller fragments. In Figure 7c) hard phases are enclosed within a deformable phase. According to Wijk (1995), these kinds of inclusions may consist of thick centres, while having elongated tails. In Figure 7d) a well-deformed and heavily elongated inclusion is presented.

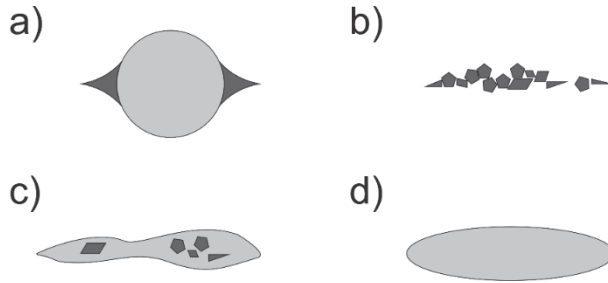


Fig. 7. Typical inclusion deformation types, reported by Holappa & Wijk (2014): a) no deformation, forms cavities; b) brittle inclusions, fragmented during rolling; c) brittle inclusions, surrounded by deformable matrix; d) a well-deformed inclusion.

It is understood that large inclusions are more affected by rolling deformation than small and uniformly distributed ones (Kiessling & Lange, 1978; Saxena, 1982). Further, Keskinilic (2011) regarded small and round sulphide inclusions as deformation-resistant.

Pure oxides or sulphides are rare in the rolled products of Ca-treated Al-killed steel. Often inclusions are a composition of oxides and sulphides, sometimes accompanied by nitrides. Ototani (1986) concluded that complex oxysulphides do not deform even during hot rolling, due to the high melting points of both calcium aluminates and calcium sulphide. According to Ototani (1986), if calcium aluminates have formed complex inclusions with spinel, they can fracture into stringers at high reduction ratios. Holappa et al. (2003) reported globular calcium aluminates surrounded by a CaS ring. According to the authors, the inclusion was nearly undeformed in the wire sample, indicating good deformation resistance.

2.4.2 Oxide–sulphide stringers

Manganese sulphides are known to deform during hot rolling into long stringers, which are especially detrimental to the bending properties of the steel. With adequate calcium additions, the formation of manganese sulphides is effectively prevented (Holappa & Helle, 1995). However, in hot rolled products, oxide–sulphide stringers are recurrently observed (Xu, Jiang, & Li, 2016). Usually their overall composition is a combination of calcium sulphides and oxide phases. In the worst cases, they can elongate into stringers with lengths of hundreds of micrometres. The stringers may be comprised of long, deformed inclusions or several inclusions that have broken into smaller pieces. In Figure 8, the formation of oxide–sulphide stringers during hot rolling is schematically illustrated.

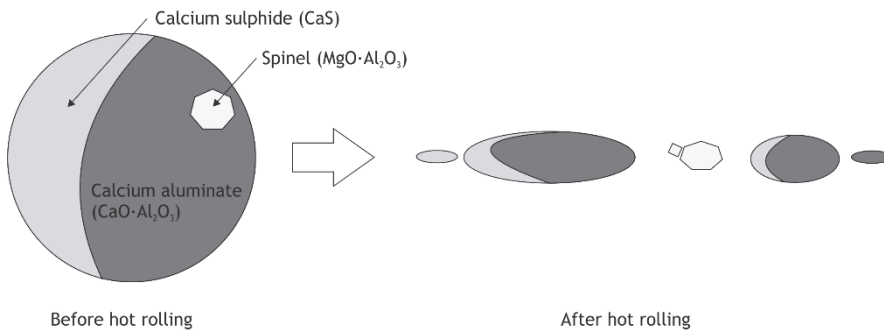


Fig. 8. Formation of oxide–sulphide stringers. Inclusion in slab and after hot rolling.

In ASTM E45 (2005), stringers are divided into two groups: continuous stringers are determined as just one very elongated inclusion, whereas discontinuous stringers contain three or more B or C type inclusions with an offset less than 15 μm and a maximum distance between two neighbouring inclusions less than 40 μm . However, the standard states that discontinuous stringers must not contain elongated inclusions, i.e., aspect ratios larger than 2. That is, a combination of continuous and discontinuous stringers is not considered. The ASTM E45 standard is developed to assess the severity of inclusions observed in a given area of a steel sample. In order to estimate and understand the formation mechanism of the stringers, rather than their potential effect on the steel properties, this type of classification of stringers might not be necessary.

To date, no extensive research on oxide–sulphide stringers has been carried out. Holappa & Helle (1995) reported that Ca-treated high sulphur steels contain

oxysulphides, which are less deformable than MnS inclusions. The researchers also stated that these oxysulphides are typically less than 5 μm in size. With these assumptions, it seems improbable that these oxysulphides could be the origin of elongated stringers in hot rolled products.

Wang et al. (2014) noted that well-deformed inclusions usually consist of low melting temperature calcium aluminates, while the non-deformed ones either contained more CaS or their CaO–Al₂O₃ ratios were out of the low-melting composition range. Similarly to Holappa & Helle (1995), Wang et al. (2014) also stated that inclusions in a CaS–CaO system would be non-deformable during hot rolling. They also postulated that large Al₂O₃–CaO low-melting inclusions could be deformed during rolling, even if a CaS–CaO surface layer had been formed on them.

According to Wang et al. (2014), after calcium treatment, liquid steel contains a large number of small sized liquid Al₂O₃–CaO inclusions. They were found to be hard to remove, and later could aggregate in clusters of 10–20 μm in size during continuous casting. Further, they are readily deformed into large stringer shaped inclusions in hot rolled plates.

Fuhr, Torga, Medina, & Cicutti (2007) and Wang et al. (2014) assumed that the elongated inclusions in hot rolled products were spherical in the slab, before hot rolling. When assuming the inclusions to be ellipsoidal plates, the diameter of the original inclusion can be estimated. In both studies, it was assessed that the original inclusion sizes were in the range of tens of micrometres in case of the longest stringers. The equations applied by Fuhr et al. (2007) and Wang et al. (2014) are presented in equations 32 and 33, respectively. It should be noted that the transverse width of an observed inclusion must be estimated; it cannot be measured from the cross section. Furthermore, it is assumed that the observed length and thickness of an inclusion are the maximum values, i.e., the cross section is cut in the centre of the ellipsoidal inclusion. On top of this, it is assumed that the cross section is perfectly parallel to the rolling direction (Karasev, Jafari, & Jönsson, 2015).

$$\frac{4}{3}\pi D^3 = LWD \quad (32)$$

$$D_{eq} = \left(\frac{3LWT}{2}\right)^{\frac{1}{3}} \quad (33)$$

where

D is the diameter of an inclusion,

L is the length of an observed inclusion,

W is the width of an observed inclusion,

D_{eq} is the equivalent diameter of a spherical inclusion,

T is the thickness of an observed inclusion.

According to Pickering (1958), the length to width ratio of the elongated ellipsoid inclusion is constant for any section parallel to the major axis of the longitudinal direction. In other words, if the inclusion is sectioned along its major axis, exposing the largest projection, the inclusion volume can be quite accurately estimated.

Various approaches for the estimation of the original inclusion size have been presented in the literature. Kanbe, Karasev, Todoroki, & Jönsson (2011) summed the areas of all inclusions in a stringer, and assumed that the area of the original spherical inclusion in a slab was equal. Calculated diameters of the original slab inclusions differ markedly, depending on the assumption used. The method used by Kanbe et al. (2011) overestimates the original inclusion size to some extent, compared to the ellipsoidal assumption.

Yang et al. (2014) reported Al_2O_3 -rich calcium aluminates aggregates in the slab. The composition of oxides was calculated to lie between CA and CA6. It was proposed that these calcium aluminates are hard and easily broken during hot rolling, forming stringer-shaped inclusions in the plate. The researchers also investigated plates, stating that stringers were most often found on $\frac{1}{2}$ and $\frac{1}{4}$ thicknesses. Further, they assumed that stringers found on $\frac{1}{4}$ thickness originated from inclusions which had risen and become trapped on the curve during continuous casting. On the other hand, stringers found on a $\frac{1}{2}$ thickness were assumed to have been pushed towards the centreline by the solidification front.

Guo et al. (2013) proposed that during rolling, CaS is easily separated from an inner Al_2O_3 based core, leaving a tail or forming a stringer. However, if the core was a low-melting calcium aluminate, the inclusion would deform as a singular inclusion, which is the less harmful alternative of these two. According to their

research, the modification of Al_2O_3 inclusions plays an essential role in reducing the detrimental effects of complex oxide–sulphide inclusions.

In their extensive work, Zhao et al. (2015) investigated the deformation of both small and large inclusions with various oxide modification ratios. They reported that partly modified inclusions surrounded by a CaS layer in a crescent shape were not deformed. On the other hand, a CaS layer with an oval shape associated with oxides was likely to separate from the oxide core along the rolling direction. Inclusions containing C3A and C12A7 were found to continuously deform. If CaS and spinel were present in addition to C3A and C12A7, a stringer containing several elongated inclusions would form. If the oxides of the stringer were less modified with calcium, they were more likely to be found to break into multiple irregular pieces. Zhao et al. (2015) postulated that small well modified calcium aluminates with either crescent or oval CaS would deform uniformly. If calcium aluminates in small inclusions are slightly modified, an oval shaped CaS will form a tail. The presence of CaS with or without spinel will make inclusions to break into several pieces, and slightly modified calcium aluminates will result in more irregular shapes. However, the effect of MgO is not discussed in their work.

It has been proposed that during rolling, CA2 may be crushed into a stringer because of its low microhardness (Xu et al., 2016). However, if the CA2 phase is surrounded by a thick layer of CaS, it might prevent the crushing down of the inclusion. The researchers also deduced that in oxide-sulphide inclusions, the melting point, and hence the deformation resistance, of the CaS shell is always higher than of the oxide core. According to Xu et al. (2016), when the composition of the oxide core of CaS-bearing inclusions changes from alumina towards C3A, the deformation of the oxide core varies from no deformation, to a low amount of brittleness, to some brittleness, to slight deformation, and finally to plastic deformation. In addition, the researchers stated that the presence of a CaS layer on the oxide phases would prevent the plastic deformation of an oxide–sulphide inclusion.

On the other hand, low-melting calcium aluminates are not always considered beneficial. Zhang et al. (2017) point out that spinel-bearing stringers contain irregularly shaped inclusions, whereas calcium aluminate with low melting temperature associated with CaS deforms into thin and slender inclusions during hot rolling. In addition, it is suggested that excess calcium additions lead to excess CaS formation on oxides, and further on deformed tails.

Several researchers have paid attention to the formation behaviour of complex oxide inclusions. Yang et al. (2012) note that a spinel core of a multiphase inclusion

is solid at steelmaking temperatures, and inevitably hard and nondeformable in the rolling process. According to the researchers, the solid spinel core is detrimental to the steel properties, and will remain undeformed, even if the surrounding phases would form stringers during hot rolling. The researchers considered the formation of liquid $\text{Al}_2\text{O}_3\text{--CaO--MgO}$ inclusions due to the calcium modification of spinel inclusions to be virtually non-existent. Instead, they suggested that the focus should be on the removal of spinels, rather than trying to modify them.

Stringered inclusions have also been seen as positive to the steel properties. Sahai & Emi (2007) state that elongated stringers are formed during hot rolling and that they are broken into small pieces, when the product is cold rolled. As the stringer is fragmented, the length of singular inclusions decreases, and the average distance of the inclusions increases. This results in less harmful inclusions, compared to a single large inclusion.

In spite of the extensive research conducted, some factors have not been completely revealed. To date, no clear consensus on the deformation tendency of various calcium aluminate phases exists. For example, Zhang (2006) considers all calcium aluminates to be non-deformable inclusions. More recent investigations have confirmed that calcium aluminates exhibit deformation during hot rolling. In the qualitative research conducted by Zhao et al. (2015), the effect of the geometry of CaS and oxide phases as well as the occurrence of spinel on the deformation ability of inclusions was assessed. In their research, calcium aluminates were divided into low-modified and well modified, the former being more prone to break into several pieces during hot rolling. Nevertheless, the effect of the occurrence of MgO phases was neglected in their studies. Zhang et al. (2017) considered low-melting calcium aluminates as the source of elongated stringers, and thus to be detrimental. Further, the formation mechanism of oxide-sulphide stringers is not fully understood in the available literature.

In order to clarify the deformation ability of typical non-metallic inclusions in hot-rolled aluminium-killed and calcium treated steels, the following factors are investigated in the research section of this dissertation. The proposed inclusion classification method enables the investigation of the deformation tendency of oxide phases in the $\text{Al}_2\text{O}_3\text{--CaO--MgO}$ system, such as calcium aluminates with varying compositions. By utilizing the dataset, the effect of the occurrence of CaS and MgO phases on the deformation behaviour of inclusions is assessed as well. As a practical application of the inclusion classification and data treatment, complex oxide-sulphide inclusions most prone to form stringers in the hot rolled product are assessed.

3 Steel sampling and inclusion analyses

Immersion samples in various sizes are used to sample liquid steel during the steelmaking processes (Bartosiaki, Pereira, Bielefeldt, & Vilela, 2015). They are mainly used to analyse the bulk concentration of alloying and impurity elements in the liquid steel with OES. However, the immersion samples are also used to analyse the non-metallic inclusions in the steel. Most of the inclusion analysis methods are time-consuming, and the results are not obtained online, unlike the bulk composition of steel. Instead, inclusions are analysed afterwards, and correcting actions to modify inclusions in the steel melt cannot be done.

The sampling and analysis method is selected, depending on the inclusion characteristics of interest. Typical factors to determine for inclusions are size distribution, chemical composition, number per area or volume, shape, and the area portion of inclusions. In some cases, a quick assessment of steel cleanliness is adequate, as a measure of the total oxygen, sulphur, or nitrogen content (Tervo, Kaijalainen, Pikkarainen, Mehtonen, & Porter, 2017).

Even with a fast cooling of the steel sample, some oxides, sulphides and nitrides are formed during the solidification. Therefore, the inclusions in the solidified sample do not depict the inclusions present in the steel melt. If we are interested in which inclusions are present in the molten steel, thermodynamic calculation packages offer a valuable tool.

The inclusion characterisation methods have been divided in various ways, according to method speed, accuracy, and the obtainable data type. The methods can be classified into indirect and direct methods. For example, the total oxygen value reveals indirect information of the inclusion content in steel. With cross sectional analyses, two-dimensional data on inclusions can be obtained, whereas the electrolytic extraction technique provides three-dimensional information. OES-PDA is applicable for online analyses. However, many others are considered offline methods for their prolonged analysis times. Extensive reviews of inclusion characterisation methods have been offered by Atkinson & Shi (2003) and Zhang & Thomas (2003), among others.

3.1 Total oxygen

The total oxygen value is the most commonly used indirect method used to assess steel cleanliness. In practice, all oxygen in solidified steel samples is found in inclusions – the amount of dissolved oxygen in the solidified steel is considered

negligible. The O_{tot} value reveals the content of evenly dispersed oxide inclusions, smaller than 50 μm (Zhang 2006). Naturally, the total oxygen value only takes into account the inclusions, that are present in the analysed volume. In the case of a large exogeneous inclusion hitting the analysed volume, a high oxygen concentration would be analysed, and a skilful operator would re-analyse the sample (Zhang & Thomas, 2003). It should be noted that the total oxygen value does not offer any information on the inclusion size, morphology or chemical composition (Dekkers, Blanpain, & Wollants, 2003). As such, it can be used as a meter for the steel cleanliness itself, but its use for research purposes is very limited.

3.2 Cross section analyses

Cross section analyses are typically made using optical or scanning electron microscopy. However, the cleanliness ratings obtained with optical methods are unsuitable for research purposes (Abraham, Raines, & Bodnar, 2013), mainly because of the lack of chemical analysis. In this work, the focus is on cross sectional analyses using scanning electron microscopy (SEM).

Automated inclusion analysis scans the specified area for particles. Scanning electron microscopy provides simultaneous recording of properties of each inclusion encountered within the sample area. Among the chemical composition data, the properties recorded include the inclusion length, aspect ratio, and direction.

The speed of the analysis depends on the following factors: the total area of interest, magnification which depends on the image resolution and the minimum particle size to analyse, the number of inclusions enclosed in the area, the imaging time, the desired analysis time per inclusion, and the detector efficiency. In the ASTM E2142 (2008) standard, it is stated that 1500 counts per inclusion is a sufficient analysis for an accurate classification of an inclusion. With modern EDS analysers, this is clearly surpassed with an analysis time of one second. Typical total areas are in the range of 50 mm^2 , containing some thousands of detected particles, of which not all are actual inclusions. The total analysis time for this kind of sample is a few hours.

Depending on the SEM operating parameters, a cut-off value for minimum inclusion size is determined. A typical cut-off value is around 1 μm (Bartosiaki et al., 2015). Firstly, the higher the cut-off value, the faster it is to scan the sample area, when the number of particles to analyse is smaller. Secondly, the EDS analysis of small inclusions is often distorted because of the matrix effect. For instance, Verma et al. (2012) and Pistorius & Patadia (2012) showed that for small inclusions,

the surrounding steel matrix distorts the analysed Ca/Al ratios, resulting in erratic inclusion analyses. Thirdly, submicron-sized inclusions are often considered not harmful for the steel properties, and the benefit of analysing them is quite questionable.

For the minimisation of the matrix effect, some researchers have determined the composition by selecting the centre point of inclusions for analysis (Deng & Zhu, 2013). This should give the best analysis for small inclusions. However, the composition analysed over the whole area gives a more representative analysis for larger inclusions. Still, Pistorius & Patadia (2012) recommend the use of centre point analysis for heterogeneous inclusions.

3.2.1 Lollipop samples

Immersion samples are routinely used to analyse the bulk steel composition, but also for inclusion characterisation. When the steel sample solidifies in the sample mould, secondary inclusions are formed because the solubility of oxygen, sulphur, and nitrogen are markedly lower in solid steel, compared to liquid steel. As a result, inclusions are not homogeneous within a sample. Secondly, the inclusions observed in the solidified sample do not depict the inclusions in liquid steel. In his dissertation, Ericsson (2010) investigated the dispersion of inclusions in lollipop samples. Sulphides precipitated heterogeneously during cooling and solidification. Ericsson recommended the middle zone of the surface part of lollipop samples for the investigation of primary inclusions, and argon protected sampling in order to protect the sample from slag entrainment. Mainly depending on the sample thickness, the solidification takes place in around 5 seconds for a 12 mm thick sample, and around 1 second for a 6 mm thick sample.

In the work by Ericsson (2010), the top zone contained markedly more primary inclusions, compared to middle and bottom zones. Surface parts contained more secondary inclusions, compared to the centre parts. Ericsson (2010) classified the inclusions as primary or secondary, using a threshold value of 0.6 μm . However, this categorisation does not take into account the actual chemical composition of inclusions, which would be a highly valuable factor in the classification. A high solidification rate hinders the formation of secondary inclusions. Therefore, for the investigation of primary inclusions, Ericsson recommended a 6 mm thick sample. Similarly, Harris, Adaba, Lekakh, O'Malley, & Von Richards (2015) recommended the surface part of the sample for investigating primary inclusions, but noted that this section is the most prone to contaminations, such as slag entrainment.

According to Ruby-Meyer, Evrard, Vergauwens, & Balland (2011), porosities in the centre parts of the samples are caused by steel shrinkage during the last solidification or incomplete filling. Later, researchers (Ruby-Meyer, Evrard, Vergauwens, & Balland, 2013) showed that the centre part solidifies last during the sampling process.

In the samples investigated by Harris et al. (2015), the centre sections had a larger fraction of inclusions, mainly owing to MnS inclusions, which form during solidification. They state that the surface section is the most representative, although it is most prone to slag entrainment or other contaminations.

Liao, Yang, Li, & Feng (2017) investigated the effect of sampler size on non-metallic inclusions. The researchers observed mainly calcium aluminates with high cooling rates. With low cooling rates, predominant inclusions shifted towards $\text{Al}_2\text{O}_3+\text{CaS}$. With smaller samplers, sulphides have no time for precipitation. However, with larger samples, and consequently, lower cooling rates, sulphides do precipitate. In addition, Liao et al. (2017) stated that inclusions do not disperse in the horizontal direction. Instead, the direction of movement was upwards, concluding from the larger inclusion size in the upper parts of the samples. Similarly, Huet, Jönsson, & Reinholdsson (1997) stated that larger inclusions tend to end up in the upper parts of the lollipop sample, whereas smaller ones are found near the inlet.

3.2.2 Rolled product samples

If the slab has been hot-rolled into a thickness of a 10–20 mm range, a longitudinal sample will reveal the inclusion deformation (Abraham et al., 2013). Unlike slab samples, the product sample is suitable for examining inclusions over the whole thickness at once. This type of examination will reveal any effects of macrosegregation, resulting in centreline manganese sulphides or inclusion bands, showing oxide inclusions concentrating on certain thickness of the continuous cast slab.

3.3 Thermodynamic calculations

While the liquid steel samples inevitably also contain secondary inclusions, the inclusion characteristics in them do not depict the inclusions present in the liquid steel. In order to assess the stability of non-metallic inclusions at steelmaking

temperatures, thermodynamic calculations can be performed. Perhaps the most often used software in the field is FactSage (Bale et al., 2002).

A straightforward method for inclusion assessment is to calculate compound mass fractions as a function of temperature. These kinds of thermodynamic stabilities calculated by FactSage have been presented by Jung, Deckerov, & Pelton (2004), Kekkonen, Leuverink, & Holappa (2017), and Nurmi et al. (2009), among others. The downside with this method is that the steel composition is fixed, and the total oxygen content should be known for accurate calculations.

In addition to stabilities as mass fractions, stability zones are also often presented in the literature. This way, the variables can be concentrations of certain elements instead of temperature. For instance, the total contents of oxygen, sulphur, and calcium markedly affect the stable compounds in steel melts, and fixing their concentrations would lead to rather limited results. The liquid window is a good example of presenting stability zones. The liquid window is the stability zone where oxide inclusions are fully liquid. One can also present the boundaries where liquid inclusions start to form. Various authors (Bielefeldt & Vilela, 2015; Holappa, 2001; Holappa et al., 2003) have presented liquid regions as a function of aluminium and calcium contents. With FactSage, liquidus lines can also be projected in arbitrary ternary diagrams, such as the $\text{Al}_2\text{O}_3\text{--CaO--CaS}$ system (Ren et al., 2014).

Lately, researchers have presented rarely used feature in FactSage, namely macros. Van Ende & Jung (2017) simulated a ladle furnace process with an effective equilibrium reaction zone model coupled with the FactSage macro processing option. Steel and liquid slag composition and inclusion fractions were calculated as a function of time, with simulated alloying and arc heating inputs. The results obtained by Van Ende & Jung (2017) compare very well to experimental data. Similarly, Ren et al. (2017) simulated the calcium treatment in the ladle process. In addition, the researchers applied FactSage macro processing in order to predict inclusion chemistry changes in the tundish during reoxidation.

Owing to the high temperature of liquid steel processing, kinetic constraints do not act as insuperable barriers. Instead, the inclusion composition can be fairly well predicted in the liquid steel, if the total composition is known accurately enough. However, if the calculation is extended to lower temperatures where solid steel is present, thermodynamic–kinetic calculation packages such as Thermo-Calc–PRISMA (Andersson, Helander, Höglund, Shi, & Sundman, 2002) or IDS (Miettinen, Louhenkilpi, Kytönen, & Laine, 2010) are recommended.

3.4 Methods used in this study

In Tables 3 and 4, a summary of the sample types, characterisation, and calculation methods is presented. The sampling locations are illustrated in Figure 1. The inclusion characterisation was conducted in the SSAB Europe Raahe steelworks. Inclusions were analysed with a Jeol JSM-7000F FESEM equipped with an EDS detector. Inclusion analyses were acquired using the Oxford INCA Feature software utilising an acceleration voltage of 15 kV. In the INCA Feature runs, inclusions larger than 1.0 μm were analysed over the whole inclusion area with a live time of one second with EDS. Representative inclusions were selected for elemental mapping with EDS.

Table 3. Characterisation methods used in this study.

| Sampling location | Sample type | Elemental analyses | Inclusion Feature runs | | |
|-------------------------------|--------------------------------------------------|------------------------------------------|---------------------------------------------|---------------------|----------------------------------------|
| | | | Equipment | Typical sample area | Elemental maps for selected inclusions |
| Ladle samples | Lollipop | OES LECO (O) | Jeol JSM-7000F FESEM-EDS, Oxford INCA | 36 mm ² | X |
| Mould samples (dispersion) | Argon-protected and metal cap protected lollipop | " | " | 90 mm ² | – |
| Mould samples | Lollipop | OES LECO (O) Mass balance* (Mg) | " | 36 mm ² | X |
| Product samples | Longitudinal section | OES LECO (O) | " | 48 mm ² | X |

* No accurate Mg analyses available, calculation procedure presented in Chapter 7.2.4.

For thermodynamic calculations, the total magnesium contents of the mould samples were estimated with the procedure presented in Chapter 7.2.4. Thermodynamic calculations were performed using FactSage version 7.1. For other

data treatment, except for constructing ternary contours of aspect ratios, MATLAB R2013b was utilised. All MATLAB ternary diagrams were plotted with the ternplot function, courtesy of Carl Sandrock. For the oxide–sulphide stringer geometry visualisation, functions from the geom2d geometry package for MATLAB were used, courtesy of David Legland.

Table 4. Samples and performed calculations used in each research section.

| Research section | Samples | Calculations | Software |
|---------------------------------------------------------|--------------------|-------------------------------------------------------|----------------|
| Elemental maps of inclusions | Ladle | IPIM | MATLAB R2013b |
| | Mould | | |
| | Product | | |
| Dispersion of inclusions | Mould (Dispersion) | IPIM Statistical tests | MATLAB R2013b |
| Evolution of inclusions during sampling of liquid steel | Mould | IPIM | MATLAB R2013b |
| | | Thermodynamic stabilities with decreasing temperature | FactSage 7.1 |
| Evolution of inclusions during continuous casting | Ladle | IPIM | MATLAB R2013b |
| | Mould | Statistical tests | |
| | Product | | |
| Elongation of inclusions during hot rolling | Product | IPIM | MATLAB R2013b |
| | | Ternary contours | OriginPro 2015 |
| Oxide–sulphide stringers | Product | IPIM | MATLAB R2013b |
| | Mould* | | |

* No correlations found between the inclusion analyses of the mould samples and the stringer characteristics in the product samples, results not reported.

4 Classification of inclusions and data treatment

4.1 Composition-based classification

Numerous means exist for the classification of inclusions. The INCA Feature results show the inclusion composition in weight percent, as is normal with EDS analyses. Therefore, the most natural way to classify the inclusions is to set arbitrary limits for each element. For example, a calcium aluminate inclusion could be classified as over 5 wt.% Al and Ca, but less than 5 wt.% Mg, Mn, S, Si, and Ti.

With a set of complex rules, quite accurate classifications can be made. For instance, Faraji et al. (2015) present complex criteria with sums and ratios to classify inclusions into various silicates, and even phases, such as spessartite, anorthite, and gehlenite. In the criteria, inclusion elemental EDS analyses are converted to oxides before classification. With a method like this, classification rules can be made with help of ternary phase diagrams, which can be readily accessed in the literature. It should be noted that Faraji et al. (2015) state that the classification is made in a separate spreadsheet, rather than in the inclusion analysis software.

Thunman & Sichen (2008) classify inclusions as mixtures of calcium aluminate, calcium sulphide, and spinel phases. However, their classification is based on EDS maps. Ren et al. (2014) present 19 rules to classify inclusions. In their method, features with excess analysed iron were regarded as stains and defects and were consequently removed from the dataset. Similarly, Pretorius, Oltmann, & Cash, (2010) state that more than 30 rules are needed to classify inclusions. However, they do not disclose the numerical values of the criteria, instead, only the names of ten classes are revealed. With these kinds of classification systems, oxides, sulphides, and complex inclusions are well categorized, but the actual oxide composition is not revealed with the criterion setup. This leads to a severe problem: if the oxide composition is not known, the overall oxide composition remains hidden. Consequently, it is hard to assess the successfulness of calcium treatment, for instance. On the other hand, with a large number of strict rules, changes in oxide compositions can be assessed only from the number of inclusions in each class.

Another issue with complex criteria is the presence of unclassified and multiclassified inclusions. In the final report of the RFCS project PREDINC

(Sancho et al., 2011), 18 inclusion classes are presented. The authors say that the criteria have been reviewed many times in order to determine the best layout.

Abraham et al. (2013) present a three-level classification scheme. The first flowsheet separates indigenous and exogenous inclusions. In short, large oxides are taken as exogenous, whereas smaller oxides, along with sulphides and nitrides, are considered indigenous. A second flowsheet is used to identify various sulphides, oxides, and nitrides, resulting in three sulphide, two carbonitride, and four oxide classes. Lastly, a third flowsheet is used to recognize the origin of exogenous inclusions: reoxidation, refractories or slag.

Winkler, Angeli, & Mayr (2007) present a sophisticated method to identify inclusion phases. After the SEM-EDS analyses with 24 inclusion types, inclusions larger than 3 μm are analysed with EPMA, providing phase maps of inclusions. This way accurate phase identification can be carried out. The authors point out, however, that more resources are needed, compared to conventional SEM analyses. Therefore, the method is not used for routine purposes.

Especially with small inclusions, the iron signal coming from the surrounding steel matrix may be significant (Nuspl, Wegscheider, Angeli, Posch, & Mayr, 2004), and the EDS spectra of the inclusions should be re-calculated without iron after the iron-containing defects have been removed from the dataset. As the analyses are always scaled to 100 wt.%, naturally the presence of iron reduces the amount of other elements. As a consequence, similar inclusions can be classified differently, depending on the analysed iron content level. Even if iron was properly removed from the analyses, inclusions with analyses near, but above and below the threshold values will be classified differently. These issues can only be avoided by using a classification method that handles ratios, not absolute values.

The other issue is that some metallic elements can be bound both to oxygen and sulphur. In calcium treated steels, the most common such element is calcium, which can be found as calcium sulphide and as an oxide, such as calcium aluminate. In complex oxide-sulphide inclusions, the Ca/Al ratio does not reveal the actual calcium aluminate phases, if the calcium bound in calcium sulphides is not deducted from the total calcium.

As a solution, a modified Ca/Al ratio has been proposed (Story, Piccone, Fruehan, & Potter, 2003), presented in Equation 34. The modified ratio takes into account sulphur as calcium sulphide, and also sulphur solubility in liquid calcium aluminate. The authors use Ca/Al ratio to assess the casting performance for heats. According to Story et al. (2003), with high values, erosion may occur. On the other hand, low ratios correlate fairly well with nozzle clogging.

$$Ca/Al = \frac{Ca - (S-2)}{Al} \quad (34)$$

where Al, Ca, S are inclusion concentrations as an atomic percent.

Nozzle clogging, ladle gate erosion, inclusion liquefaction may also be assessed with an Al–Ca–S ternary, presented on the left in Figure 9. Based on the ratios between Al, Ca, and S, Story et al. (2003), and Story, Liu, Cathcart, & Molnar (2015) constructed approximate 100% and 50% liquid areas between the CA and C3A compositions, expanding towards the CaS point. According to the authors, ladle gate erosion can happen if the inclusion composition is on the left side of the liquid window; whereas clogging can occur with an inclusion composition on the right side. On the right side of Figure 9, the liquid window at 1550°C, denoted as Slag-liq, in Al₂O₃–CaO–CaS system is calculated using FactSage.

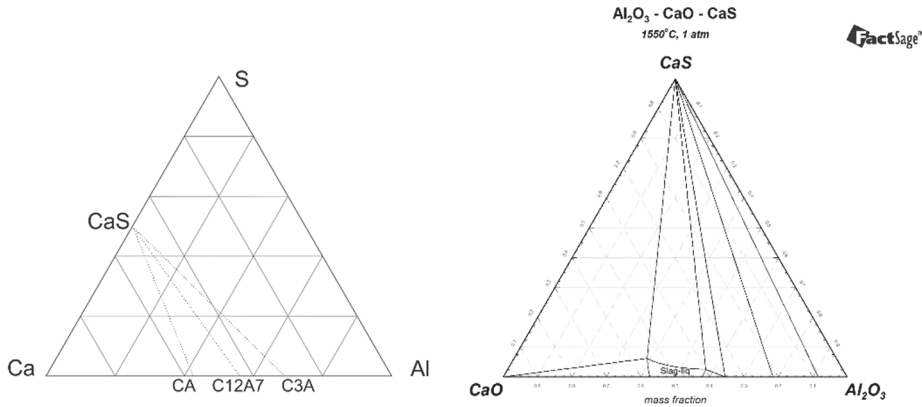


Fig. 9. Left: Al–Ca–S ternary diagram, modified from Story et al. (2003); right: Al₂O₃–CaO–CaS ternary diagram, with an all-liquid area at 1550°C.

However, even if corrected with S, the Ca/Al ratio alone does not fully reveal the oxide phases. This is mainly because the role of MgO is neglected altogether. In practice, aluminium oxides (Al₂O₃) cannot be differentiated from spinels (MgO·Al₂O₃) in such cases.

4.2 Standards

Many organisations have developed their standard testing routines for inclusion assessment. The standards provide a quick and consistent assessment of steel

cleanliness. The standards might not be very useful tools in research and development, but they serve as a reference for the customer.

Perhaps the most notable steel cleanliness standard, ASTM E45, is based on optical microscopy. In the standard, inclusions are first classified into four types based on their morphology, and secondly, they are classified into two subcategories based on their thickness or diameter. The categories are denoted as A (Sulfide), B (Alumina) C (Silicate) and D (Globular Oxide). The classification is based only on morphology, despite their naming. Abraham et al. (2013) claim that the standard is not suitable for engineering analysis or research purposes, even though it is useful for rapid assessment of steel cleanliness.

Quite similarly to ASTM E45, the Swedish standard SS11111 (Sjökvist, 2001) classifies the inclusions into four categories: A (ductile), B (brittle stringers), C (brittle–ductile), D (undeformable) inclusions. The categories are paired with a diameter parameter: thin (T), medium (M) or heavy (H). Inclusions are classified by comparing the size and shape with a chart. There are numerous other standards utilising light optical microscopy, such as ISO 4967, JIS G0555, DIN 50602, and EN 10247.

ASTM E2142 is essentially an extension of the E45 standard, utilizing a scanning electron microscope, rather than an optical one. The standard describes a test method to classify inclusions in the same manner as in E45, while making use of an EDS analyser and the chemical composition obtained for each inclusion.

The standards rely mostly on optical microscopy analyses. As Faraji et al. (2015) state, the lack of inclusion chemistry with optical methods limits the usability of the standards. In addition, complex oxide–sulphide inclusions may be hard to distinguish with optical techniques.

5 Proposed method

5.1 Component calculation

Inclusion analysis with a scanning electron microscope only provides elemental analysis of each inclusion in weight or atomic percent, depending on the user preferences. Even though the analysis might be quite accurate, it does not reveal the true composition of the inclusion, i.e., the phases it is comprised of. Various techniques must be applied in order to differentiate the amount of calcium in sulphides and oxides, simultaneously to identify the oxide phase (Ahlborg et al., 2003).

One can form simple classification rules based on the elemental analysis, using arbitrary cut-off values for each analysed element in inclusions. Even though this is simple and effective to roughly classify inclusions, it does not provide enough information to distinguish between the phases. In addition, the cut-off value is susceptible to measuring errors in oxygen, and less interesting minor components, such as zirconium.

With the following assumptions, the phase fractions of the inclusion can be estimated. The inclusions are taken as a mixture of typical compounds in commercial aluminium killed steels (Tervo et al. 2017), viz.:

- Calcium sulphide (CaS)
- Manganese sulphide (MnS)
- Titanium nitride (TiN)
- Oxide phases in the $\text{Al}_2\text{O}_3\text{-CaO-MgO}$ system.

The linear set of equations is presented in Equation 35. The set of equations answers the question: What are the molar amounts of the above-mentioned components in an inclusion containing known masses of Al, Ca, Mg, Mn, S, and Ti? Because negative molar amounts are not allowed, the condition $n_i \geq 0$ must be set.

$$\begin{bmatrix} 2M_{Al} & 0 & 0 & 0 & 0 & 0 \\ 0 & M_{Ca} & M_{Ca} & 0 & 0 & 0 \\ 0 & 0 & 0 & M_{Mg} & 0 & 0 \\ 0 & 0 & 0 & 0 & M_{Mn} & 0 \\ 0 & 0 & M_S & 0 & M_S & 0 \\ 0 & 0 & 0 & 0 & 0 & M_{Ti} \end{bmatrix} \begin{bmatrix} n_{Al_2O_3} \\ n_{CaO} \\ n_{CaS} \\ n_{MgO} \\ n_{MnS} \\ n_{TiN} \end{bmatrix} = \begin{bmatrix} m_{Al} \\ m_{Ca} \\ m_{Mg} \\ m_{Mn} \\ m_S \\ m_{Ti} \end{bmatrix} \quad (35)$$

where

M_i is the molar mass of element or component i ,

n_i is the amount of compound i in inclusion,

m_i is the mass of element i in inclusion,

$n_i \geq 0$.

The result for the set of equations is a 6-by-1 vector, containing molar amounts of Al_2O_3 , CaO , CaS , MgO , MnS , and TiN for an arbitrary-sized inclusion. The m_i values can be conveniently replaced by weight percentage analyses obtained by the EDS analyser. The solution is unambiguous, if sulphur-binding elements calcium and manganese are sufficiently available, but on the other hand, the manganese content does not exceed the need for binding all of the sulphur. Then, the molar amounts are scaled to 100%. The Al_2O_3 , CaO , and MgO amounts are summed, totalling the oxide amount, denoted here as OX. This method gives results solely based on the ratios between Al, Ca, Mg, Mn, S and Ti. The absolute values of any elements do not affect the result.

The phase identification method offers valuable information on phases of the inclusions. This data is often buried in simple inclusion classifications. The method offers the best approximation of the phases in each inclusion with minimal analysis time, if no time-consuming elemental maps are available.

With the presented method, an approximation of the phases of each inclusion can be constructed. Accurate phase contents are available only from elemental maps constructed manually for individual inclusions from a scanning electron microscope equipped with an EDS analyser. The method offers an inclusion classification tool which does not rely on arbitrary cut-off values. Instead, fundamental classification relies on the phases inclusions are comprised of.

The oxide composition is calculated independently of CaS , MnS , and TiN , and can be plotted onto conventional Al_2O_3 - CaO - MgO ternaries. Without the calculation of the CaS content of an inclusion, the ratios between CaO and Al_2O_3 or MgO will be distorted, depending on the total content of CaS . Thus, the benefit of plotting the oxide composition in a ternary diagram would be quite questionable.

The Al_2O_3 – CaO – MgO system consists of multiple phases, e.g. calcium aluminates CA6, CA2, CA, C12A7, C3A, and spinel $\text{MgO}\cdot\text{Al}_2\text{O}_3$. To date, no consensus exists on which calcium aluminates are the most favourable regarding the mechanical properties of steel. The majority of observed inclusions in hot-rolled products contain at least two of these components. In other words, pure oxides or sulphides are rarely observed in industrial samples. With the method, favourable phases from the elongation point of view can be determined. The effect of various oxide phases and the CaS content of inclusions can be assessed.

In principle, the presented method is quite similar to the procedure presented by Lind & Holappa (2010). With the presented method, an exaggeration of the MnS content can be prevented in the case where manganese is analysed, but no sulphur is detected. Oxygen is not taken as an input, because its analyses obtained with EDS were often higher than calculated. Taking oxygen as an input would shift the MgO content excessively upwards. Light elements such as nitrogen are not accurately measured with EDS (Goldstein et al., 2007). Similarly to oxygen, nitrogen is not used in the calculation.

The method can be modified with ease for other components, according to the steel grade and the inclusions in question. For instance, adding other oxides such as SiO_2 or replacing some components in the calculation is a simple task.

5.2 Phase identification

Further, fractions of oxide components (Al_2O_3 , CaO , MgO) can be used to calculate the equilibrium solidification phase fractions. In this work, the compatibility triangles are numbered 1–7 from the Al_2O_3 corner towards CaO , that is with increasing CaO content. The equilibrium triangles are listed below in Table 5, and illustrated in Figure 10.

Table 5. Compatibility triangles

| Compatibility triangle | Equilibrium phases | Notation |
|------------------------|----------------------------------|----------------------------------------|
| 1 | Aluminium oxide CA6 Spinel | Al ₂ O ₃ -CA6-MA |
| 2 | CA6 CA2 Spinel | CA6-CA2-MA |
| 3 | CA2 CA Spinel | CA2-CA-MA |
| 4 | CA Spinel MgO | CA-MA-MgO |
| 5 | C12A7 CA MgO | C12A7-CA-MgO |
| 6 | C3A C12A7 MgO | C3A-C12A7-MgO |
| 7 | CaO C3A MgO | CaO-C3A-MgO |

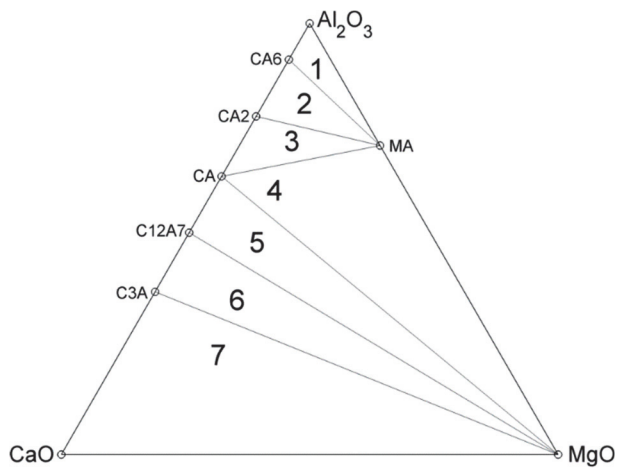


Fig. 10. Compatibility triangles in the Al₂O₃-CaO-MgO ternary diagram.

For each inclusion, the oxide composition lies inside one of these triangles. If the equilibrium solidification is assumed, the amount of the phases can be estimated with the lever rule. For instance, if the total oxide composition lies inside the 7th triangle, the oxides must be comprised of CaO, C3A, and MgO phases alone, with mass fractions directly proportional to the location inside the triangle. In that case, the mass fractions can be calculated as follows:

$$\begin{bmatrix} 0 & \frac{2M_{Al}}{M_{C3A}} & 0 \\ \frac{M_{Ca}}{M_{CaO}} & \frac{3M_{Ca}}{M_{C3A}} & 0 \\ 0 & 0 & \frac{M_{Mg}}{M_{MgO}} \end{bmatrix} \begin{bmatrix} m_{CaO} \\ m_{C3A} \\ m_{MgO} \end{bmatrix} = \begin{bmatrix} m_{Al,OX} \\ m_{Ca,OX} \\ m_{Mg,OX} \end{bmatrix} \quad (36)$$

where

M_i is the molar mass of element or component i ,

m_i is the mass of compound i in oxides,

$m_{i,OX}$ is the mass of element i in oxides.

The masses for Al, Ca, and Mg in the oxide phase are calculated for the inclusion with the molar amounts obtained in the component calculation procedure:

$$m_{Al,OX} = 2M_{Al}n_{Al_2O_3} \quad (37)$$

$$m_{Ca,OX} = M_{Ca}n_{CaO} \quad (38)$$

$$m_{Mg,OX} = M_{Mg}n_{MgO} \quad (39)$$

The result shows the total masses for the three oxide phases in an arbitrary-sized inclusion. By scaling to unity, mass fractions are obtained. It is straightforward to determine, without visual observation, in which compatibility triangle the total oxide composition of an inclusion is located. For a given inclusion, the mass fractions are calculated in each compatibility triangle. The total oxide composition lies in the only compatibility triangle, of which the calculation results in all non-negative component fractions.

The classification includes some fundamental assumptions. Oxides are comprised of Al_2O_3 , CaO, and MgO components only. The solidification of oxide phases has taken place by equilibrium. In this case, the phase fractions are estimated using the lever rule. The assumption of equilibrium solidification might not always be true; for example, with this assumption, spinel cannot occur with calcium aluminates other than CA6, CA2, and CA. However, this method provides the best estimation if no elemental maps are available. With the presented method, thermodynamically stable oxides within compatibility triangles are obtained.

Oxides are assumed to be crystalline, i.e., the solidification has not been rapid enough for amorphous inclusion solidification. This assumption is supported by the frequent observation of two distinctive calcium aluminate phases in EDS elemental maps, and precipitated MgO phases in the inclusions in the lollipop samples. Clearly, these compounds would not form if the solidification was rapid and the liquid inclusion fraction was amorphous in the solidified sample.

5.3 Inclusion classification

In this work, the inclusion classification comprises the combinations of OX, CaS, MnS, and TiN, making up a total of 15 classes, of which OX CaS is divided into two classes, depending which component totals higher. The classification criteria are shown in Table 6. The component calculation and the phase identification methods presented in the previous chapters are unambiguous. However, the classification presented here must contain more or less arbitrary cut-off values. In this case, the cut-off value was determined to be 5 mol.% for each component. In addition, inclusions that contain less than 30 wt.% Al, Ca, Mg, Mn, S, and Ti are marked as unclassified. It is evident that these kinds of inclusions cannot be reasonably described with the components studied here. The unclassified inclusions are expected false hits, not recognised during the initial removal of defects from the dataset. Alternatively, some of them may be actual inclusions, but with a non-typical composition, and thus, are not the focus of interest here.

Table 6. Inclusion classification criteria, components over 5 mol.%.

| Class | OX | CaS | MnS | TiN |
|----------------|--------------------------------------|-----|-----|-----|
| OX | X | | | |
| OX > CaS | X | X | | |
| OX < CaS | X | X | | |
| OX MnS | X | | X | |
| OX TiN | X | | | X |
| OX CaS MnS | X | X | X | |
| OX CaS TiN | X | X | | X |
| OX MnS TiN | X | | X | X |
| OX CaS MnS TiN | X | X | X | X |
| CaS | | X | | |
| CaS MnS | | X | X | |
| CaS TiN | | X | | X |
| CaS MnS TiN | | X | X | X |
| MnS | | | X | |
| MnS TiN | | | X | X |
| TiN | | | | X |
| Unclassified | Al + Ca + Mg + Mn + S + Ti < 30 wt.% | | | |

The combinations of OX, CaS, MnS, and TiN make up a total of 15 inclusion classes. This is markedly less than the comprehensive criteria presented in the literature. The class combinations, paired with ternary diagrams, provide a detailed, yet compact view of the inclusion characteristics in a sample.

As CaS can either precipitate on the surface of an existing oxide inclusion or collide during the solidification of steel, CaS contents vary greatly within this class. Therefore, OX CaS is divided into two classes, depending on which fraction is larger. Expectedly, the OX > CaS inclusion class contains the crescent shaped CaS phases, formed by precipitation, whereas the OX < CaS inclusions are more likely to be formed by a collision of oxide and sulphide inclusions, as reported by Zhao et al. (2015). Consequently, it is safe to assume the deformation mechanism of these to inclusion classes varies greatly.

6 Classification validation

6.1 Sample sets

In this dissertation, low-alloyed, aluminium killed, calcium treated steels are investigated. The composition ranges of aluminium, oxygen, sulphur, calcium, and magnesium of the studied heats are listed in Table 7. The samples were taken from the ladle after calcium treatment and from the mould during casting as lollipop samples, see Figure 1. The sample sets investigated are presented in Table 8. Two samples were prepared from the hot rolled product of each heat. The product samples are denoted as A and B, indicating the sampling locations of 10% and 35% of the width of the product.

Table 7. Steel composition in the mould samples of the studied heats.

| Element | Method | Composition range (ppm) |
|---------|------------------------------|-------------------------|
| Al | OES | 260–490 |
| O | LECO | 8–17 |
| S | OES | 0–21 |
| Ca | OES | 7–31 |
| Mg | Calculated from mass balance | 2–9 |

Table 8. Samples investigated.

| Heat | Elemental analyses | | | Inclusion Feature runs | | |
|-------|--------------------|-------|---------------------|------------------------|-------|---------------------|
| | Ladle | Mould | Hot rolled products | Ladle | Mould | Hot rolled products |
| 61154 | X | X | X | X | X | X |
| 62077 | X | X | X | | X | X |
| 62078 | X | X | X | X | X | X |
| 62468 | X | X | X | | | X |
| 62839 | | X | | X | X | X |
| 68844 | X | X | X | X | X | X |
| 68847 | X | X | X | X | X | X |
| 68852 | X | X | | X | X | X |
| 68968 | X | X | | X | X | X |
| 69274 | X | X | X | X | X | X |
| 69276 | X | X | X | X | X | X |
| 69671 | X | X | X | X | X | X |
| 69672 | X | X | X | X | X | X |
| 69673 | X | X | | | | X |
| 70255 | X | X | X | X | X | X |
| 70257 | X | X | X | X | X | X |
| 70259 | | X | X | | X | X |
| 70967 | X | X | X | X | X | X |
| 70968 | X | X | X | X | X | X |
| 75552 | | X | X | | X | X |
| 75954 | X | X | X | X | X | X |
| 76210 | X | X | X | X | X | X |
| 76211 | X | X | X | X | X | X |
| 76323 | X | X | X | X | X | X |
| 76325 | X | X | X | X | X | X |

Heats numbered 76325, 68852, and 62078 are designated as slightly modified, medium modified and overmodified with calcium, according to the overall oxide phase composition of the inclusion analyses. Three heats were chosen according to their calcium treatment success: characterised by a large amount of Al₂O₃, liquid inclusions, and CaO–CaS inclusions in slightly modified, medium modified, and overmodified heats, respectively. Heat 62078 was treated with a fixed amount of added CaSi, albeit its low sulphur content. On the other hand, heats 76325 and 68852 were produced with an experimental practice, receiving a lower CaSi addition owing to the relatively low sulphur content of the heats. In Table 9, the

total oxygen, sulphur and calcium contents of the selected heats are presented, as analysed by OES and LECO. In addition, the calcium to oxygen ratio is presented. It is clearly seen that the Ca/O_{tot} ratio increases simultaneously with the higher modification degree of oxides.

Table 9. Elemental analyses of the selected heats.

| Heat | Sample | Analyses (ppm) | | | |
|---------------------|-----------|----------------|-----|-----|---------------------|
| | | O | S | Ca | Ca/O _{tot} |
| 76325 | Ladle | 12 | 2 | 5 | 0.42 |
| "Slightly modified" | Mould | 14 | 3 | 11 | 0.79 |
| | Product A | 17 | 9 | 9 | 0.53 |
| | Product B | 13 | 7 | 11 | 0.85 |
| 68852 | Ladle | 13 | 3 | 15 | 1.15 |
| "Medium modified" | Mould | 12 | 6 | 14 | 1.17 |
| | Product A | N/A | N/A | N/A | N/A |
| | Product B | N/A | N/A | N/A | N/A |
| 62078 | Ladle | 17 | 0 | 26 | 1.53 |
| "Overmodified" | Mould | 8 | 4 | 17 | 2.13 |
| | Product A | 8 | 6 | 18 | 2.25 |
| | Product B | 7 | 8 | 21 | 3.00 |

6.2 Methods

The inclusion characterisation was conducted at the SSAB Europe Raahe steelworks. Inclusions were analysed with a Jeol JSM-7000F FESEM equipped with an EDS detector. Inclusion analyses were acquired using the Oxford INCA Feature software with an acceleration voltage of 15 kV. In the INCA Feature runs, inclusions larger than 1.0 µm were analysed over the whole inclusion area with a livetime of one second with EDS. The analysed sample areas were approximately 6 mm x 6 mm for lollipop samples, totalling 36 mm². For the hot rolled products, the total sample area comprised of a product thickness, of approximately 12 mm, with a width of 4 mm, resulting in an approximately 48 mm² scanned area. After the INCA Feature runs, elemental maps were constructed with EDS in order to reveal the prevailing phases and their geometry for selected inclusions.

6.3 Oxygen and nitrogen contents of inclusions

With the proposed method, the phase identification results only depend on the ratios between Al, Ca, Mg, Mn, S, and Ti. That is, their absolute values themselves do not affect the results. Further, this also means that the oxygen and nitrogen contents are not taken as inputs in the phase identification. Instead, the O and N contents can be used to estimate the goodness of the phase identification. If the identification was done correctly, the calculated O and N contents should be quite close to the measured ones, given that they were measured accurately enough during the INCA Feature runs. Here, the calculated and measured oxygen and nitrogen contents are presented for selected samples.

The oxygen contents for two samples of a heat are shown in Figure 11. It can be seen that the correlation is evident. Higher measured values with low oxygen concentrations are possibly caused by the presence of oxides, which are not the interest of this study, such as MnO or SiO₂. A trend of higher analysed oxygen contents, compared to the analysed ones, is clearly seen. This can be considered to be caused by the lower accuracy of the oxygen analyses.

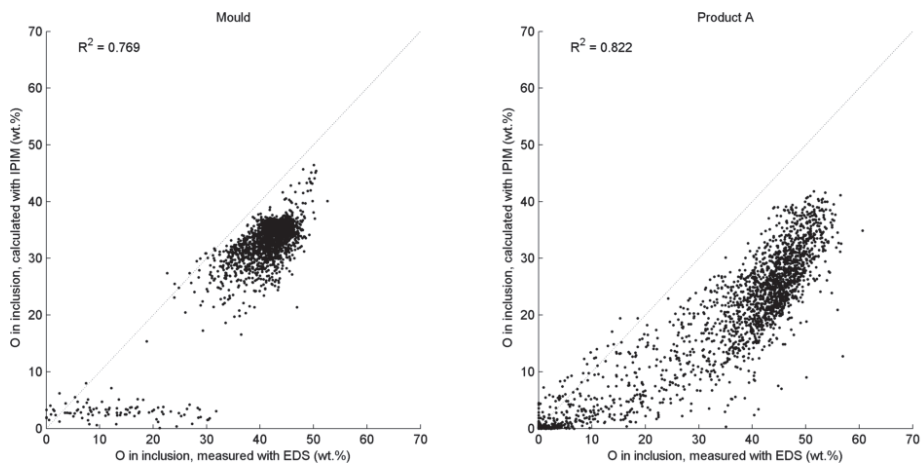


Fig. 11. Oxygen contents of inclusions on heat 76325 samples: Mould, Product A.

Similarly, the nitrogen contents of the selected samples are illustrated in Fig 12. The stoichiometric nitrogen content of TiN is approximately 22.6 wt.%, showing as a calculated upper limit on the product sample. In the liquid steel samples taken from the mould, titanium nitrides are present only in minor amounts, and the titanium concentration does not correlate well with the nitrogen analysis. There is

a great amount of variance in the nitrogen analyses even with the product samples, clearly depicting the uncertainty of the nitrogen analyses, seen in the great variance in high-titanium inclusions, i.e., measured nitrogen contents of 10–30 wt.% on calculated nitrogen limit of 22.6 wt.%. On the other hand, high calculated nitrogen contents paired with measured values close to zero might suggest the presence of titanium oxides, e.g. in a spinel solid solution. Thirdly, high nitrogen analyses accompanied by low calculated values might be associated with the presence of aluminium nitrides or boron nitrides.

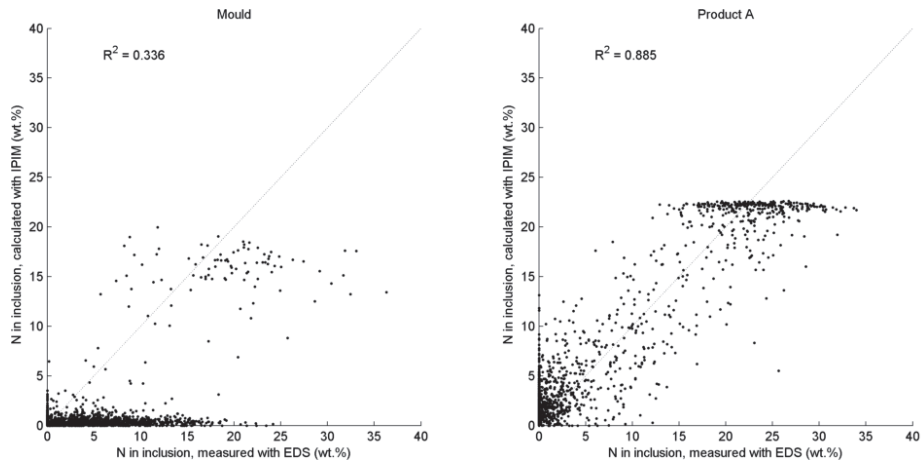


Fig. 12. Nitrogen contents of inclusions on heat 76325 samples: Mould, Product A.

6.4 Elemental maps of inclusions

Analyses obtained in the INCA Feature run were compared to elemental maps acquired after the run. Typical inclusions in the investigated steel grades are presented for the ladle furnace and mould samples as well as for the hot rolled product samples. While oxide inclusions were often observed in the ladle furnace samples, the mould samples contained inclusions containing both oxide and sulphide phases. On top of these, the inclusions observed in the hot rolled products frequently contained MnS and TiN phases. The inclusions selected for further investigation are listed in Table 10, where it can be seen that the phases calculated and detected agree very well.

Table 10. Investigated inclusions with elemental maps.

| Figure | Sample | Class | Phases calculated | Phases detected | Length |
|--------|--------------------|----------------|------------------------------------------------------------------|---------------------------------------|--------|
| 13 | 68844 LF | OX | C3A C12A7 MgO | Calcium aluminates MgO (CaS TiN) | 12 µm |
| 14 | 68847 LF | OX | C3A C12A7 MgO | Calcium aluminates MgO (CaS) | 7.0 µm |
| 15 | 68847 LF | OX | MgO CA C12A7 | Calcium aluminates MgO (TiN) | 8.7 µm |
| 16 | 69274 LF | OX TiN | CA MA MgO + TiN | Spinel Calcium aluminate (TiN) | 10 µm |
| 17 | 69274 LF | OX | C12A7 MgO (CA) | Calcium aluminate MgO (CaS TiN) | 28 µm |
| 18 | 70257 LF | OX | CA MgO MA | Calcium aluminate MgO (CaS) | 9.5 µm |
| 19 | 68844 Mould | OX > CaS | C3A C12A7 MgO + CaS | Calcium aluminate CaS (MgO TiN) | 6.1 µm |
| 20 | 68847 Mould | OX < CaS | CaS + C12A7 C3A MgO | Calcium aluminates CaS (MgO) | 8.5 µm |
| 21 | 68847 Mould | OX > CaS | C3A C12A7 MgO + CaS | Calcium aluminates CaS | 6.9 µm |
| 22 | 68844 Product A | OX | C12A7 MgO C3A | Calcium aluminates (CaS MgO TiN) | 14 µm |
| 23 | 69672 Product B | OX CaS MnS | MA Al ₂ O ₃ CA ₆ + CaS + MnS | Spinel CaS+MnS (TiN) | 8.1 µm |
| 24 | 69672 Product B | OX CaS MnS | MA CA (MgO) + MnS + CaS | Spinel CaS+MnS (TiN) | 12 µm |
| 25 | 70257 Product A | OX CaS MnS TiN | MA Al ₂ O ₃ + CaS + MnS + TiN | Spinel CaS+MnS TiN | 8.5 µm |
| 26 | 70257 Product A | OX < CaS | Al ₂ O ₃ MA + CaS | Al ₂ O ₃ CaS | 12 µm |
| 27 | 70257 Product B | OX > CaS | MA CA (MgO) + CaS | Spinel Calcium aluminates CaS | 17 µm |

6.4.1 Ladle furnace samples

In the inclusion presented in Figure 13, two calcium aluminate phases can be distinguished. The MgO and TiN phases precipitated on the surface, evidently during solidification. In addition, minor amounts of CaS can be seen inside the inclusion. The calculated composition shows the composition of the inclusion to contain more than 95 mol.% oxides, the calcium aluminates being a mixture of C3A and C12A7, which corresponds to a liquid inclusion at steelmaking temperatures. Clearly, the round shape of the inclusion confirms that it had been in a liquid state during sampling from the liquid steel.

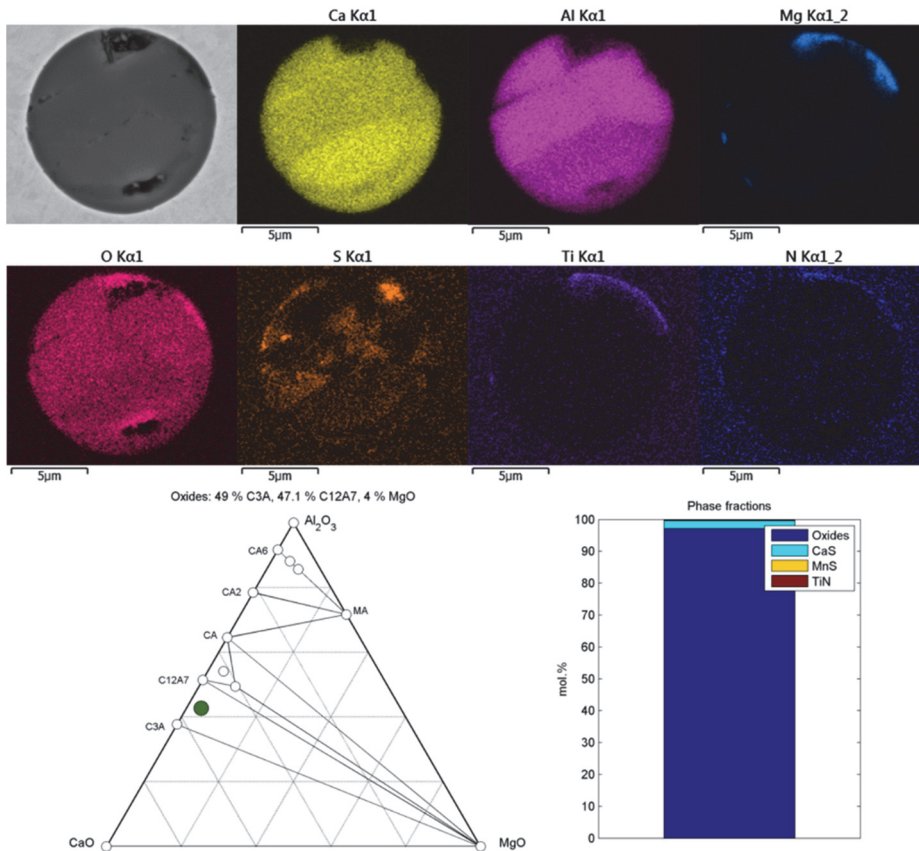


Fig. 13. Elemental maps and the calculated composition of an OX inclusion.

Again, two calcium aluminates in a composition between C3A and C12A7 can be observed in the inclusion presented in Figure 14. Similarly, magnesium oxide totalling 3.2 wt.% of the oxides, precipitated on the surface of the inclusion can also be seen. The inclusion contains more calcium sulphide phase compared to the previous one, but it is still under 5 mol.%. Some manganese was present in the feature analyses, thus a minor amount of manganese sulphide is calculated. The round shape of the inclusion evidently shows a liquid inclusion during sampling.

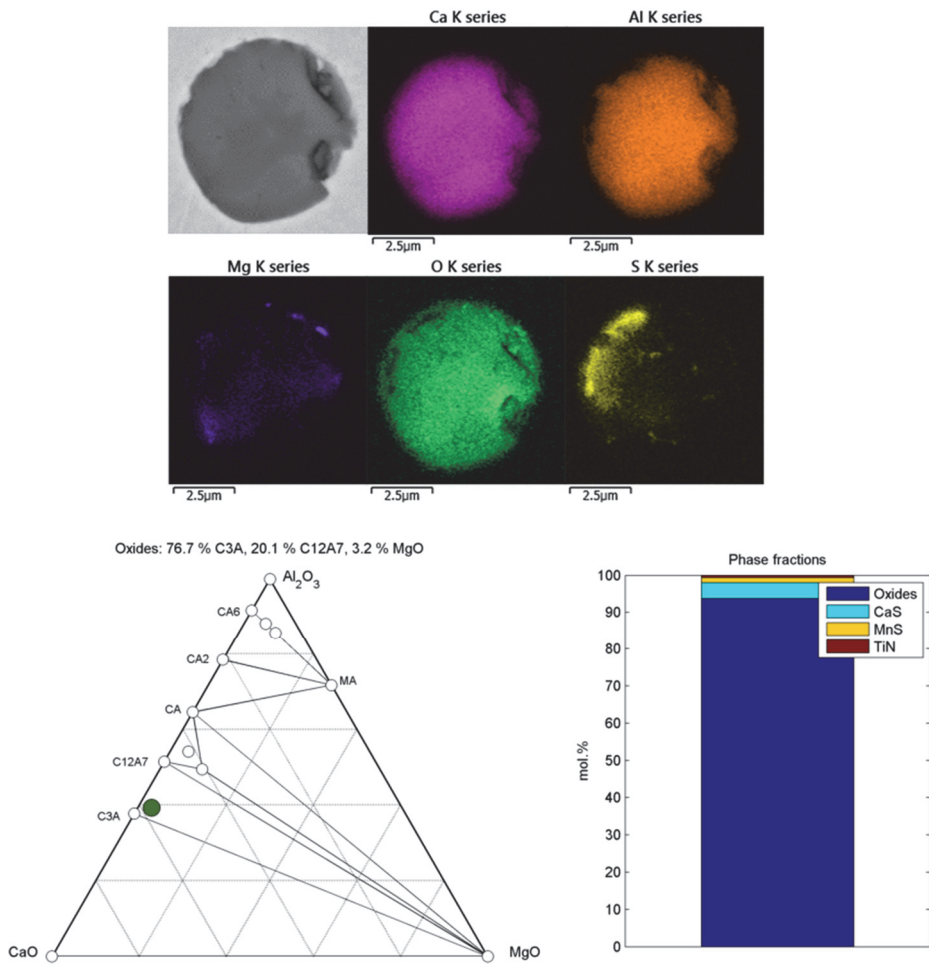


Fig. 14. Elemental maps and the calculated composition of an OX inclusion.

Here a distinctive crescent shape of calcium aluminate on a magnesium oxide inclusion is observed in Figure 15. Actually, the calculation suggests calcium aluminates are found as two compositions: C12A7 and CA. Differences in the shades of the crescent can be seen with careful observation. Titanium nitride has precipitated on the opposite side of the MgO, even though the amount is negligible, based on almost a fully oxide inclusion according to the calculation.

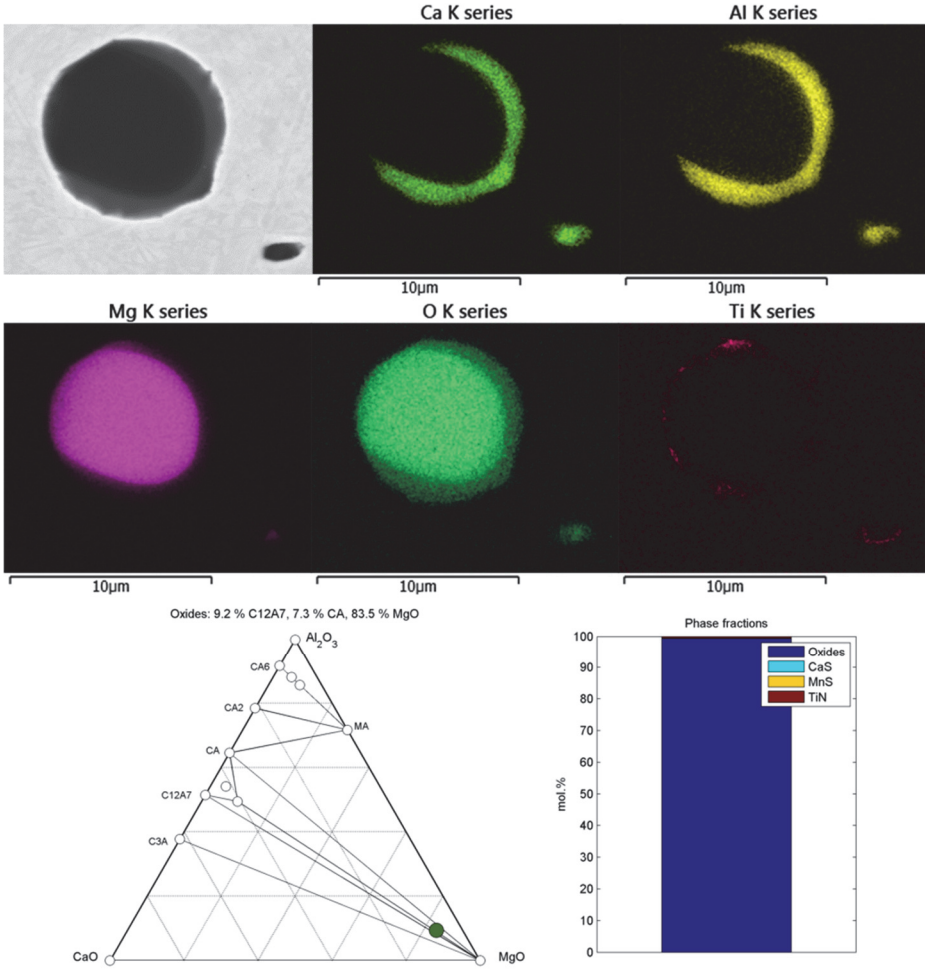


Fig. 15. Elemental maps and the calculated composition of an OX inclusion.

In the ladle sample of heat 69274, a complex inclusion of spinel and calcium aluminate can be observed in Figure 16. Almost 10 mol.% of the inclusion is estimated to be titanium nitride, based on the high titanium concentration. However, nitrogen was only mapped on the surface of the inclusion. A plausible explanation is that titanium is associated with the solid spinel solution. It is apparent that the inclusion was sampled during the modification of spinel by calcium towards the liquid calcium aluminate region. Still, spinel is found inside the inclusion in smaller particles. It is readily observed that the inclusion was comprised of liquid calcium aluminate, enclosing spinel particles before solidification. Evidently, the modification mechanism of the inclusion does not follow the unreacted core model, frequently assessed in the literature.

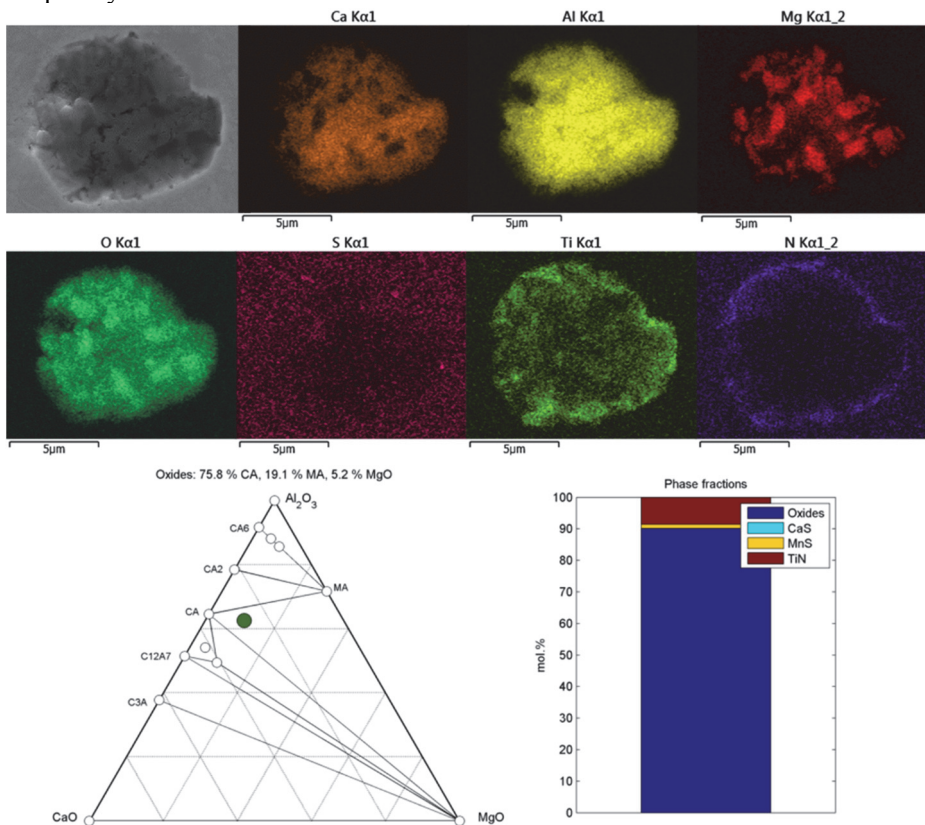


Fig. 16. Elemental maps and the calculated composition of an OX TiN inclusion.

Elemental maps for a relatively large inclusion with a diameter of 28 μm are provided in Figure 17. The brightness levels of calcium and aluminium suggest only one calcium aluminate is found within the inclusion. The calculated oxide composition lies on the C12A7–MgO line, which is in accord with the elemental maps. In this case, MgO is observed both inside and near the surface of the inclusion, yet in a round particle form. It is plausible that the MgO particles were present in the inclusion in the steel melt. Similarly, traces of sulphur are observed inside the inclusion, indicating that sulphur was present in the liquid slag solution in the steel melt. During the solidification, titanium nitrides precipitated around the inclusion on the surface.

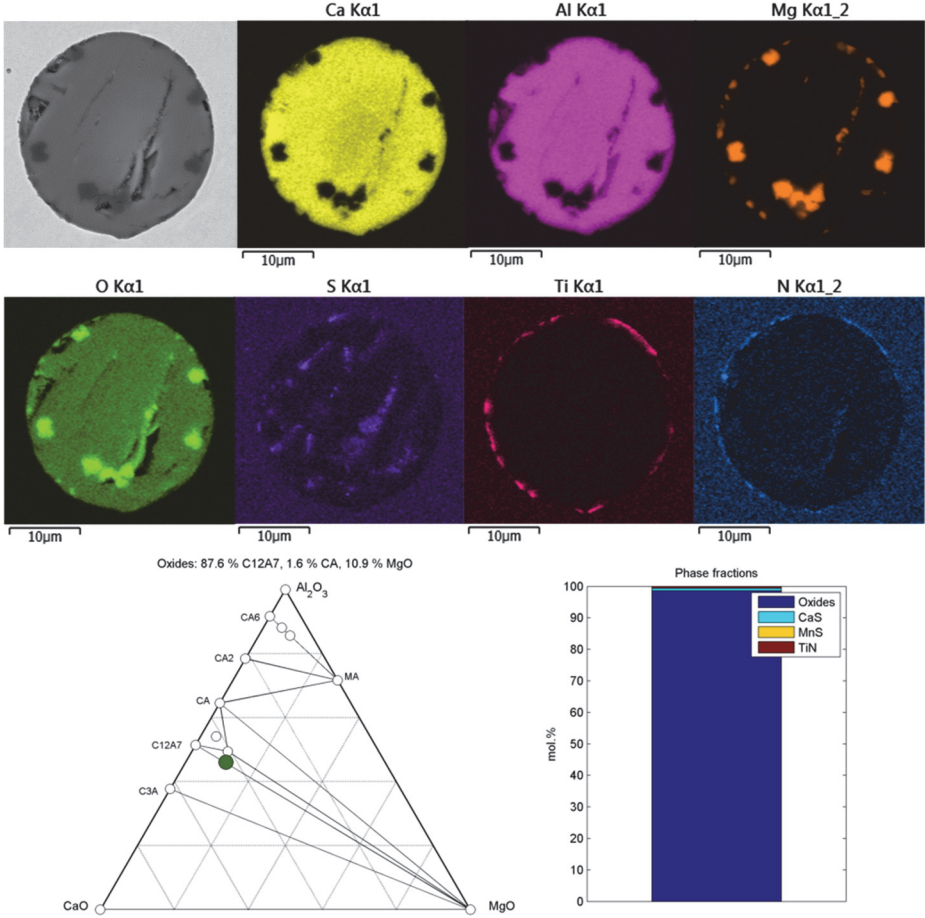


Fig. 17. Elemental maps and the calculated composition of an OX inclusion.

In Figure 18, a fully oxide inclusion can be seen, comprising a spinel core surrounded by calcium aluminate, indicating modification of the spinel by calcium. MgO phases are found on the outer rim of the inclusion, suggesting they were at least partially precipitated during solidification. The calculated oxide composition is in accord with the elemental maps.

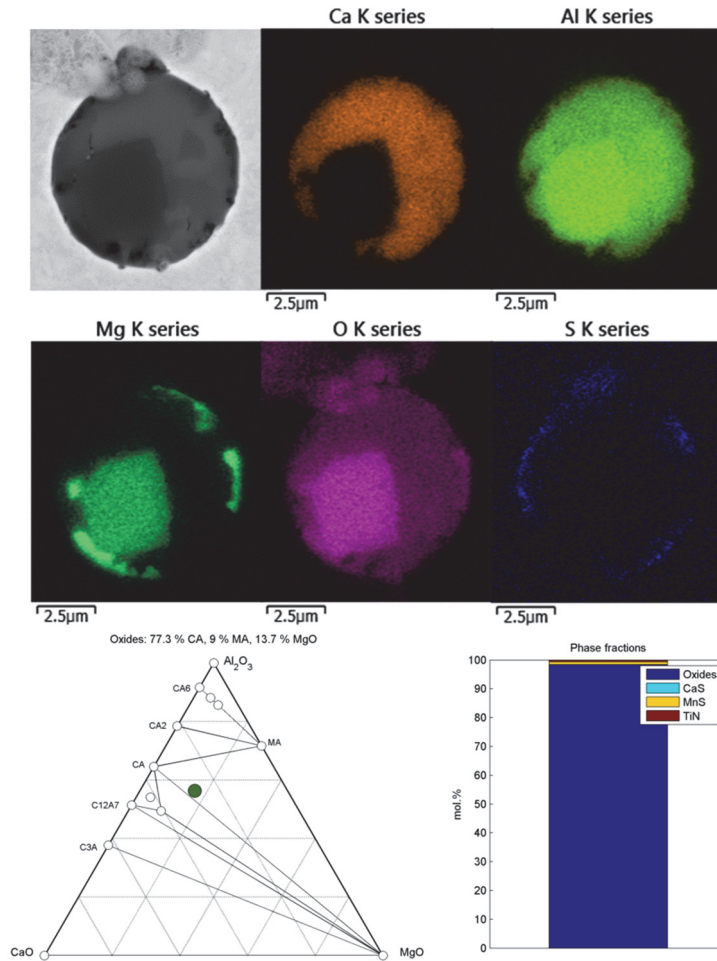


Fig. 18. Elemental maps and the calculated composition of an OX inclusion.

6.4.2 Mould samples

The inclusion presented in Figure 19 contains approximately 80 mol.% oxides, of which a majority are calcium aluminates with a composition of C3A. Some MgO and TiN has precipitated on the outer rim of the inclusion. The remaining 20 mol.% are calcium sulphides. The elemental maps and the calculations are very well comparable. The amount of sulphur in the oxide part is negligible.

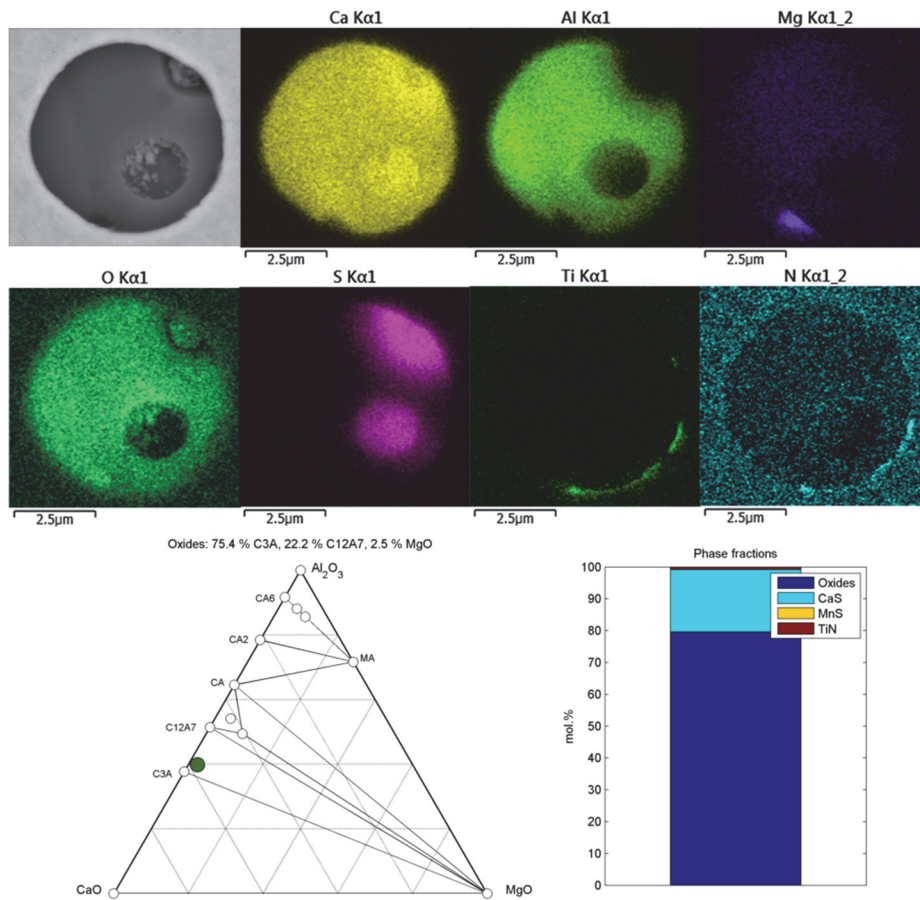


Fig. 19. Elemental maps and the calculated composition of an OX > CaS inclusion.

In the elemental maps of Figure 20, a calcium sulphide phase surrounded with two calcium aluminate phases can be clearly observed. MgO has precipitated on the surface of the inclusion during solidification. The inclusion consists of 40 mol.% oxides and 60 mol.% calcium sulphide. The estimated composition correlates well with the elemental maps. This is a good example of partial liquefaction: the inclusion is round, although the oxide fraction is less than 50 % of the inclusion composition. Understandably, inclusions like these are not likely to cause clogging during continuous casting.

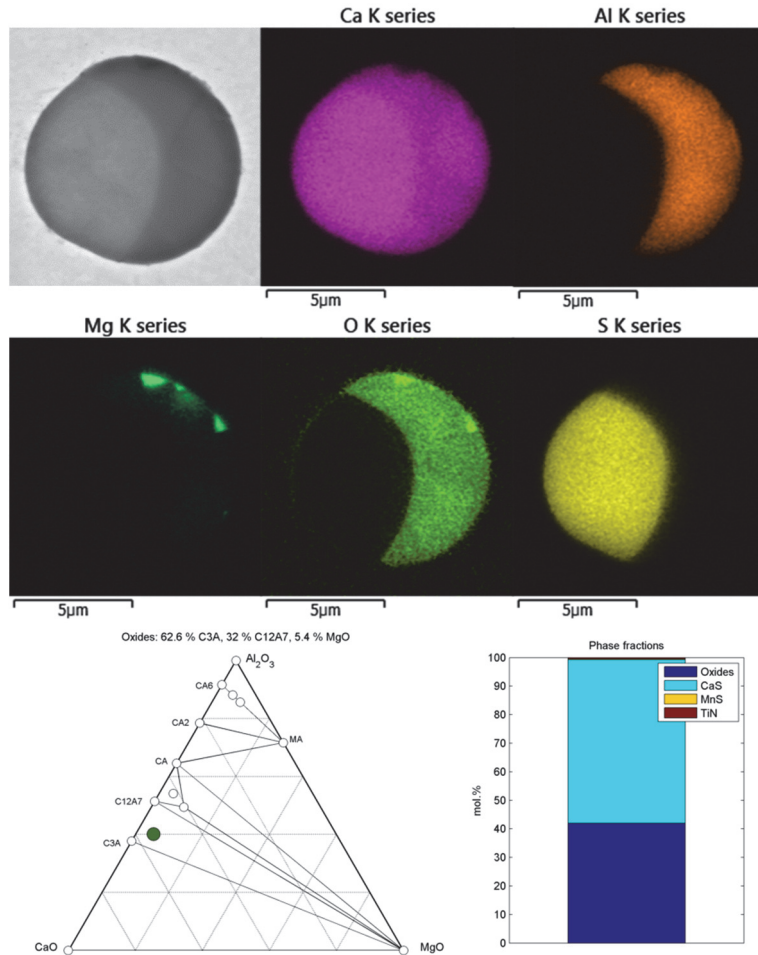


Fig. 20. Elemental maps and the calculated composition of an OX < CaS inclusion.

In the elemental maps of Figure 21, a calcium aluminate with a calculated composition very close to C3A is observed. In this case, MgO is found dispersed within the calcium aluminate phase, and no precipitates on the surface can be seen. However, the total magnesium concentration analysed is low enough to keep the oxide composition close to the C3A-C12A7 line. The calcium sulphide fraction in the inclusion is more than 25 mol.%.

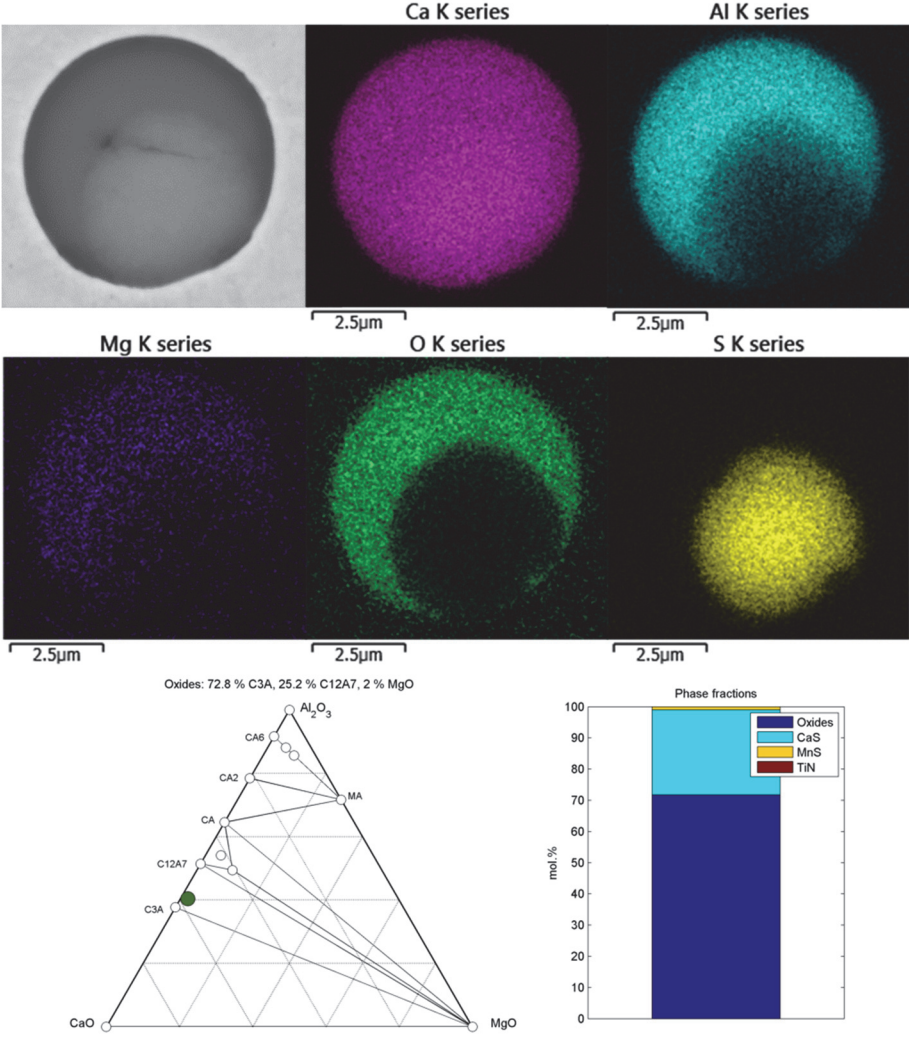


Fig. 21. Elemental maps and the calculated composition of an OX > CaS inclusion.

6.4.3 Product samples

In the elemental maps of Figure 22, two calcium aluminates can be distinguished. However, the calculation suggests that the majority of the oxide phases are C12A7. The MgO particles are quite large, yet they are found on the surface of the inclusion. A calcium sulphide phase is observed on one side, and a titanium nitride phase on the other. The calculated CaS and TiN fractions are small, owing to the relatively large diameter of the inclusion. Overall, the inclusion is very round, even though it has gone through hot rolling.

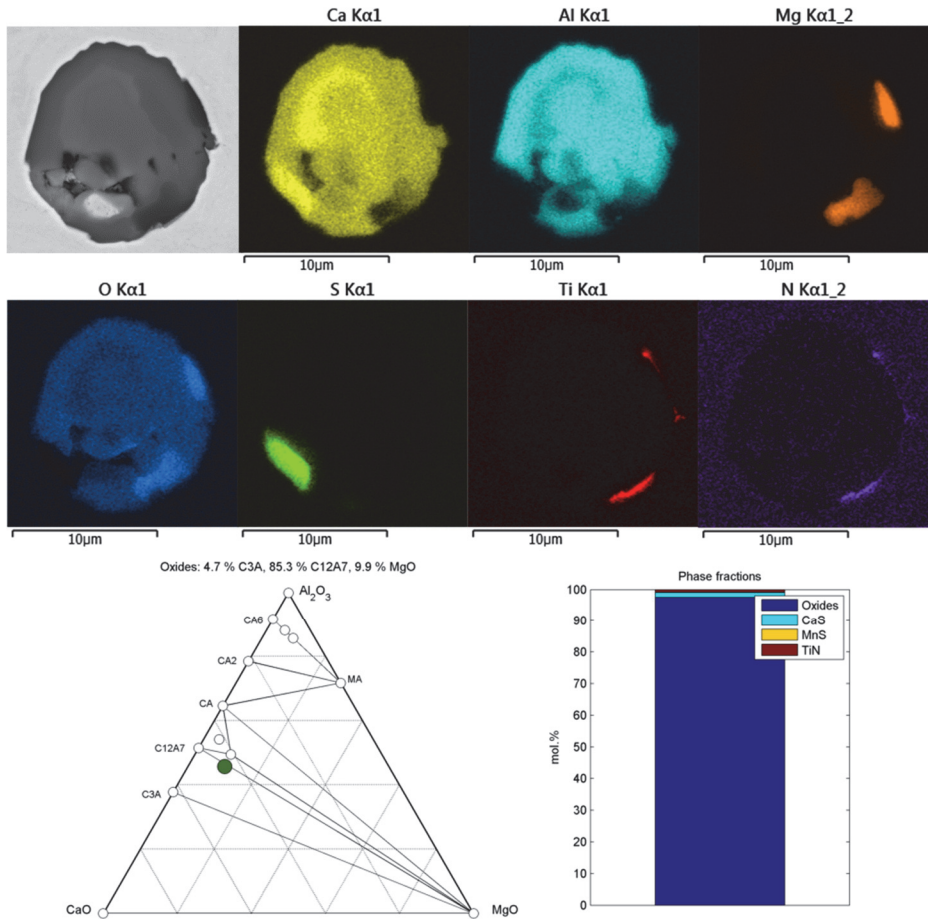


Fig. 22. Elemental maps and the calculated composition of an OX inclusion.

The inclusion presented in Figure 23 encloses a large spinel core, which has resisted deformation during hot rolling. A small amount of titanium nitride has been formed on the surface of the spinel phase. A solution of CaS and MnS is observed on both sides of the inclusion, where cone-like cavities have been formed during hot rolling. Despite of the small size of the inclusion, this kind of cavity-forming inclusion can be taken as a potential site for crack nucleation.

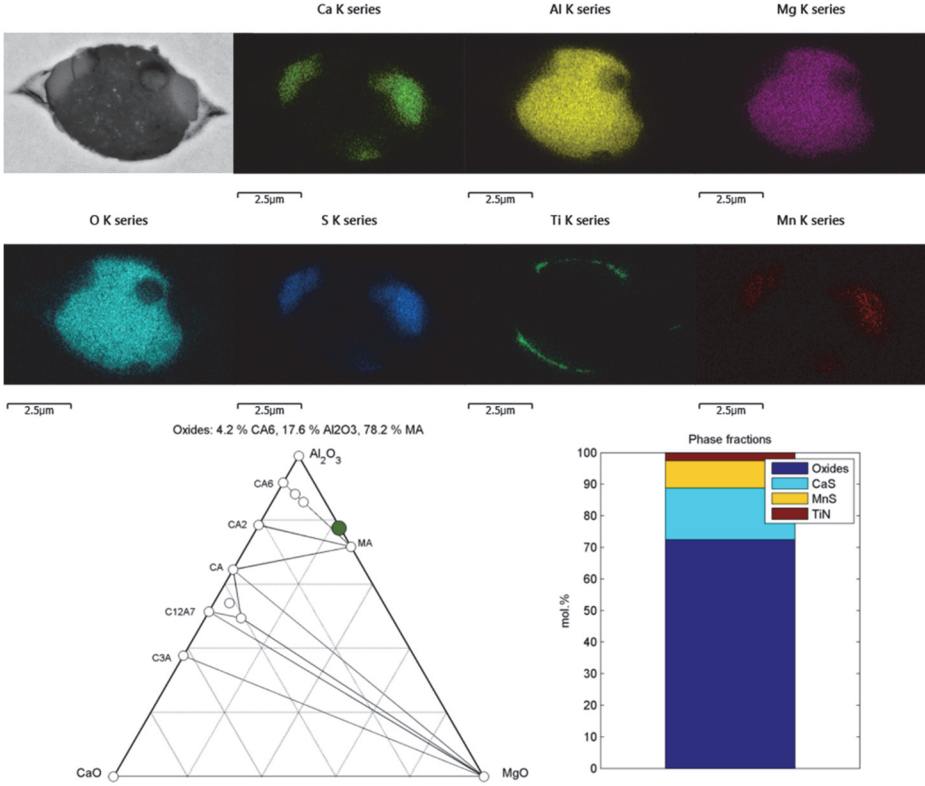


Fig. 23. Elemental maps and the calculated composition of an OX CaS MnS inclusion.

Figure 24 shows an example of a very elongated inclusion. In the core, a spinel phase is found. A solution of CaS and MnS has surrounded it and has become heavily deformed during hot rolling. As can be seen, the calculated oxide composition lies in the imminent vicinity of the spinel composition. As expected, the presence of MnS drastically affects the deformation behaviour of the inclusion.

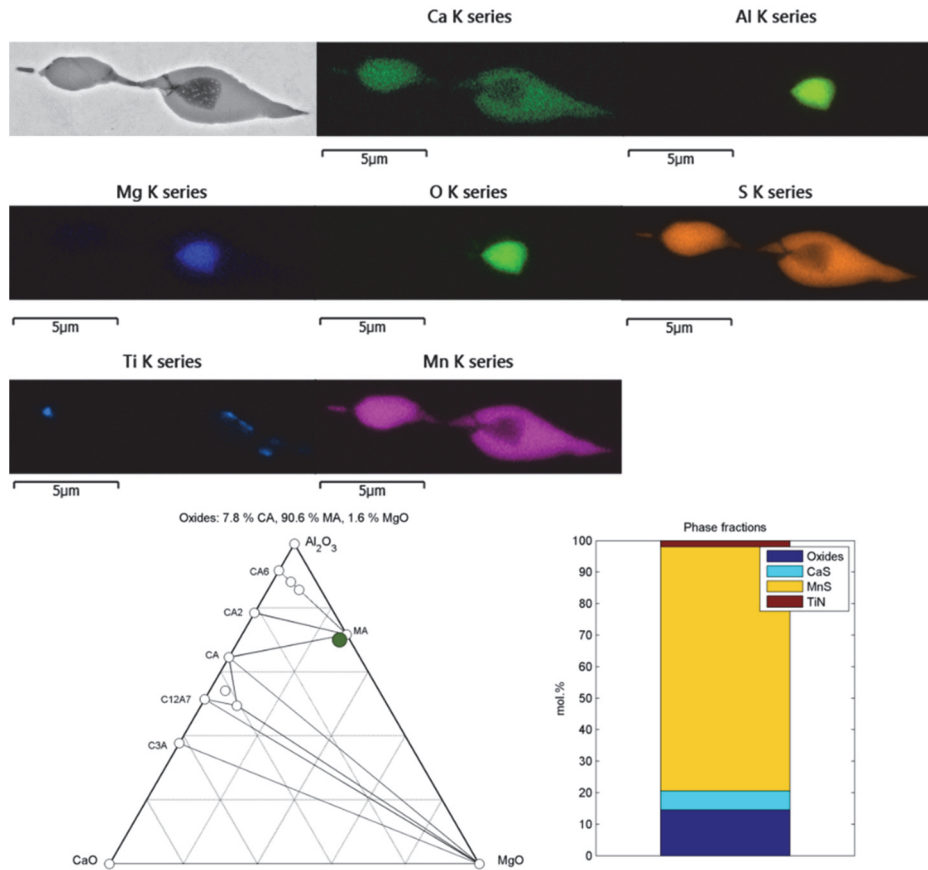


Fig. 24. Elemental maps and the calculated composition of an OX CaS MnS inclusion.

The inclusion illustrated in Figure 25 shows a spinel core surrounded by a (Ca,Mn)S phase. Unlike the previous one, this inclusion had the ability to resist the deformation, owing to the largest fraction of oxide phases. During hot rolling, a cavity has formed on the left-hand side of the inclusion.

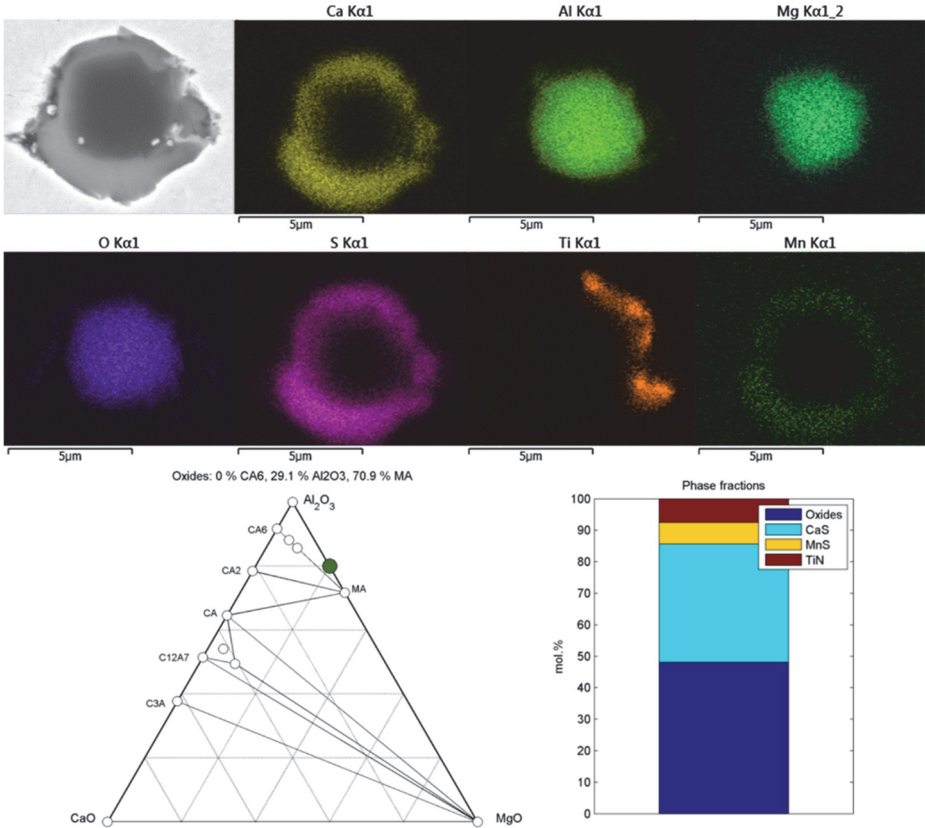


Fig. 25. Elemental maps and the calculated composition of an OX CaS MnS TiN inclusion.

Here, an aluminium oxide phase enclosed in calcium sulphide can be observed. The elemental maps shown in Figure 26 also show traces of an Al_2O_3 phase on the surface of the calcium sulphide phase, probably formed during the solidification on the sample.

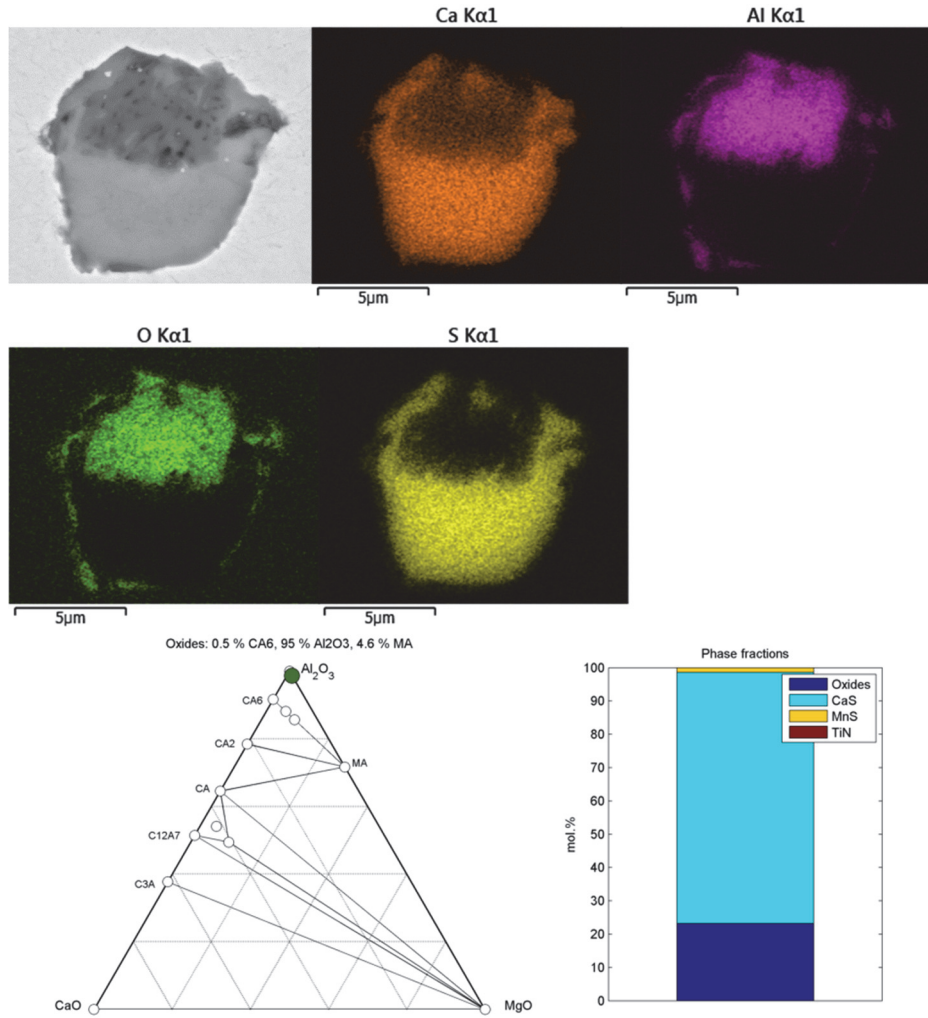


Fig. 26. Elemental maps and the calculated composition of an OX < CaS inclusion.

The inclusion in Figure 27 contains spinel, calcium aluminate phases, and calcium sulphide. Some titanium nitride has precipitated during solidification on the surface of the inclusion. In this case, the liquid calcium aluminate lies in the centre of the inclusion, between spinel and CaS phases. There are also visible tips on both sides of the inclusion, formed during hot rolling. Apparently, they are composed of calcium aluminates and calcium sulphide. However, the inclusion can be considered quite round, with an observed aspect ratio of only 1.32.

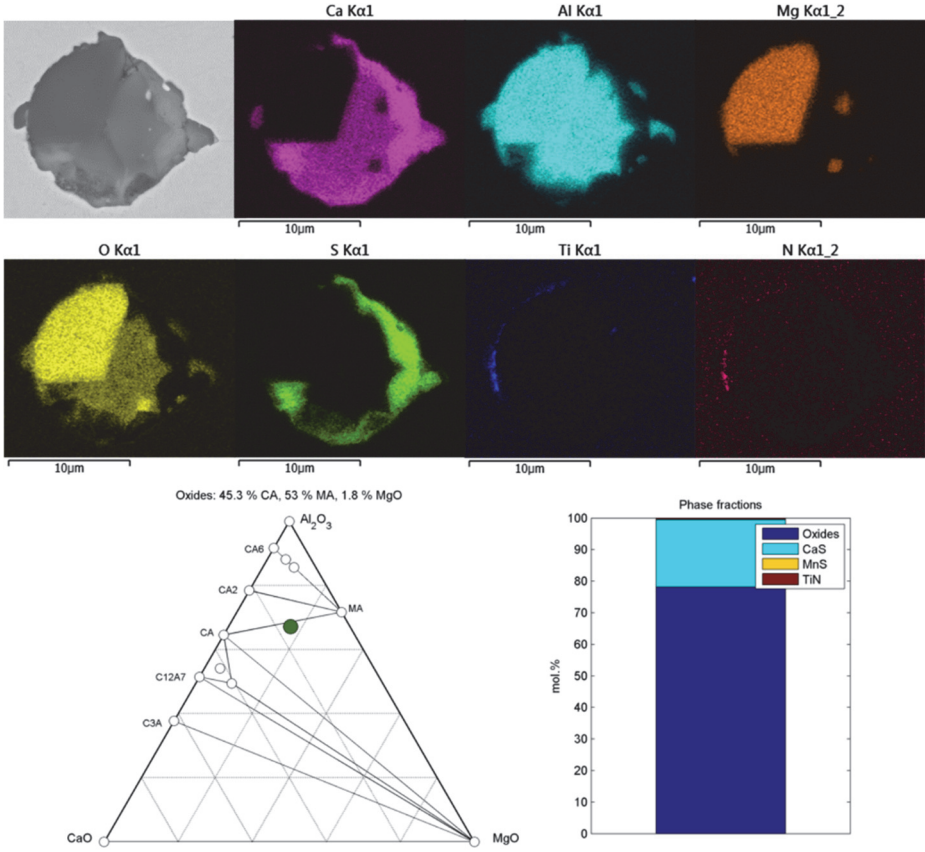


Fig. 27. Elemental maps and the calculated composition of an OX > CaS inclusion.

7 Practical applications of the new classification method

7.1 Dispersion of inclusions in a lollipop sample

From heats 62077 and 62078, samples were taken from the mould during casting with both the conventional sampling method and with an argon-protected sampler, with a sample thickness of 12 mm. The total oxygen, sulphur, and calcium contents for the heats are presented in Table 11, all of which are essentially higher in heat 62077. Additionally, the magnesium content calculated from the inclusion mass balance is presented in the table.

Table 11. Elemental analyses for the heats, obtained by OES and LECO from the mould samples.

| Heat | Analyses (ppm) | | | Calculated from mass balance* (ppm) |
|-------|----------------|----|----|-------------------------------------|
| | O | S | Ca | Mg |
| 62077 | 15 | 19 | 31 | 3 |
| 62078 | 8 | 4 | 17 | 1 |

* No accurate Mg analyses are available, and the calculation procedure presented in Chapter 7.2.4

In order to assess the dispersion and solidification of inclusions during sampling, lollipop samples were cut and prepared in the manner illustrated in Figure 28. Accordingly, they were divided into four sections: These were the top and bottom parts on both the surface and centre side. The four sections were analysed with a Jeol JSM-7000F FESEM equipped with an EDS detector. Inclusion analyses were obtained using the Oxford INCA Feature software with an acceleration voltage of 15 kV. In the INCA Feature runs, inclusions larger than 1.0 μm were analysed over the whole inclusion area with a live time of one second with EDS. The analysed sample areas were approximately 90 mm² for each section, resulting in thousands of inclusions per section. The inclusions were classified with the method described in Chapter 5.3 in order to distinguish various inclusion classes.

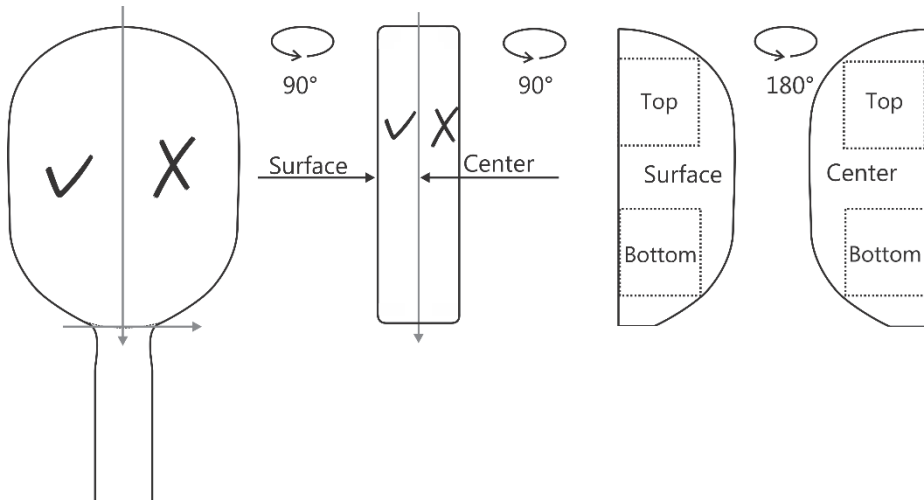


Fig. 28. Investigated sections of the lollipop samples.

In this case, the dispersion of inclusions was investigated with non-parametric tests, because the inclusion sizes or the elemental analyses are not normally distributed. Mann–Whitney U tests were used to determine if the medians differed, and further, Kolmogorov–Smirnov tests can be used to confirm which one is larger. Rather than comparing the number of inclusions per analysed area, the median sizes of inclusions were compared. In addition, the magnesium content distributions in the inclusions were compared, in order to assess the precipitation behaviour of MgO. The following factors were investigated with Mann-Whitney U tests:

- Are the median sizes of inclusions belonging to selected classes different between the centre and surface sections?
 - Null hypothesis: Equal medians
 - Alternative hypothesis: Unequal medians
- Are the medians of Mg concentration of inclusions belonging to selected classes different between the centre and surface sections?
 - Null hypothesis: Equal medians
 - Alternative hypothesis: Unequal medians

Further, the following factors were investigated using one-sided Kolmogorov-Smirnov tests:

- Are inclusions belonging to selected classes larger in the centre than on the surface?
 - Null hypothesis: Inclusions come from the same population
 - Alternative hypothesis: Larger in the centre
- Are the Mg concentrations of inclusions belonging to selected classes larger in the centre than on the surface?
 - Null hypothesis: Inclusions come from the same population
 - Alternative hypothesis: Larger in the centre

7.1.1 Size distributions

OX inclusion class

In Figure 29, OX inclusion size distributions on the 62077 MC surface and centre parts are illustrated as box plots. According to the figure, the inclusions on the surface parts of the sample have a larger median, and the size distribution is broader. The p-value is 0.012, indicating a statistical difference between the medians.

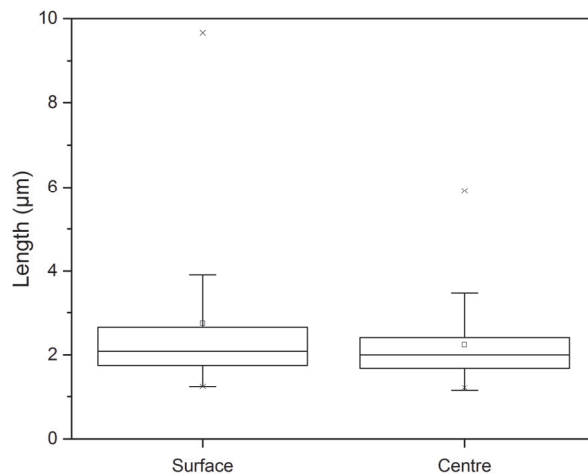


Fig. 29. Size distributions of inclusions in the OX class of the 62077 MC sample, for the surface and centre.

In the tables, p-values lower than 0.05 indicate the rejection of the null hypothesis. In the following tables, a conclusion for each pair of tests is also presented. As seen in Table 12, the Mann-Whitney U test confirms a difference between the size distributions of the OX inclusions in the abovementioned 62077 MC sample. However, the Kolmogorov-Smirnov test shows the inclusions are not larger in the centre part. On the contrary, it is safely concluded that the OX inclusions are larger on the surface part. In addition, this conclusion holds for the other samples as well, not taking into account the 62078 Ar sample.

Table 12. p-values for the size distribution comparison, for the OX inclusion class.

| Sample | Number of inclusions | | Median size (μm) | | Centre vs. Surface p-values | | Conclusion |
|----------|----------------------|-----|-------------------------------|------|-----------------------------|-------|---------------|
| | S | C | S | C | M-WU | K-S | |
| | 62077 MC | 490 | 461 | 2.09 | 2.00 | 0.012 | |
| 62077 Ar | 469 | 248 | 2.16 | 2.02 | 0.022 | 1.000 | " |
| 62078 MC | 82 | 55 | 1.71 | 1.48 | 0.016 | 0.960 | " |
| 62078 Ar | 44 | 42 | 1.45 | 1.50 | 0.353 | 0.372 | No difference |

OX > CaS inclusion class

Similarly, the p-values for the size distribution comparison of the OX > CaS inclusion class is presented in Table 13. In three samples out of four, the OX > CaS inclusions tend to be larger on the surface parts of the samples.

Table 13. p-values for the size distribution comparison, for the OX > CaS inclusion class.

| Sample | Number of inclusions | | Median size (μm) | | Centre vs. Surface p-values | | Conclusion |
|----------|----------------------|------|-------------------------------|------|-----------------------------|-------|-------------------------------------------|
| | S | C | S | C | M-WU | K-S | |
| | 62077 MC | 1427 | 1356 | 2.24 | 2.12 | 0.002 | |
| 62077 Ar | 1912 | 1029 | 2.24 | 1.99 | <0.001 | 0.992 | " |
| 62078 MC | 556 | 913 | 1.55 | 1.55 | 0.448 | 0.434 | No difference |
| 62078 Ar | 316 | 603 | 1.65 | 1.54 | 0.002 | 0.687 | OX > CaS inclusions larger on the surface |

OX < CaS inclusion class

Compared to OX > CaS, the OX < CaS class has more variation in the results, as presented in Table 14. In three of the four samples, the inclusions are larger on the surface, but actually larger at the centre in one of the samples.

Table 14. p-values for the size distribution comparison, for the OX < CaS inclusion class.

| Sample | Number of inclusions | | Median size (μm) | | Centre vs. Surface p-values | | Conclusion |
|----------|----------------------|------|-------------------------------|------|-----------------------------|--------|-------------------------------------------|
| | S | C | S | C | M-WU | K-S | |
| | 62077 MC | 2117 | 2591 | 3.00 | 2.63 | <0.001 | |
| 62077 Ar | 3870 | 2629 | 2.73 | 2.34 | <0.001 | 0.997 | " |
| 62078 MC | 1824 | 2403 | 1.77 | 1.82 | 0.010 | 0.002 | OX < CaS inclusions larger at the centre |
| 62078 Ar | 998 | 1813 | 2.03 | 1.84 | <0.001 | 0.976 | OX < CaS inclusions larger on the surface |

CaS inclusion class

The number of pure calcium sulphides in the studied samples is quite low, as seen in Table 15. From the data, we cannot state whether there would be a difference between the median sizes of the CaS inclusions. The low total number of pure calcium sulphides indicates they are not abundantly precipitated during the cooling of the samples.

Table 15. p-values for the size distribution comparison, for the CaS inclusion class.

| Sample | Number of inclusions | | Median size (μm) | | Centre vs. Surface p-values | | Conclusion |
|----------|----------------------|----|-------------------------------|------|-----------------------------|-------|---------------|
| | S | C | S | C | M-WU | K-S | |
| | 62077 MC | 75 | 29 | 2.88 | 3.31 | 0.044 | |
| 62077 Ar | 25 | 33 | 3.30 | 3.57 | 0.994 | 0.659 | No difference |
| 62078 MC | 1 | 3 | 3.00 | 2.65 | 0.655 | 0.759 | " |
| 62078 Ar | 4 | 7 | 2.57 | 2.43 | 0.850 | 0.204 | " |

TiN inclusion class

The centre parts of the samples contain a markedly higher number of TiN inclusions, as depicted in Table 16. Further, it is reasonable that they are usually also larger in the centre parts, as confirmed by the Kolmogorov–Smirnov tests.

Table 16. p-values for the size distribution comparison, for the TiN inclusion class.

| Sample | Number of inclusions | | Median size (μm) | | Centre vs. Surface p-values | | Conclusion |
|----------|----------------------|-----|-------------------------------|------|-----------------------------|--------|-------------------------------------|
| | S | C | S | C | M-WU | K-S | |
| | | | | | | | |
| 62077 MC | 73 | 870 | 1.46 | 1.58 | <0.001 | <0.001 | TiN inclusions larger at the centre |
| 62077 Ar | 47 | 247 | 1.50 | 1.80 | <0.001 | <0.001 | " |
| 62078 MC | 58 | 488 | 1.51 | 1.52 | 0.775 | 0.893 | No difference |
| 62078 Ar | 59 | 368 | 1.46 | 1.76 | <0.001 | <0.001 | TiN inclusions larger at the centre |

7.1.2 MgO content

OX inclusion class

In Figure 30, we see the oxide phase compositions for OX inclusions in 62077 MC sample. Clearly it can be seen that in the centre parts, higher MgO contents have been analysed, indicated by the expansion of the composition of the inclusions from the liquid calcium aluminate area towards the MgO corner.

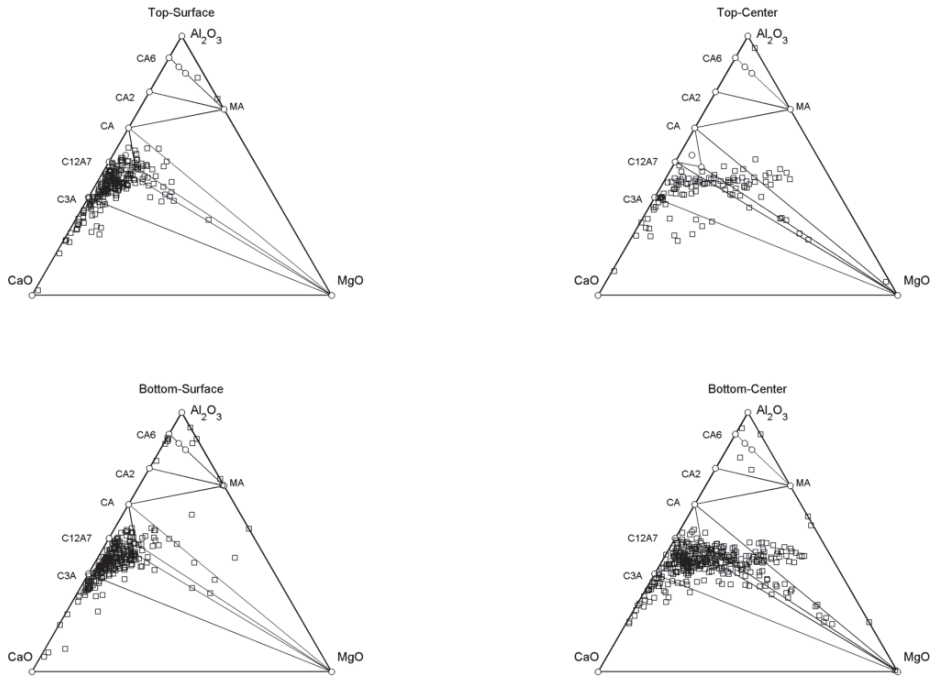


Fig. 30. Oxide phase compositions of OX inclusions in different sections of the 62077 MC sample.

In Table 17, the observation is confirmed with the Mann-Whitney U and Kolmogorov-Smirnov tests. For the OX inclusions, the same behaviour can be confirmed for the other samples, excluding 62078 Ar.

Table 17. p-values for the MgO content comparison, for the OX inclusion class.

| Sample | Centre vs. Surface | | Conclusion |
|----------|--------------------|--------|--------------------------------------------------|
| | M-WU | K-S | |
| 62077 MC | <0.001 | <0.001 | Mg content of OX inclusions higher at the centre |
| 62077 Ar | <0.001 | <0.001 | " |
| 62078 MC | 0.004 | <0.001 | " |
| 62078 Ar | 0.119 | 0.511 | No difference |

OX > CaS inclusion class

For the OX > CaS inclusions, the statistical tests confirm that in each studied sample, the magnesium contents are higher in the centre parts of the samples. As can be seen in Table 18, in each test, the p-values were lower than 0.001, strongly indicating the difference in the distributions.

Table 18. p-values for the MgO content comparison, for the OX > CaS inclusion class.

| Sample | Centre vs. Surface | | Conclusion |
|----------|--------------------|--------|--------------------------------------------------------|
| | M-WU | K-S | |
| 62077 MC | <0.001 | <0.001 | Mg content of OX > CaS inclusions higher at the centre |
| 62077 Ar | <0.001 | <0.001 | " |
| 62078 MC | <0.001 | <0.001 | " |
| 62078 Ar | <0.001 | <0.001 | " |

OX < CaS inclusion class

Similarly to the OX > CaS inclusions, the magnesium contents are higher in the centre parts of the samples. According to Table 19 for the 62077 MC sample, the p-value of the Mann–Whitney U test is slightly above 0.05. However, the p-value of the Kolmogorov–Smirnov test falls below 0.001, indicating higher magnesium contents in the centre parts.

Table 19. p-values for the MgO content comparison, for the OX < CaS inclusion class.

| Sample | Centre vs. Surface | | Conclusion |
|----------|--------------------|--------|--------------------------------------------------------|
| | M-WU | K-S | |
| 62077 MC | 0.075 | <0.001 | Mg content of OX < CaS inclusions higher at the centre |
| 62077 Ar | <0.001 | <0.001 | " |
| 62078 MC | <0.001 | <0.001 | " |
| 62078 Ar | <0.001 | <0.001 | " |

7.1.3 Summary

It has been stated that the sample filling practically always occurs in a turbulent manner (Zhang et al. 2010). Because of the turbulent sample filling, inclusion characteristics vary heavily within the samples. In addition, secondary inclusions precipitate during the solidification of the sample. Ericsson (2010) recommended a fast-cooling sample and the surface parts for investigating primary inclusions. However, Ericsson (2010) did not investigate the chemical composition of the inclusions, instead he used a threshold value of 0.6 μm to distinguish between primary and secondary inclusions.

In this section, median sizes and the MgO contents of inclusions were compared between the surface and centre parts of lollipop samples. One can hypothesise that a larger median size of inclusions and a higher magnesium content indicate a lower cooling rate. For the OX and OX CaS classes, inclusions tended to be larger on the surface parts of the sample. This could be explained by the turbulent flow and filling of the sample mould – it is probable that for inclusions existing in the liquid steel, the fluid flows have a larger effect on size than the cooling rate of the sample. On the other hand, TiN inclusions are formed only after the sample filling, during solidification, which explains their larger number and size in the centre parts. In this case, the cooling rate is the dominant factor determining the inclusion size. Moreover, a reduction in the cooling rate may allow slightly sub-micron sized inclusions to grow and to be detected with the SEM setup used here. In the investigated samples, the number of pure CaS inclusions is quite small, and no differences in their sizes were observed. It is clear that the vast majority of the CaS component was formed during sampling as precipitates on the surface of existing inclusions.

For the assessment of primary inclusions, the surface parts of the samples are recommended. The inclusions in the centre parts are higher in MgO content, which was caused by MgO precipitation from the steel melt. The total MgO contents in the oxides in the solidified samples were markedly higher than the solubility of MgO in the liquid inclusions at steelmaking temperatures, indicating abundant MgO precipitation from the steel melt during the solidification of the samples. Even if the liquid inclusions were saturated with MgO, it cannot explain the total oxide composition outside the liquid window in the $\text{Al}_2\text{O}_3\text{--CaO--MgO}$ ternary. However, the MgO phases detected inside calcium aluminate phases in some of the ladle samples indicate that some amount of MgO might have precipitated from the liquid inclusion phases.

Not only the inclusion size differed within sections of the lollipop samples, but also the composition varied. Therefore, the inclusions in the lollipop sample do not represent the inclusions in the liquid steel as such. In order to estimate the primary inclusions present in the liquid steel, e.g. with online applications such as OES-PDA, the most suitable section is near the surface of the sample, where the MgO and TiN contents are lower.

7.2 Evolution of inclusions during sampling

Here, the inclusions analysed in the mould samples are presented as a percentage of the component area, estimated with the phase identification method. For simplicity, CA6 and CA2 are denoted as solid calcium aluminates, whereas CA, C12A7 and C3A are treated as liquid calcium aluminates. On top of this, the average oxide phase compositions are presented for the OX and OX CaS inclusion classes for each heat.

For comparison, the stable inclusion masses in the mould samples were calculated using the FactSage software. For this investigation, mould samples from three heats were chosen according to their calcium treatment success, characterised by a large amount of Al₂O₃ in slightly modified, liquid inclusions in medium modified, and CaO–CaS inclusions in overmodified heats, numbered 76325, 68852, and 62078, respectively.

For the thermodynamic calculations, the FactSage 7.1 Equilib module was utilised to calculate stable inclusions. The calculation took into account pure solids from the FactPS, FToxid, FSstel databases, in addition to FCC, BCC, spinel, olivine, and monoxide as solid solutions, and liquid steel and slag solutions. With the bulk chemical analysis of the steel samples obtained with OES, stable inclusions were calculated with descending temperatures from 1550°C to 1450°C, encompassing typical steel temperatures for mould during continuous casting, as well as the solidification of the steel. While the solidification of steel does not follow equilibrium, calculations below liquidus temperature of steel show which inclusion compounds are the first to form during the cooling and solidification of the steel. In the FactSage result figures, the star markers show the composition of the liquid slag at the highest temperature where it is stable, and squares denote the composition of CaO or MgO monoxides.

7.2.1 Slightly modified heat 76325

Despite the large amount of liquid calcium aluminates, more than 25% of the inclusions in this heat were either solid Al_2O_3 or spinel inclusions, as seen in Figure 31. It is a strong indicator that the calcium addition has not been adequate. However, the average oxide phase compositions of OX and OX > CaS lie near the C12A7–MgO line, indicating the presence of liquid inclusions. No OX < CaS inclusions were detected in the sample. The low fraction of CaS is easily explained by the low sulphur content of 3 ppm in the sample. A significant amount of titanium nitrides were also observed, possibly accompanied with spinels.

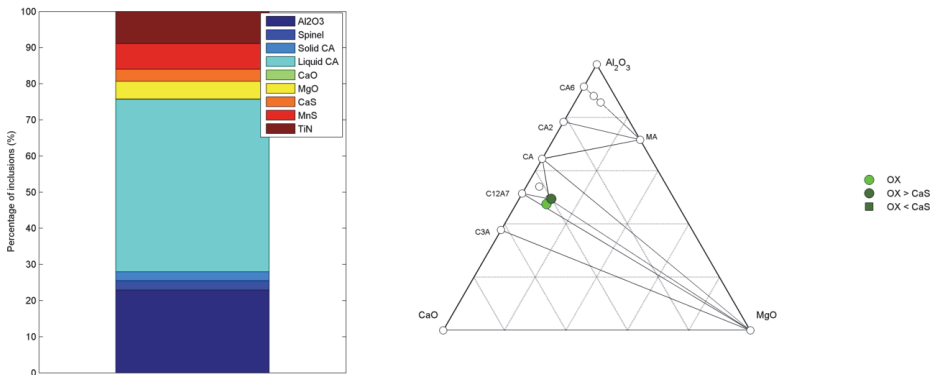


Fig. 31. Inclusion types and oxide composition in slightly modified heat 76325.

The FactSage calculations presented in Figure 32 show that at steelmaking temperatures, the inclusions were comprised of liquid inclusions and MgO monoxides. At high temperatures, the sulphur content of liquid inclusions was quite small, and the fraction of Al_2O_3 , CaO and MgO in them was larger than 90 %. From the results, it is expected that the CaS fraction of OX CaS inclusions would be quite small in the solidified sample. On the other hand, the calculations do not predict the occurrence of Al_2O_3 and spinel.

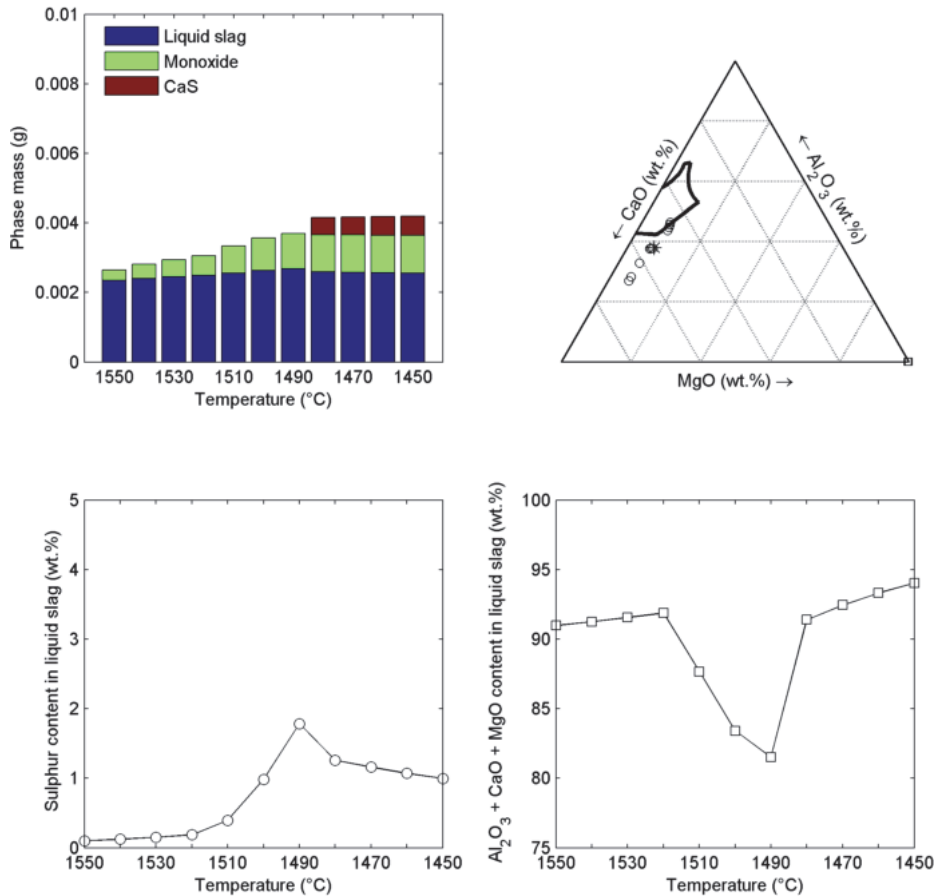


Fig. 32. FactSage calculated inclusions in slightly modified heat 76325.

7.2.2 Medium modified heat 68852

As seen in Figure 33, over 70 % of the mould sample inclusions were liquid calcium aluminates, which is considered excellent from the casting success point of view. In addition, the oxide phase compositions of OX and OX CaS inclusions were very close to each other, between C3A and C12A7 calcium aluminates. Furthermore, some slightly modified calcium aluminates CA2 and CA6 occurred, according to the phase identification. In this heat, the total sulphur content in the mould sample was analysed at 6 ppm. As a result, the CaS fraction of the inclusions was very low.

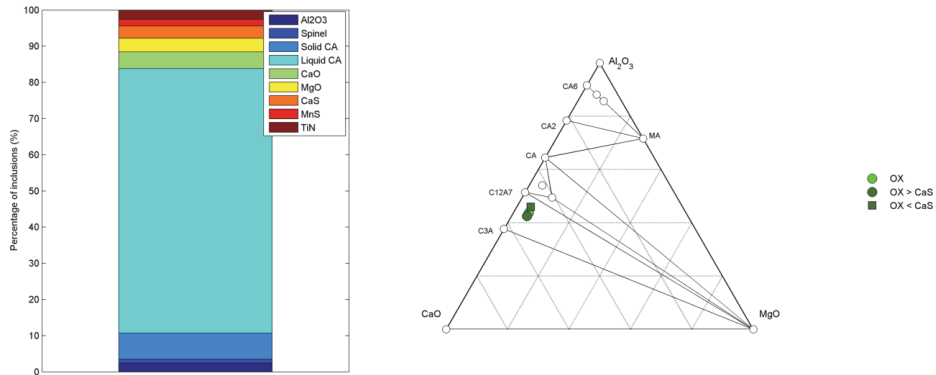


Fig. 33. Analyzed inclusion types and oxide composition in medium modified heat 68852.

According to the FactSage calculations, at casting temperatures, all thermodynamically stable inclusions were in a liquid state. As seen in Figure 34, the composition of liquid inclusions at 1550°C is outside the liquid window of pure $\text{Al}_2\text{O}_3\text{--CaO--MgO}$ system. The S contents, among other components, expands the actual liquid window towards the CaO corner. However, during sampling, and with a decreasing temperature, MgO and CaS precipitated, and the total $\text{Al}_2\text{O}_3\text{--CaO--MgO}$ content in the liquid inclusions increased. The FactSage calculations are in good agreement with the observed inclusions.

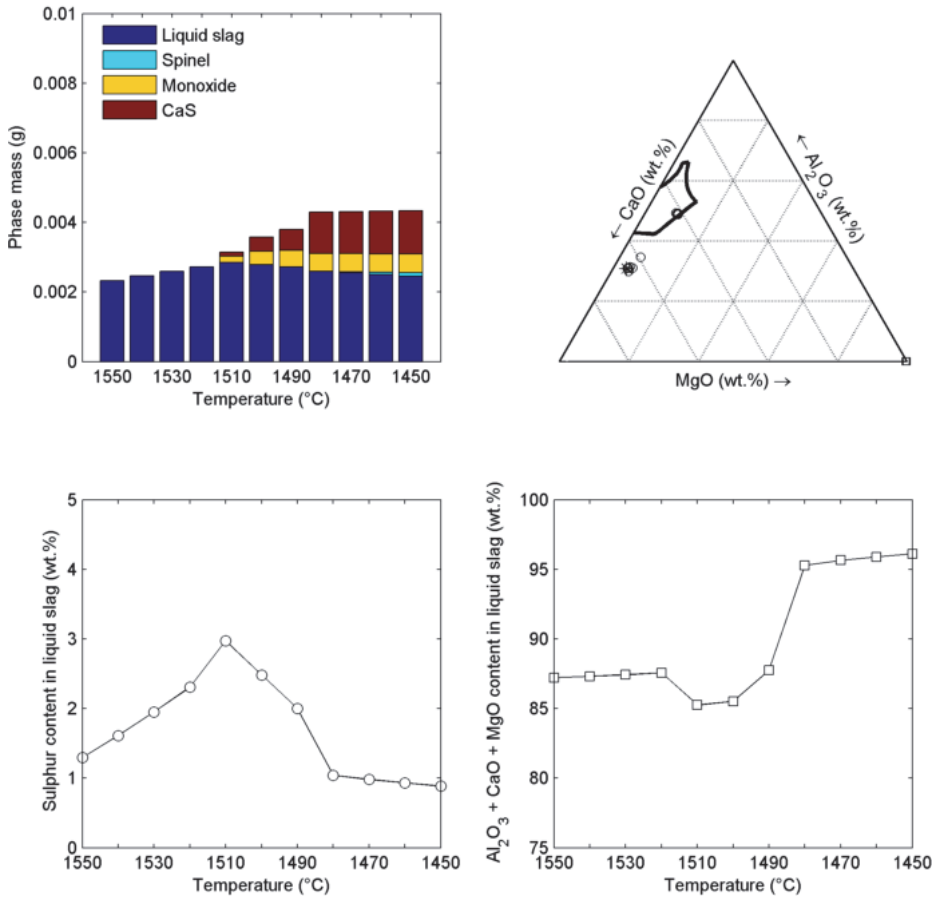


Fig. 34. FactSage calculated inclusions in medium modified heat 68852.

7.2.3 Overmodified with calcium, heat 62078

This heat is characterised by a vast amount of CaO and CaS in the mould sample, as depicted in Figure 35. The average OX inclusion composition lies on the CA–MgO line, i.e., outside the liquid window at steelmaking temperatures. However, the OX CaS classes contained CaO as a majority. Even with a low sulphur level of only 4 ppm, a marked portion of the analysed inclusion components were calcium sulphides.

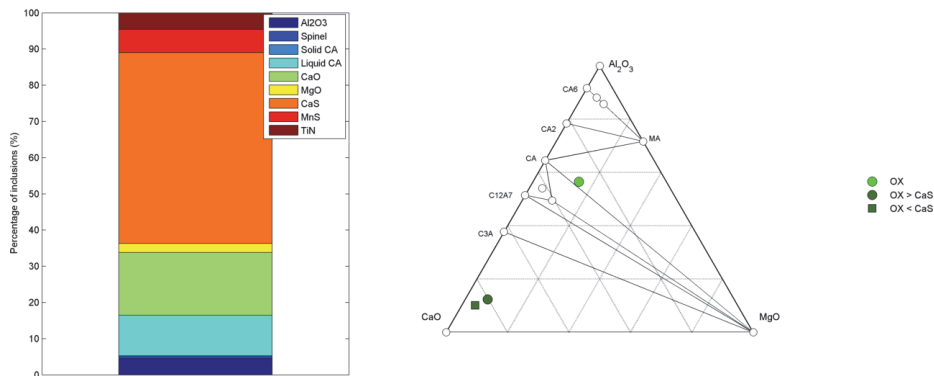


Fig. 35. Analyzed inclusion types and oxide composition in overmodified heat 62078.

According to the FactSage calculations, virtually all inclusions at casting temperatures in this heat were CaO monoxides. According to Figure 36, liquid slag and CaS would be formed only after the temperature decrease. The almost negligible amount of liquid inclusions is relatively low in $\text{Al}_2\text{O}_3\text{-CaO-MgO}$ content, totalling around 80 wt.%, which heavily expands the liquid window towards the CaO corner. Further, the high calcium content originating from abundant calcium treatment, forms calcium silicates after the solidification of steel, according to the FactSage calculations. Naturally, such inclusions were not observed in the sectioned mould samples.

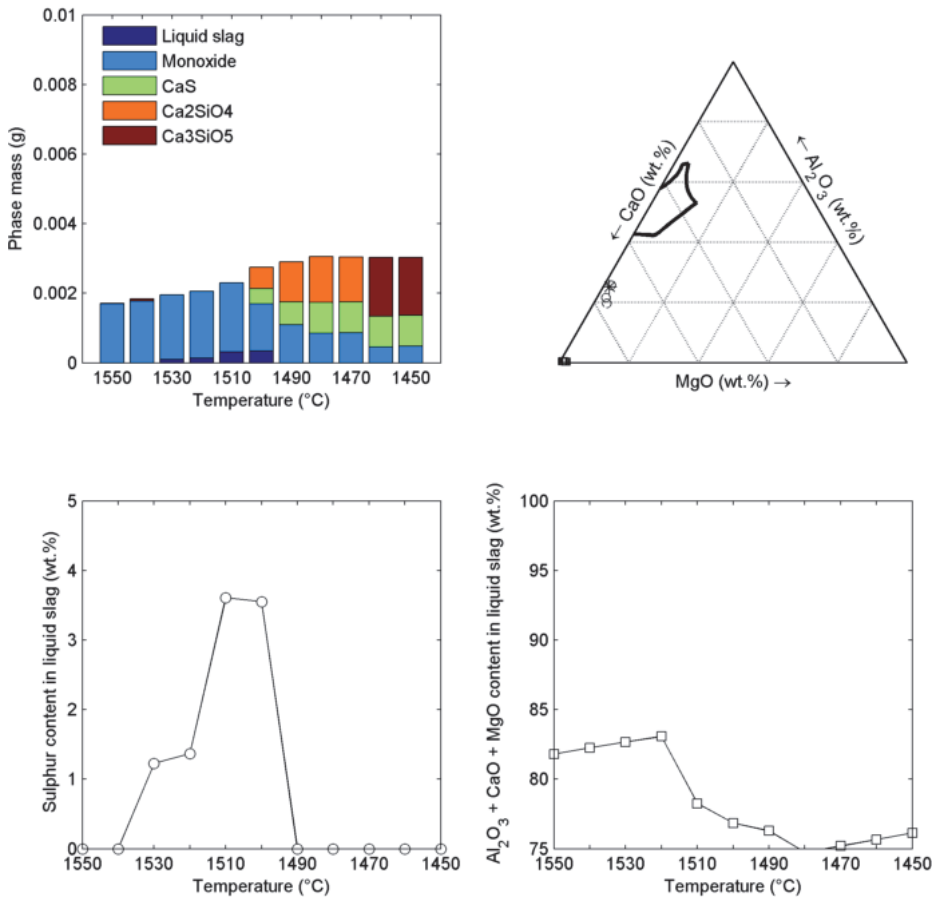


Fig. 36. FactSage calculated inclusions in overmodified heat 62078.

7.2.4 Discussion

Inclusions observed in the mould samples do not fully correspond to the stable phases calculated by FactSage. According to the thermodynamic calculations of the steel compositions in question, aluminium oxides are not a stable phase at steelmaking temperatures, still, they were analysed in the samples. This indicates that the inclusions in the mould had not reached the equilibrium state, i.e., calcium modification was still on-going. For the slightly Ca-modified heat, liquid oxides and MgO were the thermodynamically stable phases at casting temperatures, but Al₂O₃ inclusions were abundant in the analysed sample. In the medium Ca-

modified heat, liquid inclusions were the vast majority in the mould sample. According to the FactSage calculations, all stable inclusions were fully liquid at temperatures over 1520°C. In addition, MgO and CaS would be the first compounds formed during cooling of the sample. In the sample of the overmodified heat, CaO–CaS were the prevailing inclusions in the analysed sample. According to the thermodynamic calculations, almost all stable inclusions were CaO at steelmaking temperatures. However, liquid slag high in CaO and S is stable at casting temperatures above 1500°C. It is possible that some of the CaO–CaS inclusions may have been in a liquid state in the molten steel, as suggested by the expansion of the liquid slag composition towards the CaO corner in the Al₂O₃–CaO–MgO ternary diagram.

With the FactSage calculations, it is possible to assess the distribution of sulphur between inclusions and molten metal at sampling temperatures. Here, the sulphur content in the inclusions and the molten steel are presented at 1520°C, in order to assess the sulphur precipitation during solidification of the sample. In Figure 38, for each heat, the dissolved sulphur content at 1520°C, obtained from the above calculations, is plotted as a function of the total analysed sulphur content, analysed by OES. As illustrated in Figure 37, in heats with sulphur contents up to 10 ppm, virtually all the sulphur is found to be dissolved in the molten steel. As the total sulphur content in the heats increases, the sulphur content bound to inclusions simultaneously increases. For instance, for the heats with analysed total sulphur contents of around 20 ppm, the dissolved S is in the range of 8–13 ppm, meaning approximately half of the total sulphur content in molten steel is bound to inclusions. Keeping in mind that pure oxide inclusions are relatively rare in the lollipop samples even for low-sulphur heats, it is reasonable to state that a marked portion of sulphides precipitate during sampling of the liquid steel.

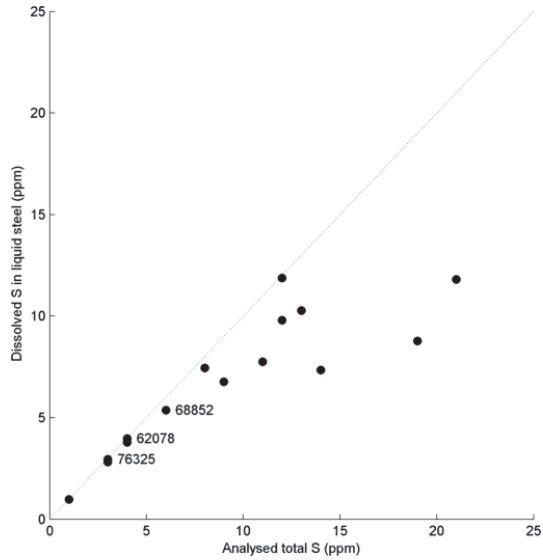


Fig. 37. Analysed sulphur content (OES), and dissolved sulphur content in molten steel at 1520°C, calculated by FactSage.

During the solidification of the sample, some amount of the total sulphur is precipitated as inclusions. Here, the total sulphur content and the sulphur content calculated from the inclusion data obtained from the INCA Feature runs of the mould samples are compared. The sulphur content in the solidified mould samples was calculated from the mass balance with the following assumptions, modified from Harris (2015). The volume fraction of inclusions is assumed equal to the area fraction. Further, the density of all inclusions is considered half of the density of the steel. The procedure to calculate the sulphur bound to the inclusions is presented in Equations 40–42.

$$\frac{V_{inc}}{V_{steel}} = \frac{A_{inc}}{A_{steel}} \quad (40)$$

$$\frac{\rho_{inc}}{\rho_{steel}} = \frac{1}{2} \quad (41)$$

$$W_{i,steel} = \frac{\sum_{k=1}^n A_k w_{i,k} \rho_{inc}}{A_{steel} \rho_{steel}} \quad (42)$$

where

V_{inc} is the volume fraction of the inclusions,

A_{inc} is the area fraction of the inclusions,

V_{steel} is the volume of the steel,

A_{steel} is the analysed area of the steel,

ρ_{inc} is the density of the inclusions,

ρ_{steel} is the density of the steel,

$w_{i,steel}$ is the mass fraction of element i in the steel,

n is the number of inclusions in the analysed area,

A_k is the area of an analysed inclusion k,

$w_{i,k}$ is the mass fraction of element i in an inclusion k.

In Figure 38, it can be clearly seen that the calculated S contents from the inclusion data of the mould samples tend to be smaller than the analysed contents. The reason for this is that the OES analysis takes into account the bulk analysis of the steel, whereas inclusions only larger than 1 μm were analysed in the INCA Feature runs. Firstly, it is evident that not all sulphur is in the observed inclusions in the solidified steel sample. Secondly, the inclusion composition alters during sampling, cooling and solidification.

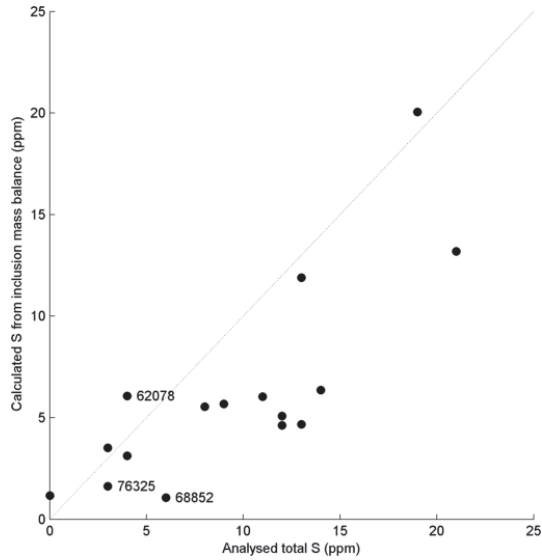


Fig. 38. Calculated sulphur content from inclusion data and analysed sulphur (OES) contents in the mould samples.

Similarly to sulphur, the total calcium contents analysed with OES and dissolved calcium contents at 1520°C calculated by FactSage, are plotted in Figure 39. It is noteworthy that the dissolved calcium content in the molten steel is quite constant, at around 3–5 ppm for most samples, irrespective of the total calcium content. During solidification, most of the dissolved calcium precipitates in inclusions as CaO or CaS components in calcium aluminates or sulphides, respectively. As the sample solidifies, the dissolved calcium content is rapidly consumed by the dissolved sulphur or oxygen, forming calcium sulphides or oxides. During further solidification, the remaining dissolved sulphur reacts with the components in the existing inclusions, rather than with dissolved calcium. With the steel grades investigated, excess calcium treatment did not act as a buffer for reoxidation, as reported by Geldenhuis & Pistorius (2000).

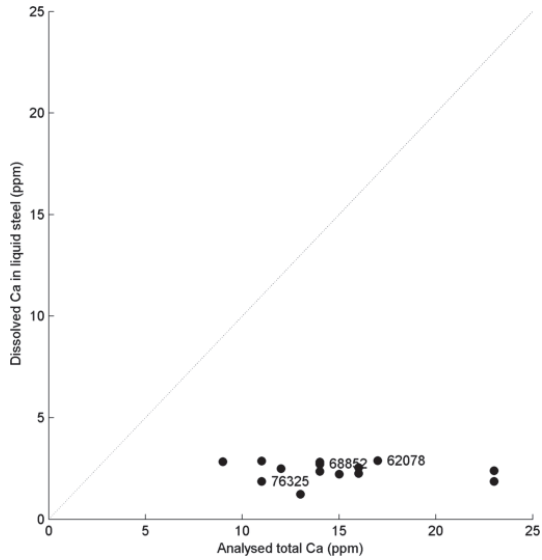


Fig. 39. Analysed calcium content, and dissolved calcium content in molten steel at 1520°C, calculated by FactSage.

7.3 Evolution of inclusions during continuous casting

Successful casting is ensured by the adequate liquefaction of inclusions, and the prevention of solid CaS forming in the mould. However, plenty of time is available for inclusion composition changes during continuous casting. Along with sulphur, also the oxygen, calcium, and magnesium solubilities decrease with decreasing temperatures. Inevitably, this results in the composition change of oxides in the solidifying steel.

As shown in Chapter 7.2, the inclusions in low-sulphur heats may be fully liquid, and virtually the entire sulphur content might be found in the molten steel at casting temperatures. In such cases, all the sulphur will precipitate as CaS inclusions or on existing inclusions as a CaS phase. In the worst case, no calcium will be available to bind the dissolved sulphur content in the steel, resulting in the occurrence of heavily elongated MnS inclusions in the product.

The optimal inclusion composition during casting is not necessarily the optimal inclusion composition in the final product. Here, inclusion evolution during casting is assessed.

7.3.1 Slightly modified heat 76325

In the mould sample of the slightly modified heat, the inclusions were a mixture of calcium aluminates and calcium sulphide, as seen in the Al–Ca–S ternaries presented in Figure 40. In the hot rolled products A and B, the oxide composition has shifted to mainly aluminium oxides and calcium sulphides. As illustrated by the Al₂O₃–CaO–MgO ternaries in Figure 41, not many oxide inclusions without CaS were observed in the hot rolled products. This is understandable as the CaS phase has precipitated on the existing OX inclusions, shifting their composition to OX CaS classes.

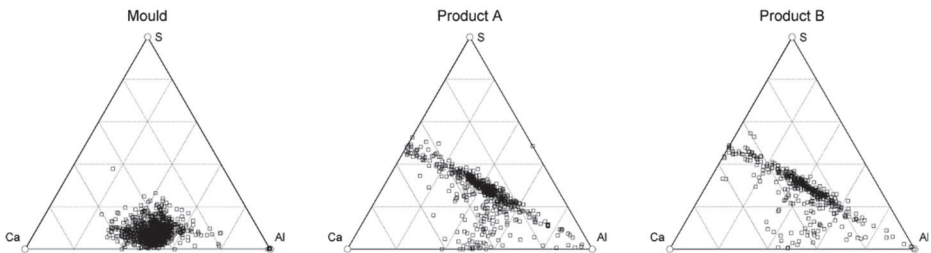


Fig. 40. The composition of OX and OX CaS inclusions in heat 76325 samples, projected on Al–Ca–S ternary diagrams.

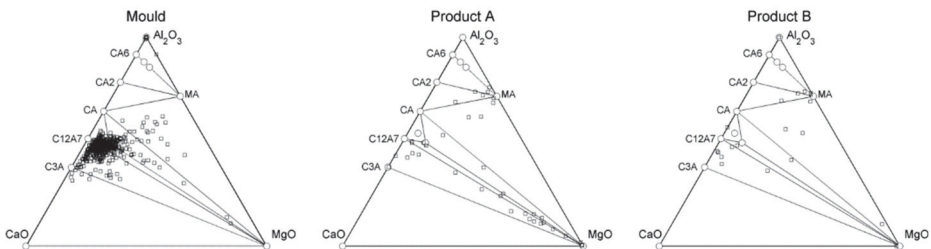


Fig. 41. The composition of OX inclusions in heat 76325 samples, projected on Al₂O₃–CaO–MgO ternary diagrams.

Even though Figure 40 suggests that the OX CaS inclusions are a mixture of Al₂O₃ and CaS, it can be seen in Figure 42 that in fact, the oxide composition of the majority of the inclusions consist of spinel instead of alumina. During continuous casting, a significant amount of dissolved magnesium has reacted with the Al₂O₃ component of calcium aluminates, forming spinel inclusions.

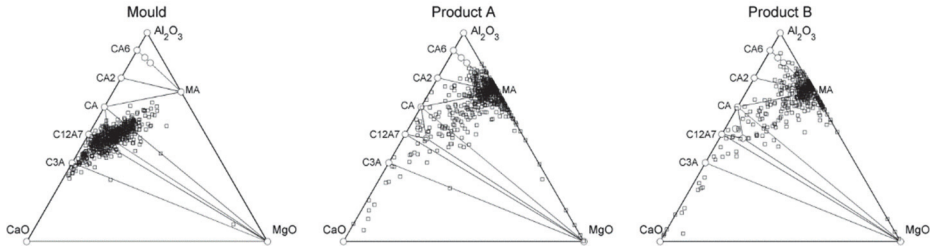


Fig. 42. The composition of OX CaS inclusions in heat 76325 samples, projected on $\text{Al}_2\text{O}_3\text{--CaO--MgO}$ ternary diagrams.

7.3.2 Medium modified heat 68852

In this case, both the mould and product samples reveal a mixture of calcium aluminates and calcium sulphides, as plotted on the ternaries in Figure 43. It can be seen in Figure 44 that in the mould sample, the calcium aluminates are richer in CaO contents, compared to the slightly Ca-modified case. Consequently, the precipitated MgO components are found in a mixture of calcium aluminates, MgO phase and CaS. This is clearly seen in the oxide composition ternaries in Figure 45, where the majority of inclusions lie between C3A and CA, with greatly varying MgO contents. In addition, some CaO and spinel oxide phases can also be observed. With a higher calcium treatment in this heat, the occurrence of spinels in the product samples has been greatly hindered.

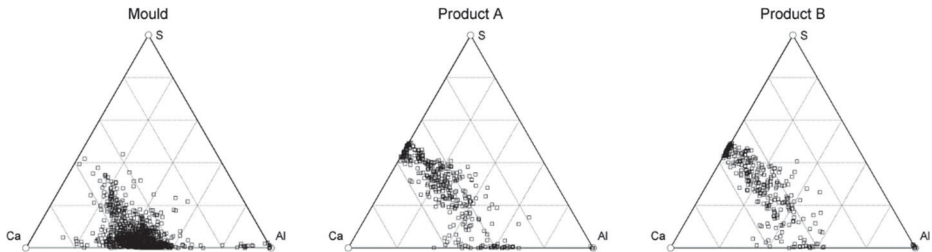


Fig. 43. The composition of OX and OX CaS inclusions in heat 68852 samples, projected on Al--Ca--S ternary diagrams.

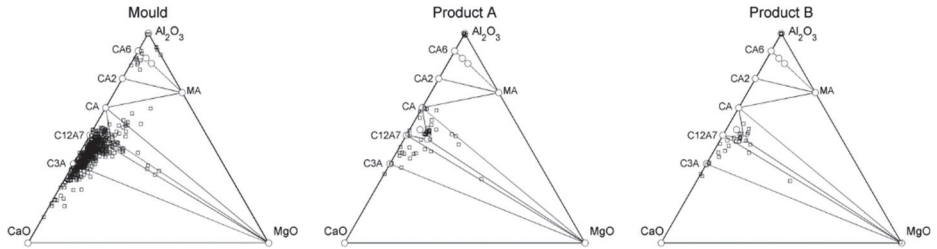


Fig. 44. The composition of OX inclusions in heat 68852 samples, projected on Al_2O_3 – CaO – MgO ternary diagrams.

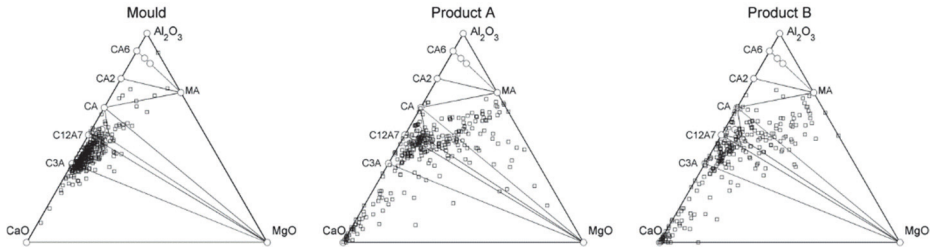


Fig. 45. The composition of OX CaS inclusions in heat 68852 samples, projected on Al_2O_3 – CaO – MgO ternary diagrams.

7.3.3 Overmodified with calcium, heat 62078

In the mould sample of the overmodified heat, a majority of inclusions in the mould and product samples lie on or very close to the Ca–S line, as observed in Figure 46. The occurrence of CaS inclusions can be considered a result of overmodification with calcium. Pure oxides were very rare in the samples, as seen in Figure 47. The inclusions in the mould samples are mostly of a CaO–CaS type, observed in Figure 48. It is reasonable that during casting, magnesium has precipitated as an MgO phase on these inclusions, instead of spinel. The overmodification with Ca has prevented the occurrence of Al_2O_3 and spinel inclusions altogether.

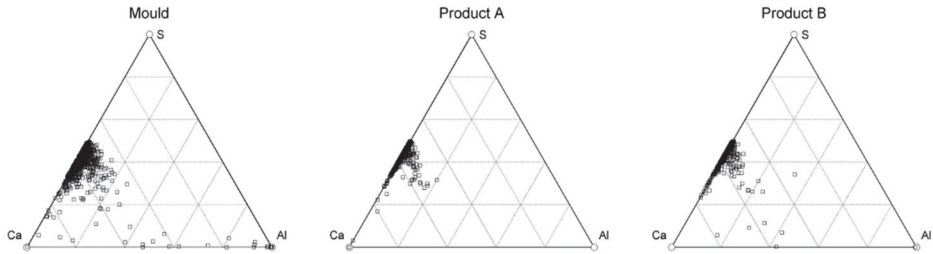


Fig. 46. The composition of OX and OX CaS inclusions in heat 62078 samples, projected on Al–Ca–S ternary diagrams.

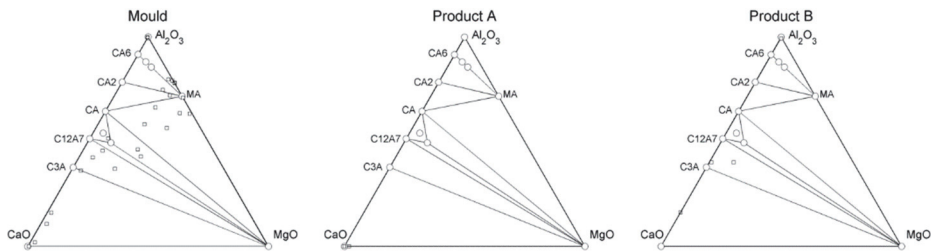


Fig. 47. The composition of OX inclusions in heat 62078 samples, projected on Al_2O_3 –CaO–MgO ternary diagrams.

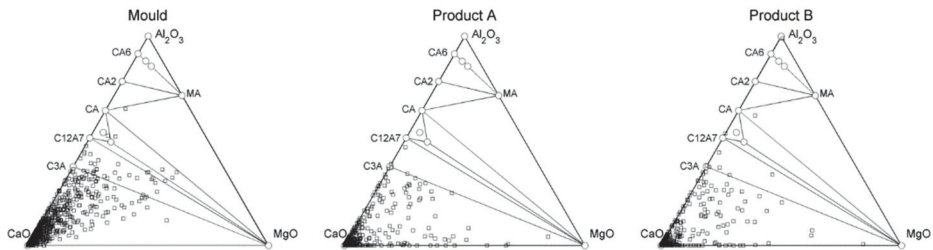
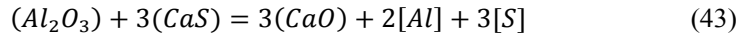


Fig. 48. The composition of OX CaS inclusions in heat 62078 samples, projected on Al_2O_3 –CaO–MgO ternary diagrams.

7.3.4 Discussion

The reaction occurring during continuous casting can be written as:



If the compound activities are assumed to be unity, the equilibrium constant for the reaction is:

$$K = a_{[Al]}^2 a_{[S]}^3 \quad (44)$$

The heats of the dataset were classified depending on whether the reaction had proceeded from right to left or not. Mann-Whitney U tests were performed to confirm, whether the medians differed. According to the results, the sulphur content in the mould plays a significant role. As illustrated in Figure 49, a sulphur concentration larger than 10 ppm in the steel melt leads to back-modification of calcium aluminates and leads to Al_2O_3 or spinel inclusions in the hot rolled products. However, the total calcium and total oxygen do not explain the occurrence of the reaction confirmed by Figures 50–51. As a conclusion, the presence of Al_2O_3 or spinel phases in the product samples is not necessarily a sign of reoxidation. Furthermore, the area fractions of Al_2O_3 , CaS or CaO inclusion components in the mould samples do not affect the reaction, as observed in Figures 52–54.

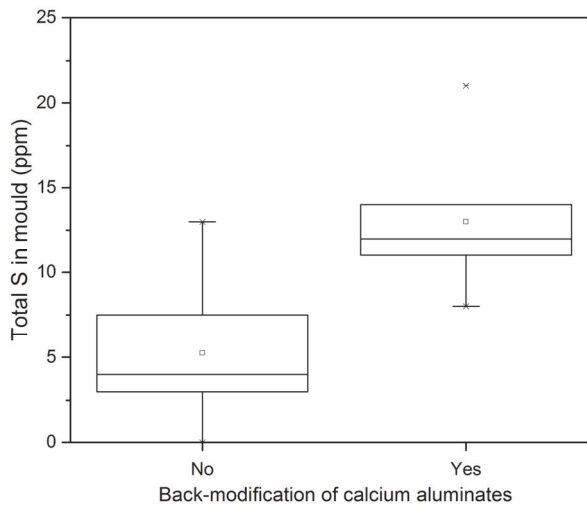


Fig. 49. Total sulphur content in the mould samples.

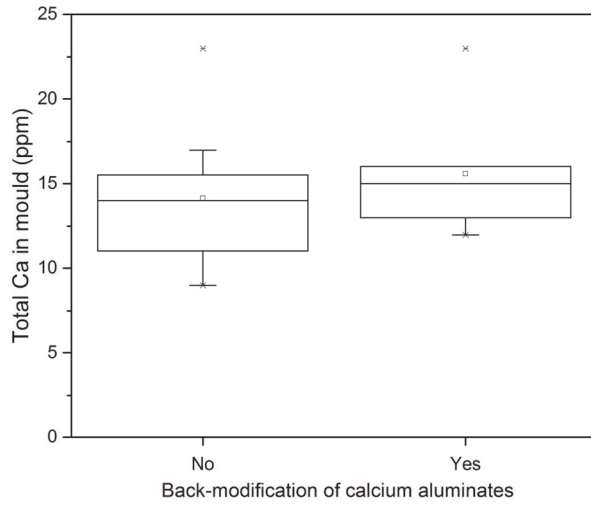


Fig. 50. Total calcium content in the mould samples.

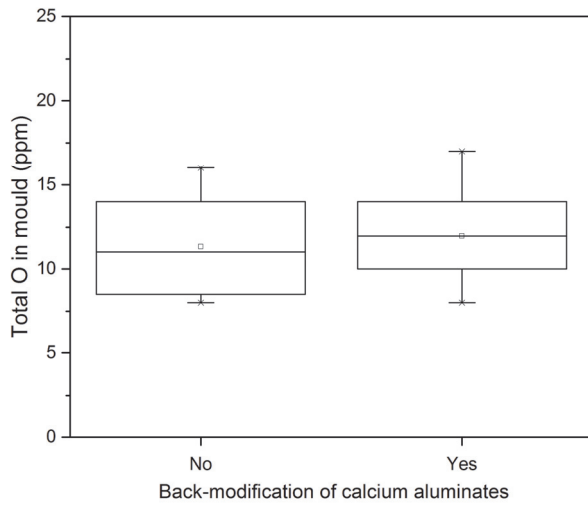


Fig. 51. Total oxygen content in the mould samples.

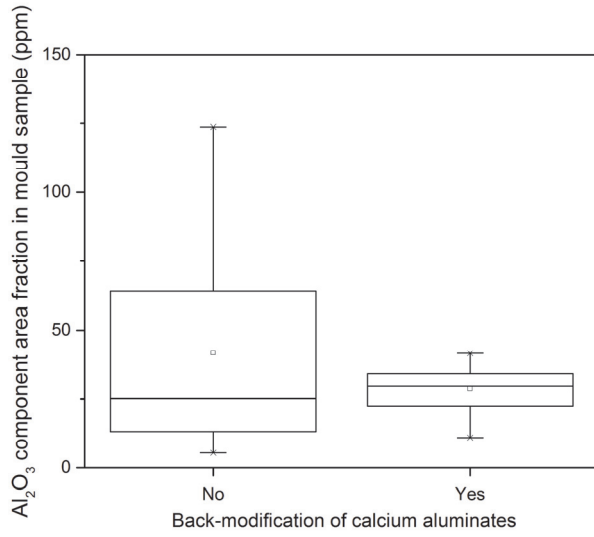


Fig. 52. Al_2O_3 component area fraction in the mould samples.

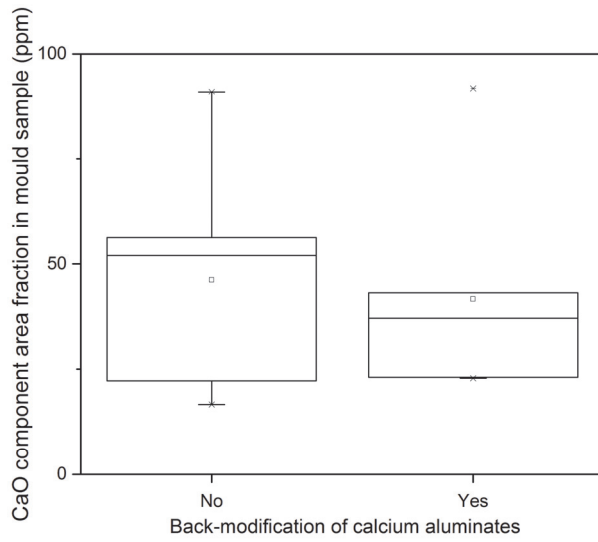


Fig. 53. CaO component area fraction in the mould samples.

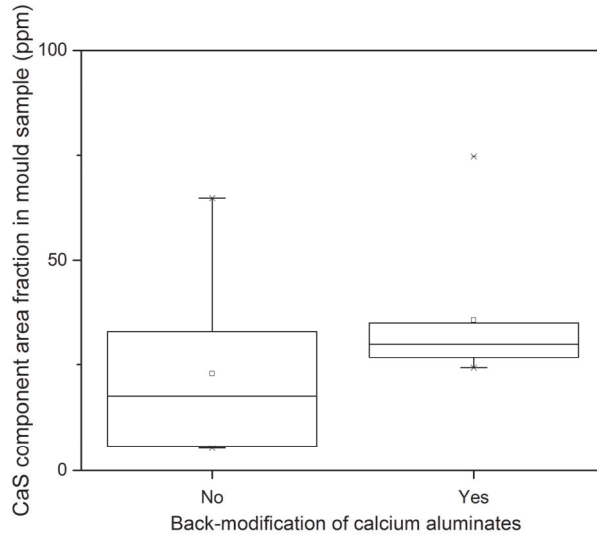


Fig. 54. CaS component area fraction in the mould samples.

Ahlborg et al. (2003) state that the reverse reaction of Equation 43 cannot occur during the sampling of liquid steel, because the solidification of the sample takes place rapidly. According to this reasoning, if $\text{Al}_2\text{O}_3+\text{CaS}$ inclusions would be found in liquid steel samples taken from the mould, we could conclude at least some aluminium oxide would be present in the steel melt, presumably also most of the calcium sulphides. However, Liao et al. (2017) investigated different-sized samplers and observed calcium aluminates with high cooling rates, whereas the transformation into $\text{Al}_2\text{O}_3+\text{CaS}$ inclusions occurred at low cooling rates.

The oxide composition of inclusions may vary greatly from a mould sample to a hot-rolled product. In assessing inclusion composition, the use of Al–Ca–S ternary diagrams can be misleading, mainly because they do not differentiate between Al_2O_3 and spinel inclusions. The reverse reaction direction of $(\text{Al}_2\text{O}_3)+3(\text{CaS})=3(\text{CaO})+2[\text{Al}]+3[\text{S}]$ is dominated by the total sulphur concentration in the steel, as expected by the equilibrium constant of the reaction. With sulphur contents higher than 10 ppm, calcium aluminates are back-modified to alumina and spinel inclusions during casting. However, with decreasing S, and simultaneous adequate calcium treatment of oxides, the formation of Al_2O_3 and spinel during the solidification of the steel can be hindered or even avoided. On the other hand, the area fractions of inclusion components Al_2O_3 , CaS, and CaO did not affect the occurrence of the reverse reaction.

During the formation of CaS, existing liquid calcium aluminates are transformed into solid ones, as stated by Choudhary (2008). For instance, Yang et al. (2017) observed the transformation of liquid calcium aluminates into complex Al_2O_3 –CaO–MgO–CaS inclusions. Verma et al. (2012) pointed out that for spinel modification, the reaction is identical than for alumina identification, with no role of MgO. The most effective way to prevent the back-modification is to reach low sulphur contents, preferably less than 10 ppm.

7.4 Elongation of inclusions during hot rolling

After continuous casting, slabs go through hot rolling, where the thickness of the slab, typically at around 200–300 mm, is reduced to the thickness of hot rolled plate, which is around 10 mm. Hard and non-deformable inclusions do not elongate, but may form cracks during the hot rolling of steel. On the other hand, readily deformable inclusions may form stringers in the finished product, worsening the mechanical properties of the steel. With constantly more demanding product quality requirements, it is important to modify inclusions with a controlled calcium treatment.

It can be clearly observed that some inclusions tend to deform during hot rolling of the steel slab. Undoubtedly, one of the most important factors that determine the tendency to elongate during rolling is the composition of a given inclusion, or more accurately, the phases it is comprised of. The INCA Feature run does not provide information on the geometry of the phases within an inclusion, but many other parameters for each inclusion is stored. Among others, these include the maximum length, coordinates and orientation. The aspect ratio shows the ratio of the maximum and minimum length. For a circle, the aspect ratio is exactly one, and for elongated inclusions, the aspect ratio increases. It should be noted that inclusions that are solid in the liquid steel and show sharp or irregular forms in the finished plate even without elongation, naturally have aspect ratios larger than one.

7.4.1 Fraction of elongated inclusions

In each of the inclusion classes containing oxides, the oxide composition may differ greatly. Therefore, the elongation tendency varies within inclusion classes, depending on the oxide composition. For each inclusion containing oxide phases, the compositional triangle is determined along with the oxide phase fractions

assuming equilibrium cooling. The compositional diagrams are denoted as numbering 1–7, with generally increasing CaO contents, see Figure 10.

In order to assess the effect of oxide composition in each inclusion class, the aspect ratio and the compositional triangle of each inclusion containing oxide phases in the hot rolled product samples were determined. Using the dataset, the percentages of elongated inclusions for each class and compositional triangle were calculated with varying aspect ratio limits of: 1.3, 2, and 3. The results are plotted in Figure 55.

The following conclusions can be made. In the pure oxides class OX, the large values in the first triangle are caused by irregular alumina inclusions. In general, the $OX < CaS$ inclusions are slightly more elongated than the $OX > CaS$ inclusions, indicating an increased tendency towards elongation when CaS phase is dominant. According to the dataset, the most prone to elongate are the OX MnS inclusions. However, their number in the hot rolled plates is relatively low. OX CaS TiN and OX CaS MnS TiN both show similar trends as the OX CaS classes: i.e. an increasing aspect ratio with an increasing CaO content. The OX CaS MnS inclusions elongate almost irrespective of the oxide compositional triangle. It is therefore reasonable to assume that the sulphide phases determine the elongation tendency, especially if the oxide phases are enclosed inside the sulphide phases. In the figure, it can be clearly seen that in each inclusion class, inclusions with oxide phases located in triangles 6 and 7 are the most elongated. In conclusion, abundant calcium treatment should be avoided, because increased CaO content in the inclusions causes excess elongation.

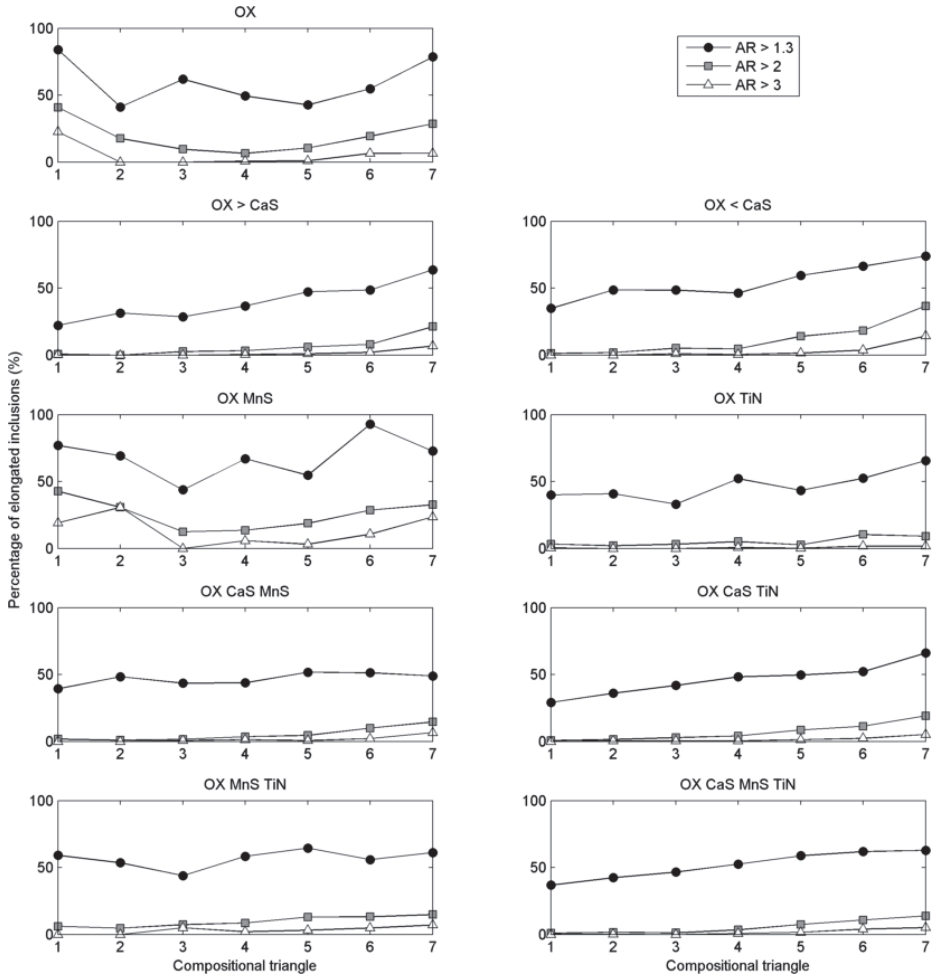


Fig. 55. Fractions of elongated inclusions with various aspect ratio thresholds.

7.4.2 The effect of CaS and MgO on the tendency to elongate

The previous approach did not take into account the effect of CaS and MgO on the aspect ratio of the inclusions. In Figure 56, the aspect ratios of all inclusions belonging to OX, OX CaS, and CaS classes in the hot rolled products are plotted as a function of CaS content of the inclusion. Further, the graphs are divided into two sections, whether the inclusion contains less or more than 5 mol.% of MgO component, showed on left and right column, respectively.

Pure aluminium oxides are irregular by nature, and as seen in the figure, they do not contain CaS at all. Otherwise, inclusions in compositional diagrams 1–3 are not prone to elongate, and they usually contain more than 5 mol.% MgO component, presumably in a spinel phase. Some inclusions in triangles 4 and 5 are slightly elongated with aspect ratio values around 5.

From compositional triangles 6 and 7, the following observations can be made. Inclusions with no CaS are more prone to elongate, compared to the ones containing CaS up to 20 mol.%. The most elongated inclusions contain 60–80 molar percent CaS in these graphs. The most elongated inclusions lie in triangle 7, containing less than 5 mol.% MgO. This is in contrast to the findings by Wang et al. (2014), who prevented the occurrence of stringers through the treatment of inclusions in the CaO–CaS system.

It is clear that inclusions located in compositional triangles 6 and 7 are more prone to elongate than others. In addition, the effect of the CaS content on inclusion elongation tendency is not linear.

It should be noted that the low melting $\text{Al}_2\text{O}_3\text{--CaO(–MgO)}$ inclusions in the C12A7–CA–MgO triangle are not the most elongated oxide inclusions in the hot rolled product. This can be considered the target composition for oxides with calcium treatment. In addition, the CaS content has little effect on the elongation of the low melting $\text{Al}_2\text{O}_3\text{--CaO(–MgO)}$ inclusions.

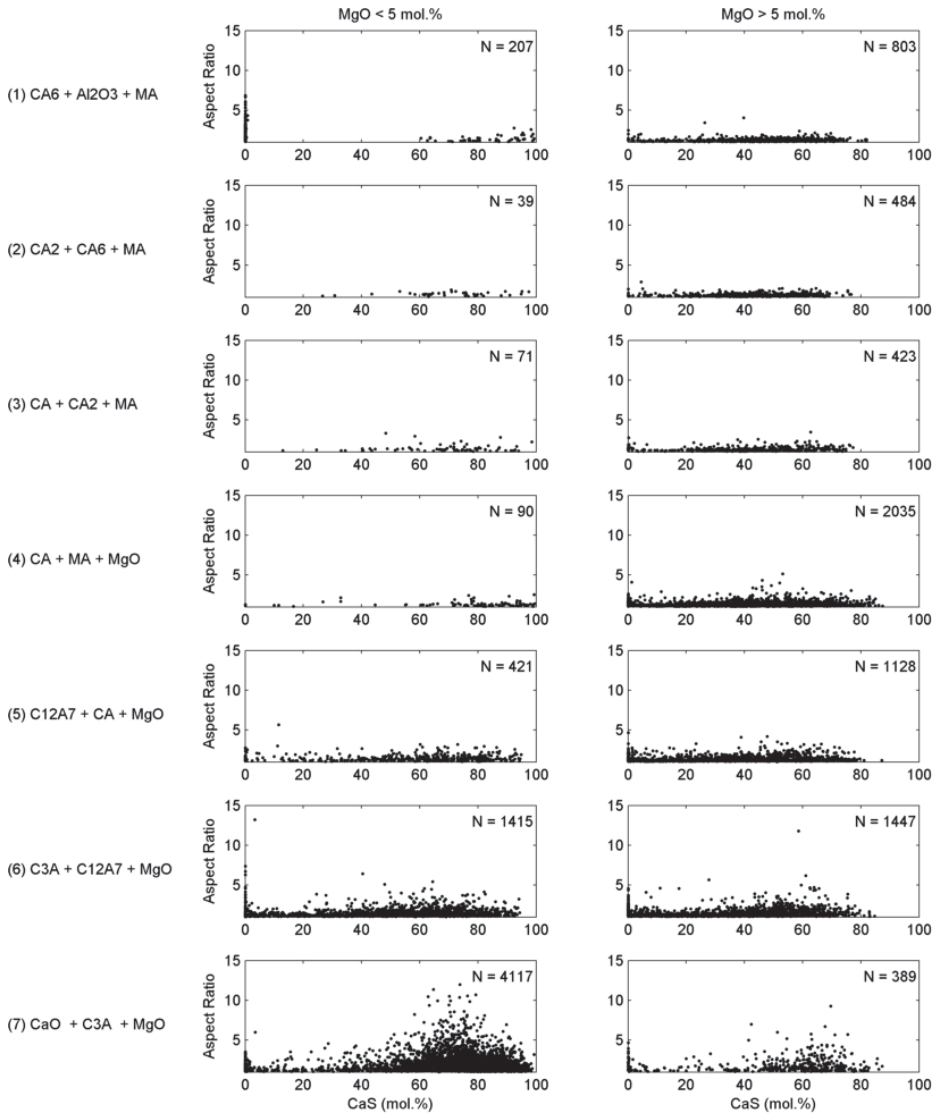


Fig. 56. Aspect ratios of OX, OX CaS, and CaS classes, divided into oxide phase triangles and MgO contents.

In the OX CaS MnS class illustrated in Figure 57, the most elongated are the inclusions with an oxide composition in the fourth compatibility triangle, with an MgO over 5 mol.% and CaS content below 40 mol.%. In this case, the MnS fraction is undoubtedly high. Similarly to the OX CaS inclusions, heavily elongated

inclusions are also found in the seventh compatibility triangle, with CaS contents of approximately 80 mol.%. It is clear that the occurrence of the CaO component in the inclusions should be prevented by applying a moderate calcium treatment.

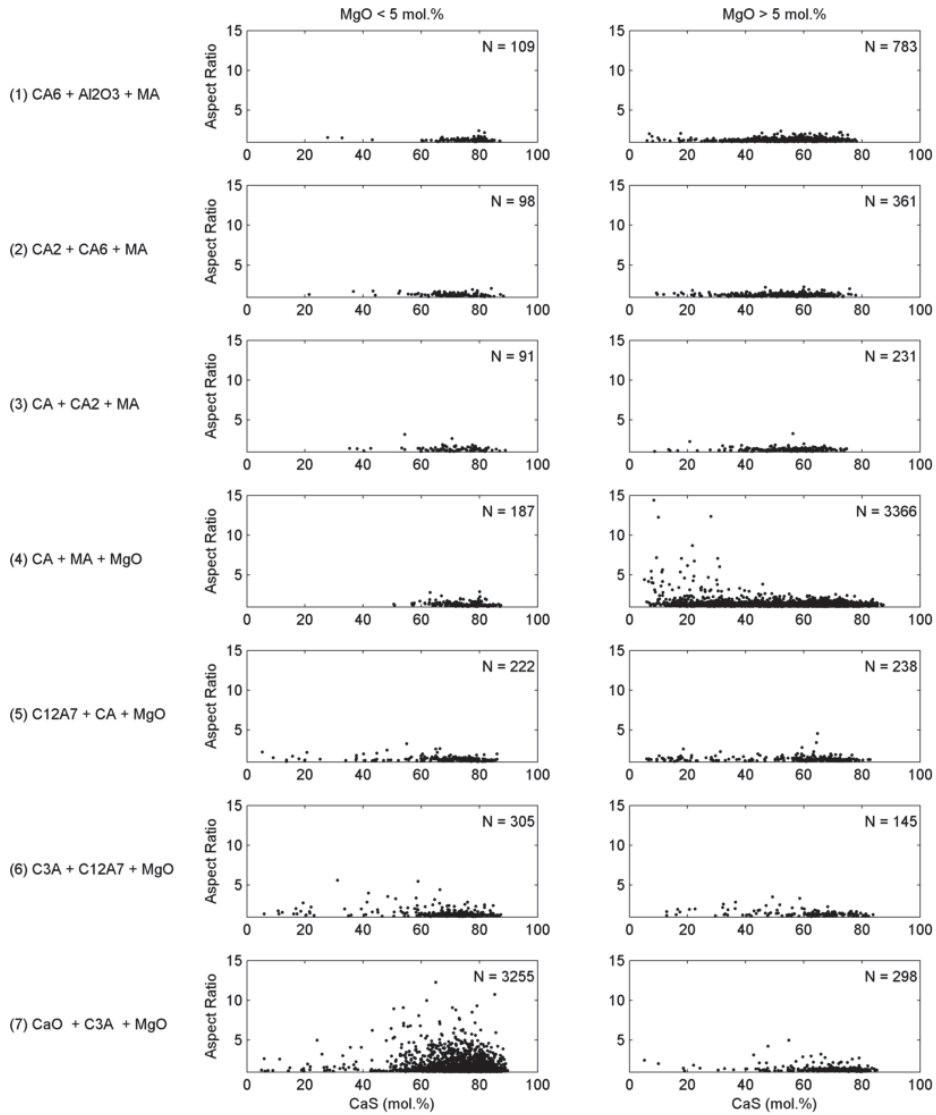


Fig. 57. Aspect ratios of OX CaS MnS inclusions, divided into oxide phase triangles and MgO contents.

The number of detected OX CaS TiN inclusions with MgO contents lower than 5 mol.% were considerably lower than inclusions with a higher MgO content, as seen in Figure 58. The largest number of OX CaS TiN inclusions was found in the fourth compatibility triangle, indicating the tendency for the occurrence of TiN together with the spinel phase. The most elongated OX CaS TiN inclusions are found in the seventh triangle, with MgO contents less than 5 mol.%.

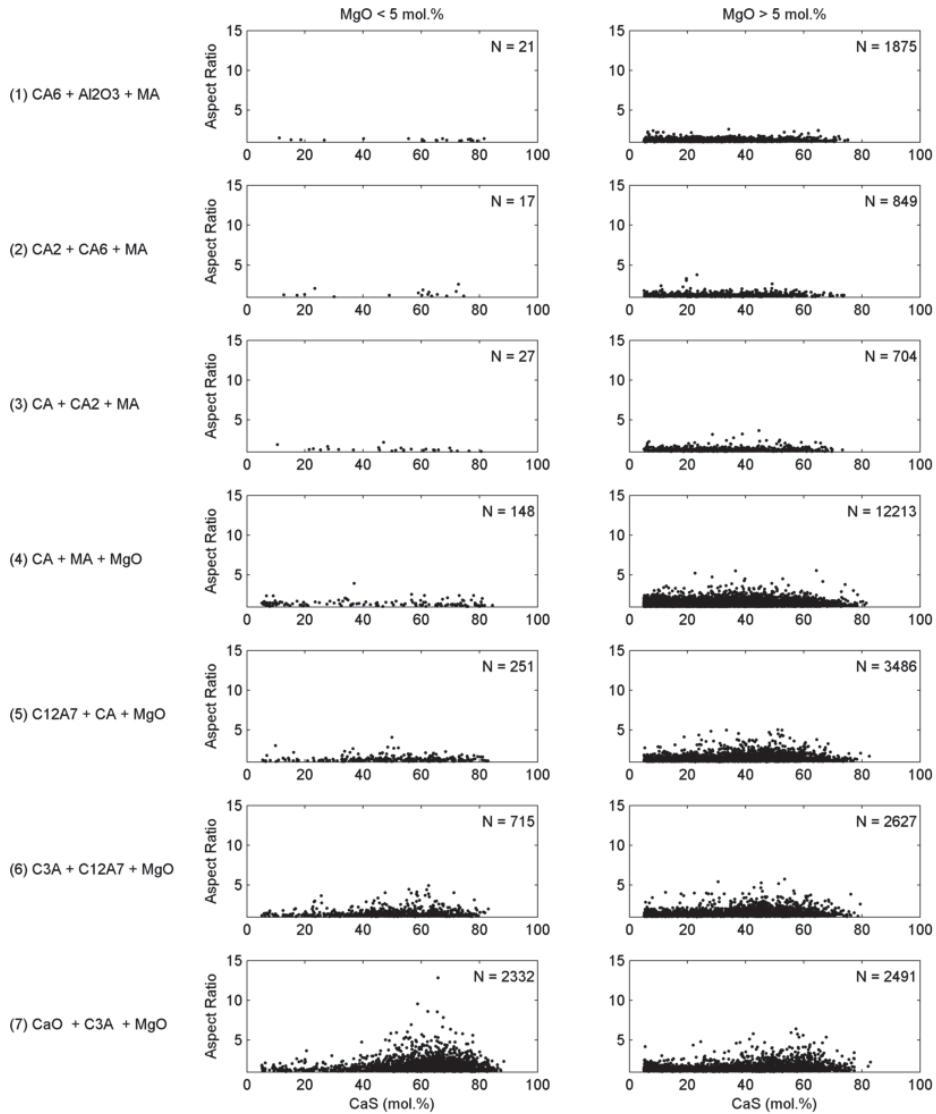


Fig. 58. Aspect ratios of OX CaS TiN inclusions, divided into oxide phase triangles and MgO contents.

In the OX CaS MnS TiN class presented in Figure 59, the most elongated are inclusions with an oxide composition in the fourth compatibility triangle, an MgO over 5 mol.% and CaS content below 30 mol.%. Similarly to the OX CaS MnS inclusions, the MnS fraction is assumedly high in the elongated inclusions. Some

elongated inclusions are also found in the seventh compatibility triangle, with CaS contents in the range of 50–80 mol.%.

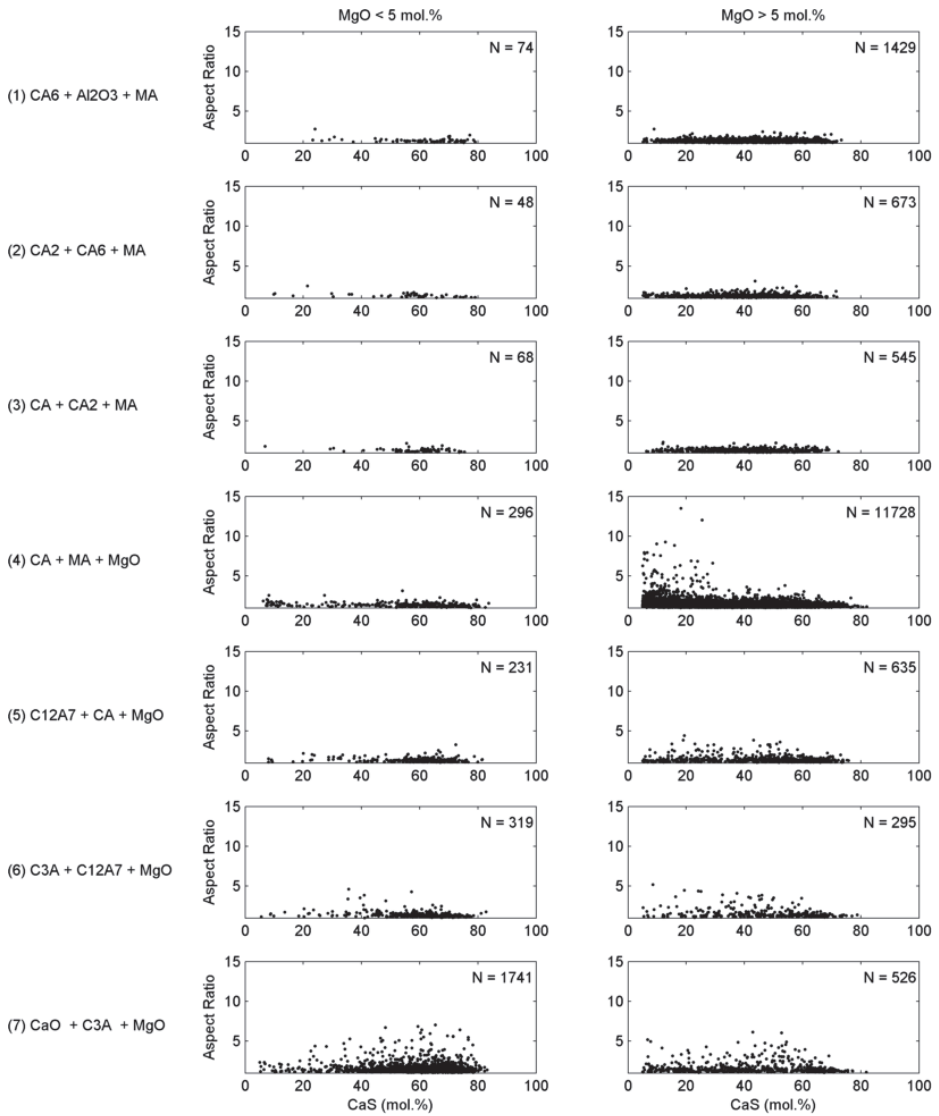


Fig. 59. Aspect ratios of OX CaS MnS TiN inclusions, divided into oxide phase triangles and MgO contents.

7.4.3 Ternary contours

The effect of MgO was not fully disclosed in the above graphs. In order to clarify the effect of MgO, ternary contours of aspect ratios were constructed for the classes containing the largest number of inclusions, namely OX, OX > CaS, OX < CaS, and OX CaS TiN. Inclusions with lengths over 3 μm were selected for the construction of the plots.

Inclusions enclosing a spinel phase, i.e., where the oxide composition is located above the CA–MgO line strongly resist the deformation during hot rolling. Spinel inclusions are hard and nondeformable, and may act as cavity nucleation sites during hot rolling, even when accompanied with some sulphides. As disclosed in the ternary diagrams, it is clearly observed that the effect of the MgO content is not linear. Not taking into account OX inclusions, the most elongated inclusions are in the CaO–C3A–MgO triangle.

OX inclusion class

Aluminium oxides without MgO are irregularly shaped, which shows as larger aspect ratios in the Al_2O_3 corner of Figure 60. Calcium aluminates with a C3A composition are often elongated, irrespective of the MgO content, as seen on larger aspect ratios on the C3A–MgO line. The effect of MgO on elongation of C12A7 calcium aluminate is not linear.

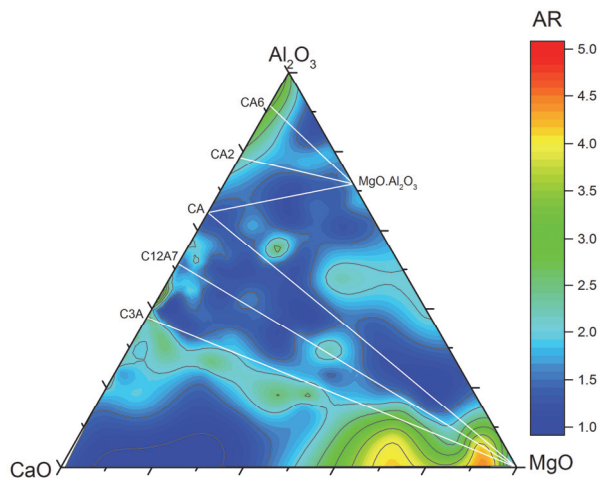


Fig. 60. Contour lines of aspect ratios of inclusions in the OX class.

OX > CaS inclusion class

No clear trends above the C12A7–MgO line are observed, where aspect ratios vary quite randomly between values of 1–2. However, inclusions located in the CaO–C3A–MgO triangle are often severely elongated, as observed in Figure 61. Local maxima in aspect ratios are found in three locations: in the CaO corner, in between CaO and C3A compositions, and on the C3A–MgO line.

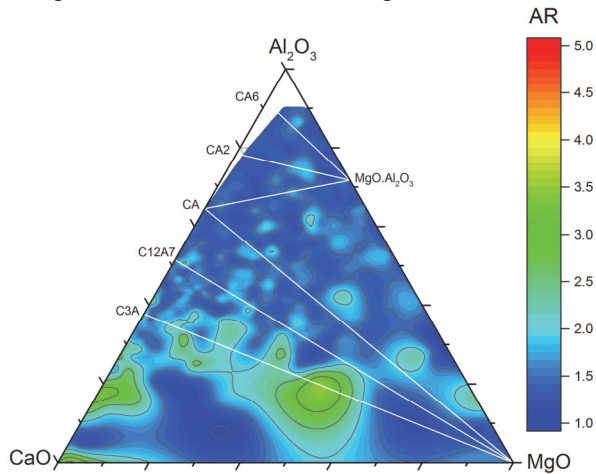


Fig. 61. Contour lines of aspect ratios of inclusions in the *OX > CaS* class.

OX < CaS inclusion class

Compared to the inclusions with a lower oxide fraction, *OX < CaS* inclusions are more likely to elongate, as seen in Figure 62. Calcium aluminates C3A, C12A7, and CA often have aspect ratios around 2. However, data from the MgO corner are missing; no such inclusions were observed in the dataset. The most elongated inclusions are comprised of a mixture of CaO, C3A and MgO, and seen as heavily deformed inclusions with aspect ratios over 4.

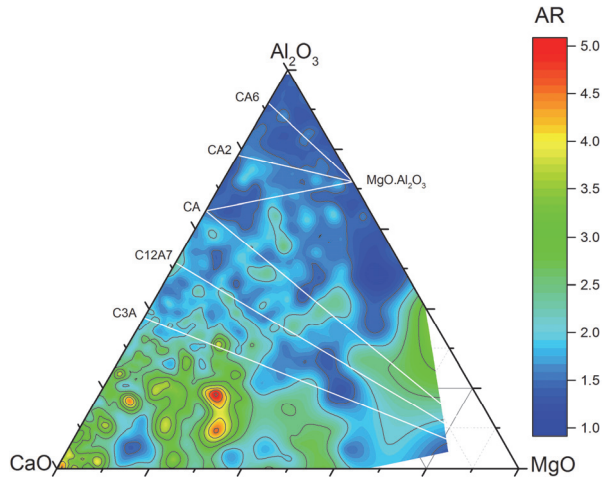


Fig. 62. Contour lines of aspect ratios of inclusions in the OX < CaS class.

OX CaS TiN inclusion class

This inclusion class is the most prevalent in the hot rolled products. The inclusions often have an aspect ratio larger than 2, except for spinels, alumina, and inclusions in the CA–CA2–MA triangle, as seen in Figure 63. Again, inclusions in the CaO–C3A–MgO triangle are the most elongated. Maxima are found near the CaO corner. Inclusions with a C3A oxide composition are elongated, especially when the MgO content is less than approximately 40 wt.%. Other calcium aluminates C12A7 and CA are the most elongated with MgO contents of around 30 wt.%.

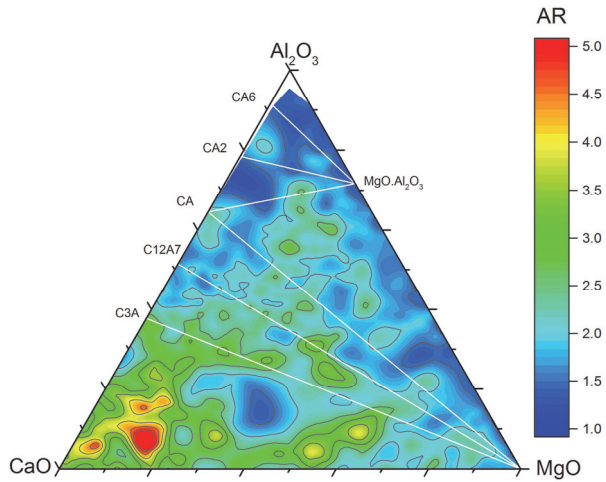


Fig. 63. Contour lines of aspect ratios of inclusions in the OX CaS TiN class.

7.4.4 The effect of thickness location

In order to evaluate the effect of the location of the inclusion in the vertical direction of the hot rolled product, box plots were constructed for each oxide compositional triangle. Further, the product thickness was divided into three equally sized sections: upper, middle, and lower, denoted in the graphs with U, M, and L, respectively.

In conclusion, OX inclusions with compositions located in triangles 5–7 were less elongated in the lowest vertical section of the product. For the other inclusion classes, no clear differences were observed.

OX inclusion class

Oxides in compositional triangle 1, i.e., Al_2O_3 –CA6–MA, had the large aspect ratios because of irregular alumina inclusions. Otherwise, pure oxide inclusions did not tend to elongate easily. As seen in Figure 64, the inclusions in triangles 6 and 7 are the most elongated.

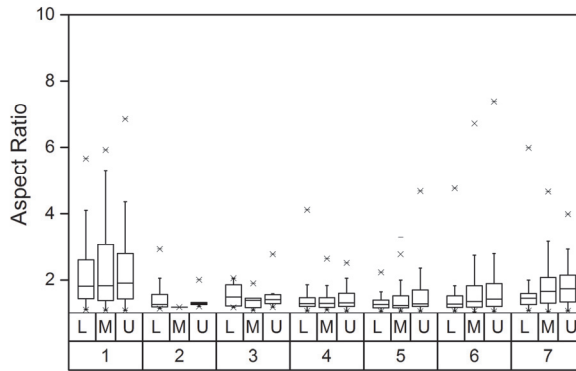


Fig. 64. Aspect ratios of inclusions in the OX class, grouped by oxide compatibility triangle and location on the rolled product.

OX > CaS inclusion class

Inclusions tend to elongate more with an increasing CaO content, readily seen in Figure 65. The most elongated inclusions were found in the seventh triangle, i.e., CaO–C3A–MgO inclusions. Triangles 5 and 6 were also comprised of liquid inclusions, and evidently, elongated inclusions were observed. Unlike pure aluminium oxides, the inclusions belonging to the first triangle were not elongated or irregular, when accompanied with CaS.

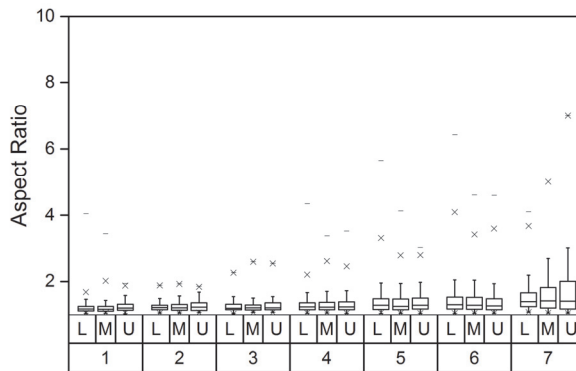


Fig. 65. Aspect ratios of inclusions in the OX > CaS class, grouped by oxide compatibility triangle and location on the rolled product.

OX < CaS inclusion class

In this inclusion class an increased CaS content has led to slightly more elongated inclusions than in the previous inclusion class. In Figure 66, it can be observed that the most elongated inclusions are located in the seventh triangle.

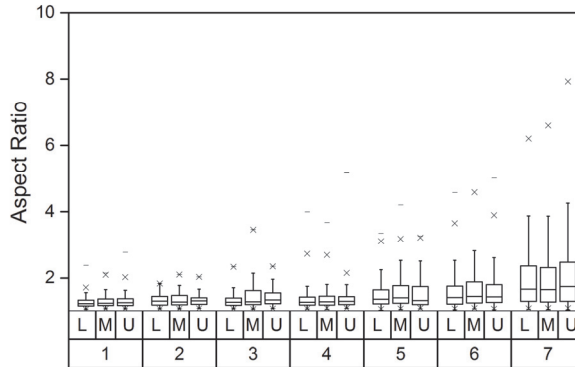


Fig. 66. Aspect ratios of inclusions in the OX < CaS class, grouped by oxide compatibility triangle and location on the rolled product.

OX CaS TiN inclusion class

OX CaS TiN is the most prevalent inclusion class in the hot rolled products. As observed in Figure 67, the aspect ratios are generally lower than in the OX CaS classes. It may be concluded that the presence of TiN hinders the elongation. Compared to ternary contours, lower aspect ratios can be observed. Here, inclusions with lengths 1–3 are also taken into account.

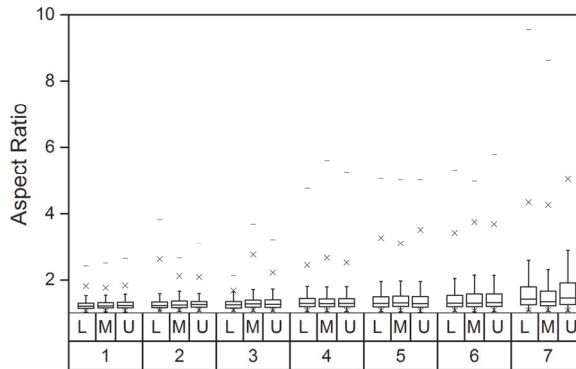


Fig. 67. Aspect ratios of inclusions in the OX CaS TiN class, grouped by compatibility triangle and location on the rolled product.

7.5 Oxide–sulphide stringers

As a case study, the inclusion classification method and the data treatment was utilised in order to enhance the investigation of oxide–sulphide stringers. It is well known that oxide–sulphide stringers are detrimental to the mechanical properties of steel, similarly to elongated manganese sulphides. It is possible to identify stringers from available inclusion data, and to calculate the phase composition of each inclusion. Further, it is possible to estimate the size and composition of original, unfragmented inclusions in the slab before hot rolling. In this context, “original inclusion” refers to an assumed single inclusion in the slab, which has fragmented into several smaller inclusions, i.e., a stringer. The size of the original inclusion corresponds to the total estimated volume of the stringered inclusions. Furthermore, the composition of the original inclusion is a weighted average of the phase fractions of inclusions in the stringer. The aims of this study were to determine the effect of the vertical location and the composition of inclusions on the occurrence of stringers, and to determine the inclusions most prone to form oxide–sulphide stringers during hot rolling.

7.5.1 Parameters

The following parameters were adopted in order to find and analyse stringers in the hot rolled product samples. The oxide–sulphide stringers were located by a

MATLAB script that handles Excel spreadsheets exported from the INCA Feature software. In Table 20, the parameters used in this case are presented. The parameters were chosen so that they eliminate other than oxide-based stringers, such as manganese sulphides. In addition, the stringers must be horizontal, i.e., assumedly formed during the hot rolling of the steel. Compared to the ASTM E45 standard, the threshold values differ slightly. In the ASTM standard, the maximum distance between inclusions is 40 μm , and the maximum vertical offset is 15 μm .

Table 20. Parameters for stringer recognition.

| Parameter | Threshold value | Note |
|-----------------------------------------------------------------------|-----------------------|-----------------------------------------------------------------------------|
| Number of inclusions | ≥ 3 | After deducting inclusions which contain TiN + MnS in total over (90 mol.%) |
| Horizontal distance between inclusions | $< 30 \mu\text{m}$ | |
| Average horizontal distance between inclusions | $< 20 \mu\text{m}$ | |
| Vertical distance between inclusions | $< 8 \mu\text{m}$ | |
| At least one inclusion must contain oxides | $> 10 \text{ mol.}\%$ | |
| Calculated TiN + MnS phase fractions in undeformed inclusion in total | $< 50 \text{ mol.}\%$ | |
| Stringer aspect ratio OR | > 8 | Eliminates clusters and inclined stringers |
| R ² value of linear fit of inclusion coordinates AND | > 0.9 | |
| Stringer aspect ratio | $2 < \text{AR} < 8$ | |

7.5.2 Assessing the characteristics of an unfragmented inclusion

For each inclusion in a stringer, the volume is estimated. The inclusions are assumed to be ellipsoids with the major axis parallel to the rolling direction, as presented by Fuhr et al. (2007) The observed inclusion area is considered the area of a projection of an ellipsoid. Further, the aspect ratios for the observed inclusion and the approximation are assumed equal. Equations 45–47 and Figure 68 present the procedure to calculate the volume of each inclusion in a stringer.

$$A_1 = A_{1A} \quad (45)$$

$$\frac{L_1}{B_1} = \frac{L_{1A}}{B_{1A}} \quad (46)$$

$$V_1 = V_{1A} = \frac{4}{3}\pi \frac{L_{1A}}{2} \left(\frac{B_{1A}}{2}\right)^2 \quad (47)$$

where

A_1 is the observed area of an observed inclusion,

A_{1A} is the area of an ellipsoid,

L_1 is the length of an observed inclusion,

B_1 is the breadth of an observed inclusion,

L_{1A} is the length of an ellipsoid,

B_{1A} is the breadth of an ellipsoid,

V_1 is the approximated volume of an observed inclusion,

V_{1A} is the volume of an ellipsoidal inclusion.

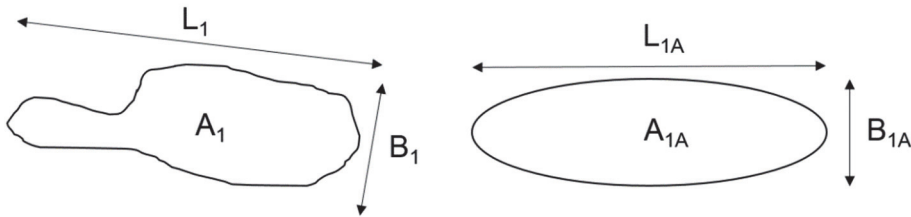


Fig. 68. Geometrical approximation of inclusion size.

Further, we can estimate the volume of an unfragmented inclusion in the slab as the sum of all inclusion volumes in the stringer. For convenience, the size of the original inclusion is presented as a diameter of a sphere with the same volume. The composition of the original inclusion is – independent of its shape – the average phase composition of stringer inclusions, weighted with the volumes of the stringered inclusions.

7.5.3 Results

In the figures, the vertical thickness location is converted into a dimensionless number, where 0% denotes the upper side, and 100% denotes the lower side of the product. Most of the long stringers, with total lengths over 100 μm , locate on the upper half of the rolled product. As can also be seen in Figure 69, shorter stringers are more evenly dispersed throughout the thickness of the product. In the dataset,

the longest stringers have total lengths of over 200 μm . A possible explanation for the occurrence of the longest stringers is the flotation of liquid inclusions upwards in the melt during casting, corresponding to the formation of inclusion bands.

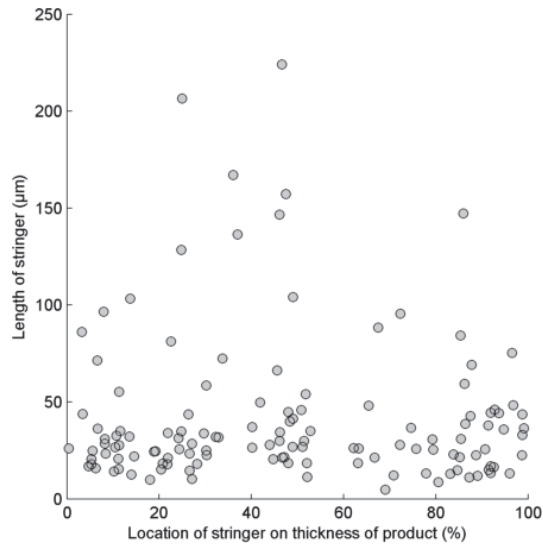


Fig. 69. Length of stringer as a function of the location of the stringer on the thickness of product.

When we examine the number of stringers as a function of the thickness location in Figure 70, it can clearly be seen that it is consistent with the previous figure. The longest stringers comprised of nearly 20 inclusions. On the lower side of the hot rolled product, only one stringer including more than ten inclusions can be observed.

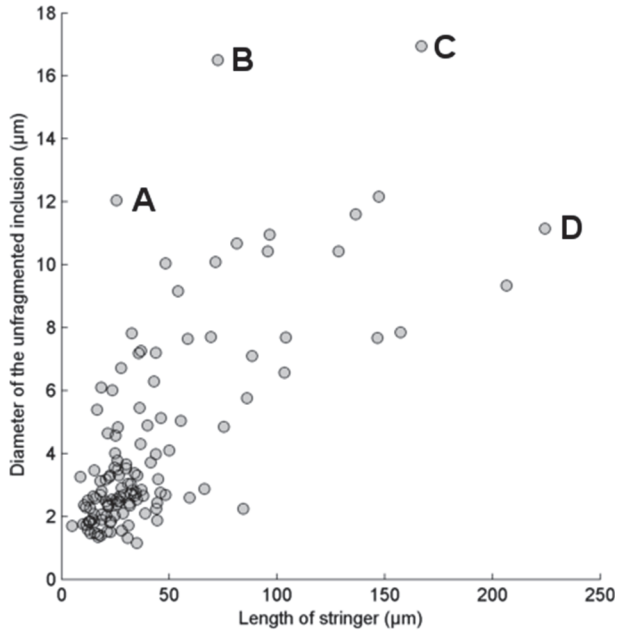


Fig. 71. Length of stringers vs. the diameter of unfragmented inclusions.

The stringer A presented in Figure 72 includes a large OX < CaS inclusion with an oxide composition between C12A7 and C3A, and two smaller inclusions. Owing to the small sizes of the other two inclusions, the original calculated inclusion size is extremely close to the diameter of the first inclusion in the stringer. It should be noted that the first inclusion itself is hardly deformed during hot rolling, though still being a part of a stringer.

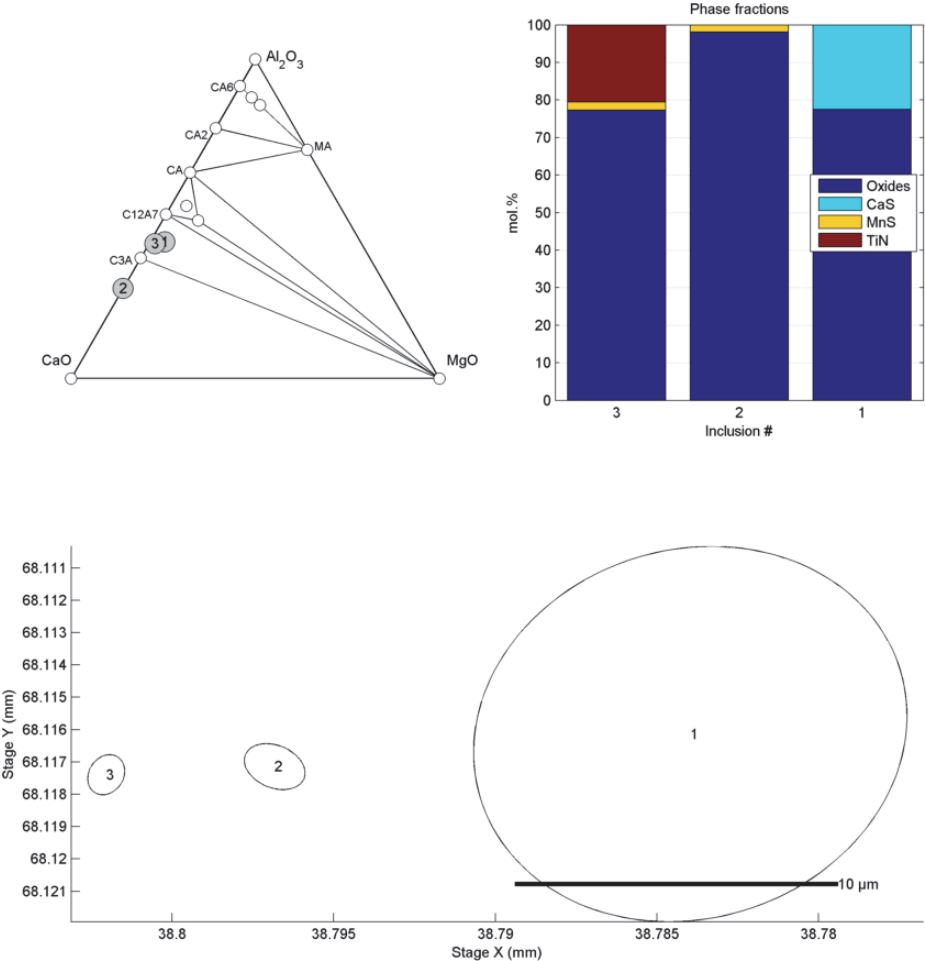


Fig. 72. Stringer A, calculated composition and geometrical visualisation.

The oxide compositions of inclusions in stringer B are located in the sixth compatibility triangle, as seen in Figure 73. The low-melting inclusions are slightly elongated and have formed a stringer with a length of 70 μm . The largest inclusion in the stringer contains more MgO phase than the others, and is not very elongated. According to the volume estimation, the stringer has formed from an original inclusion with a diameter of 17 μm .

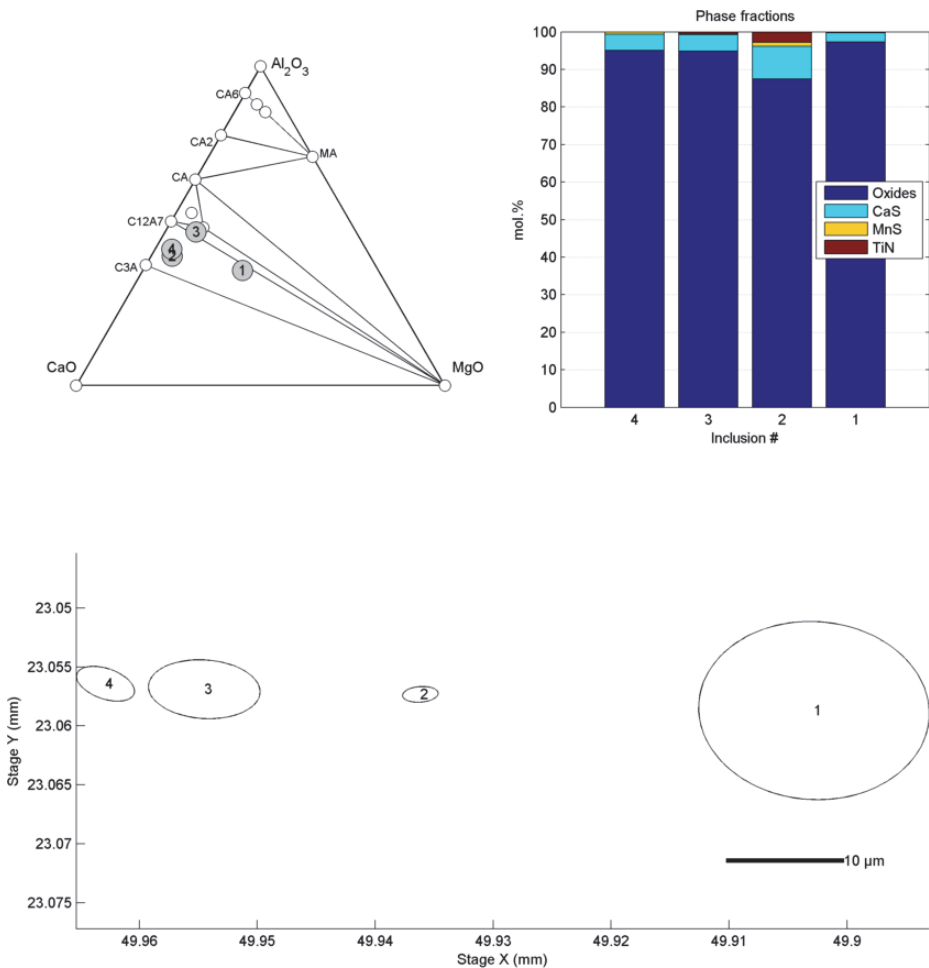


Fig. 73. Stringer B, calculated composition and geometrical visualisation.

Stringer C presented in Figure 74 has a total length of 150 μm . Inclusion no. 7 is an elongated calcium sulphide, but all the others contain a marked fraction of oxide phases, located inside the sixth compatibility triangle. The original inclusion diameter was estimated to be 17 μm in the calculation procedure.

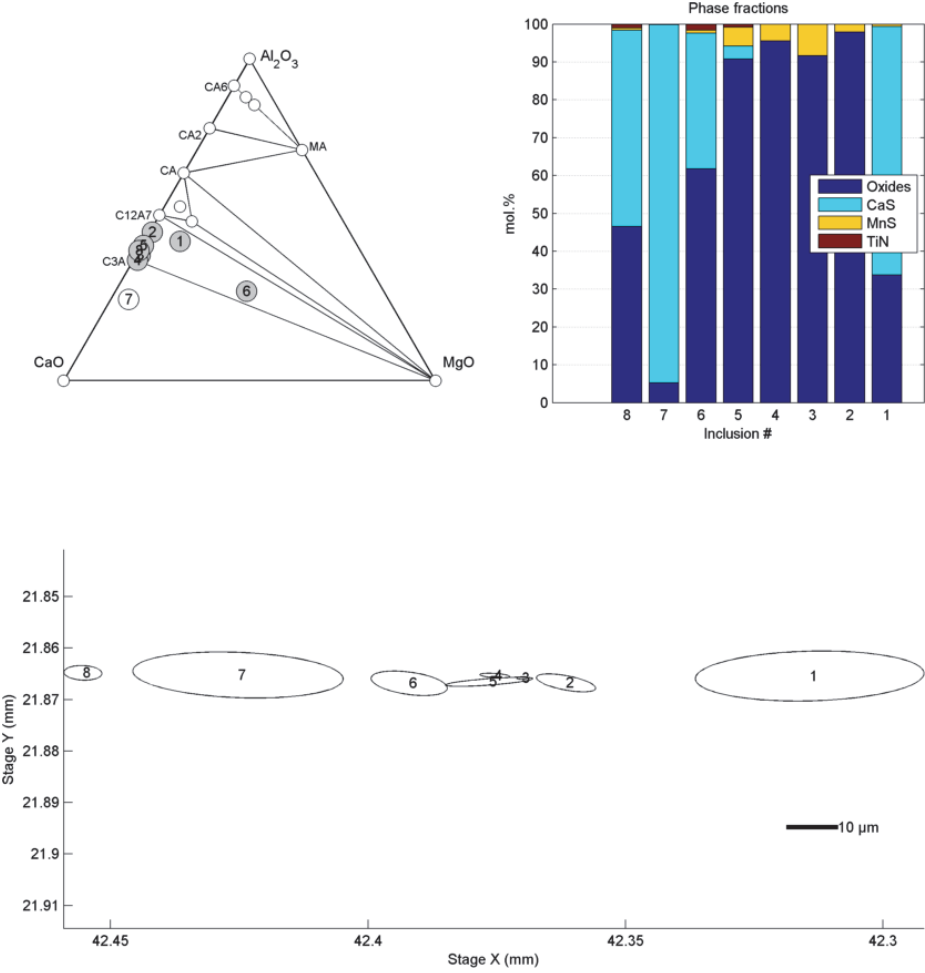


Fig. 74. Stringer C, calculated composition and geometrical visualisation.

Stringer D is heavily elongated, with a total length over 200 μm , as observed in Figure 75. All the inclusions contain oxide phases in the range of 80–100 mol.%. For the most part, the oxide compositions are located in the seventh triangle. The inclusions are quite small; therefore, the estimated volume of the original inclusion is only 11 μm .

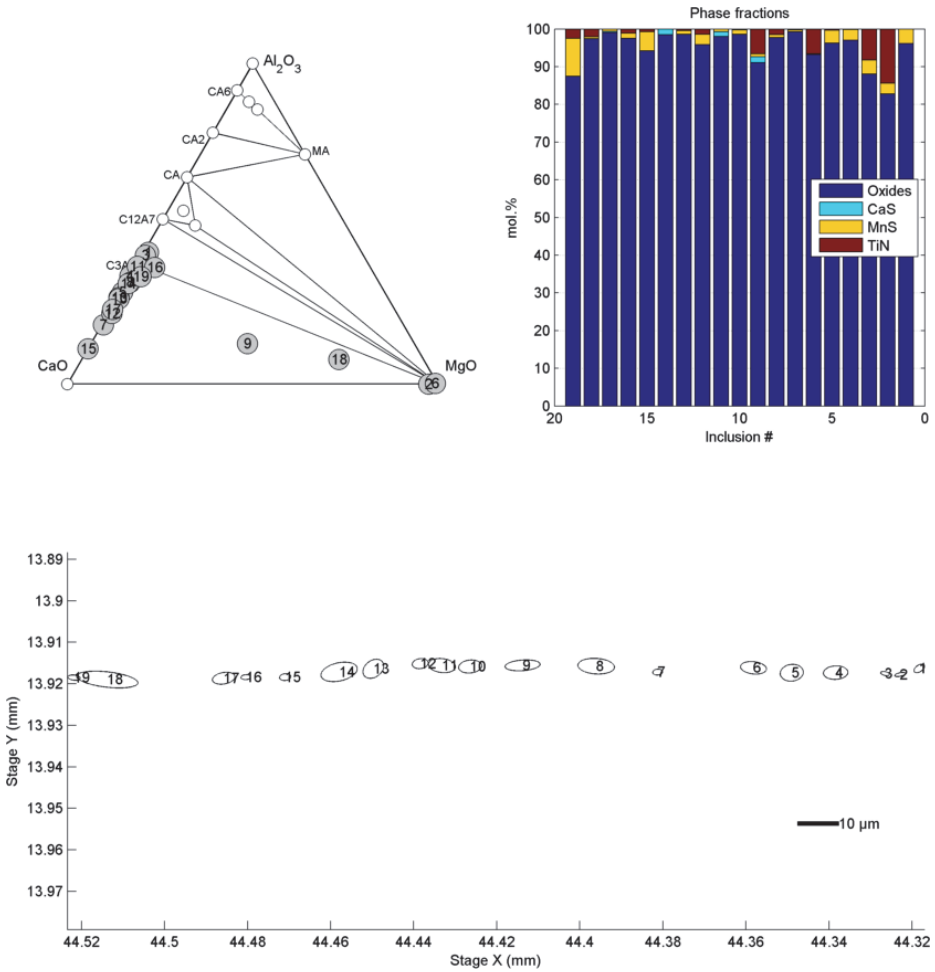


Fig. 75. Stringer D, calculated composition and geometrical visualisation.

Inclusion phase fractions vs. thickness location

The composition of unfragmented inclusions before hot rolling was calculated according to the procedure presented in Chapter 7.5.2. Here, the correlation between the fractions of aluminium oxide, calcium aluminates, and calcium sulphides and the vertical location of stringers on the hot rolled product is assessed. As observed in Figure 76, inclusions with notable aluminium oxide contents were concentrated at approximately 20% and 80% of the thickness on the hot rolled product. Presumably, the columnar-to-equiaxed transition (CET) zones are located in these regions in the slab, and solid inclusions could have been pushed into the zone by the dendritic solidification fronts. Accordingly, Yang et al. (2014) observed large Al_2O_3 -rich agglomerates on $\frac{1}{2}$ and $\frac{1}{4}$ thicknesses of slabs.

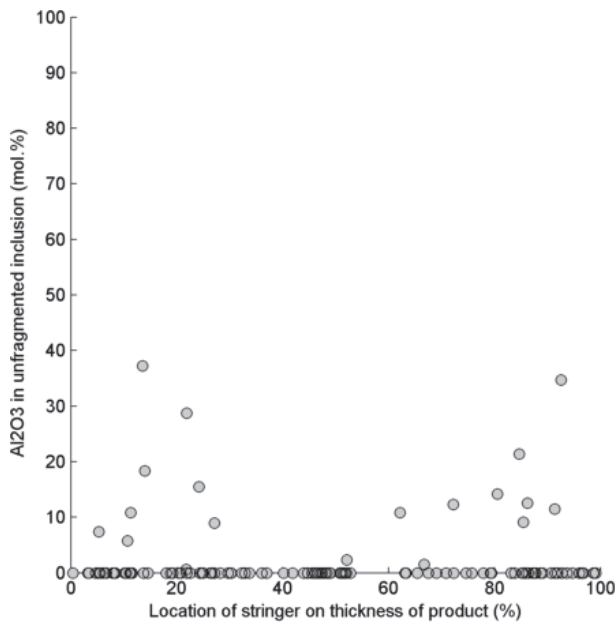


Fig. 76. Aluminium oxide content in an unfragmented inclusions vs. the location of the stringer.

The effect of the calculated calcium aluminate fraction in the unfragmented inclusions is presented in Figures 77–79, depicting CA, C12A7, and C3A phases. Calcium aluminates with a composition close to C12A7 are fully liquid at steelmaking temperatures, while pure CA and C3A compounds are solid. With high

C12A7 contents, inclusions have formed stringers on the upper half of the hot rolled product. Stringers with C3A contents are often found near the centreline, possibly caused by the original inclusions pushed by the solidifying steel front during casting.

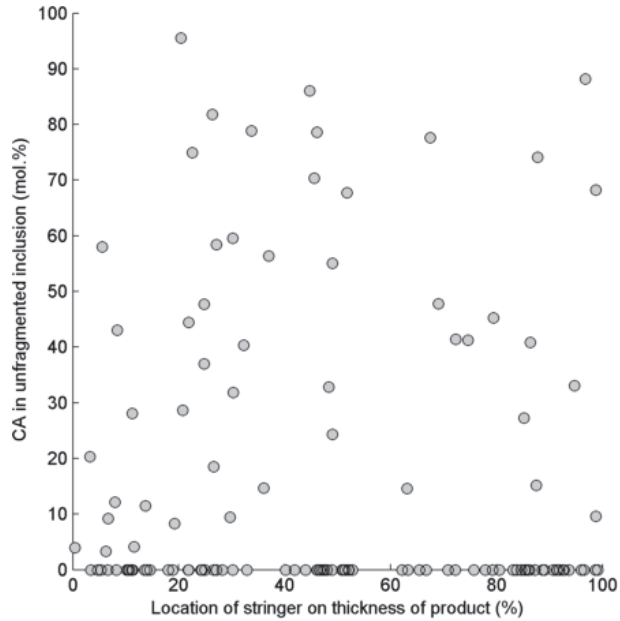


Fig. 77. CA content in an unfragmented inclusions vs. the location of the stringer.

CaO–CaS stringers were observed in the lower section of the product, which were seen as high concentration of both CaO and CaS inclusions in the 80–100% thickness of the product in Figures 80 & 81. Otherwise, stringers containing calcium sulphides were quite evenly distributed throughout the sample thickness. The calcium sulphide phases usually precipitate on the surface of existing inclusions, which easily explains the even distribution of calcium sulphides.

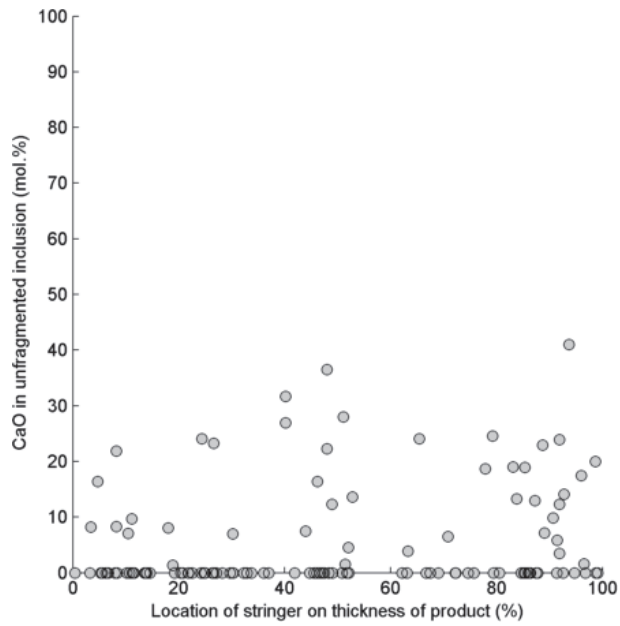


Fig. 80. CaO content in an unfragmented inclusion vs. the location of the stringer.

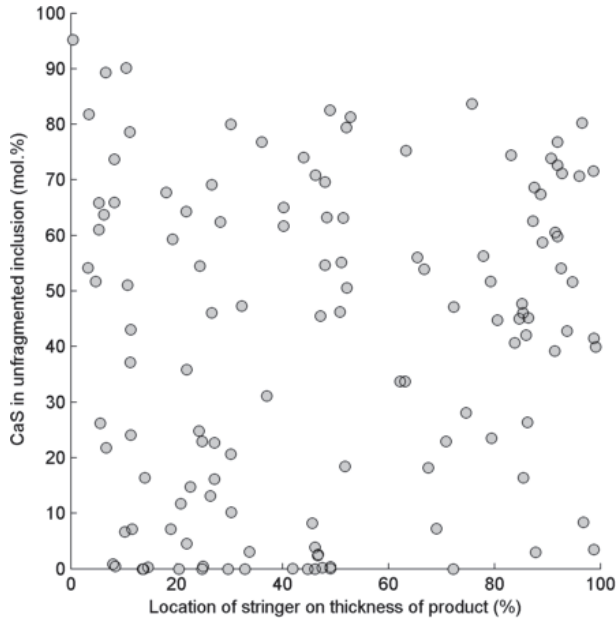


Fig. 81. CaS content in an unfragmented inclusion vs. the location of the stringer.

Inclusion phase fractions vs. stringer length

Here, the correlation between fractions of aluminium oxide, calcium aluminates, calcium oxide, and calcium sulphide in the original inclusions and the thickness location of stringers on the hot rolled product is assessed. According to Figure 82, stringers containing an aluminium oxide phase are typically short, and are under 50 μm in length.

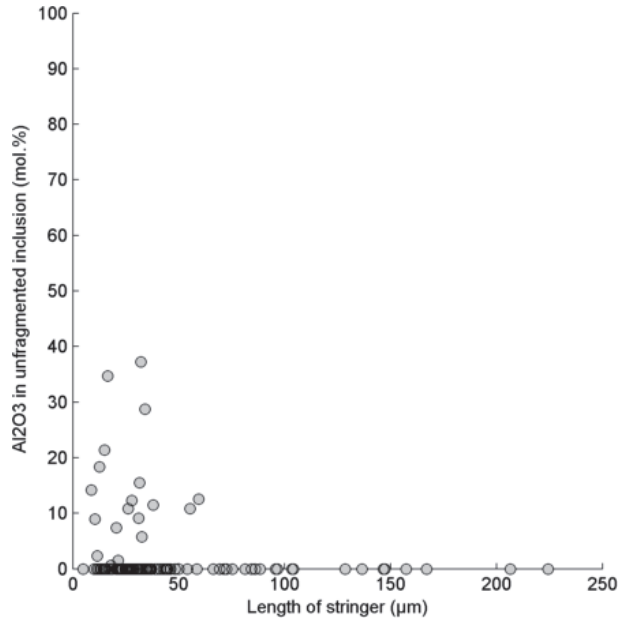


Fig. 82. Aluminium oxide content in an unfragmented inclusion vs. the stringer length.

Stringers under 100 µm often contained CA calcium aluminate phases, illustrated in Figure 83. However, stringers with lengths over 150 µm contained marked amounts C12A7 or C3A phases, revealed in Figures 84 & 85. In conclusion, oxide inclusions with a composition of C3A–C12A7 are more prone to form stringers, compared to the C12A7–CA composition.

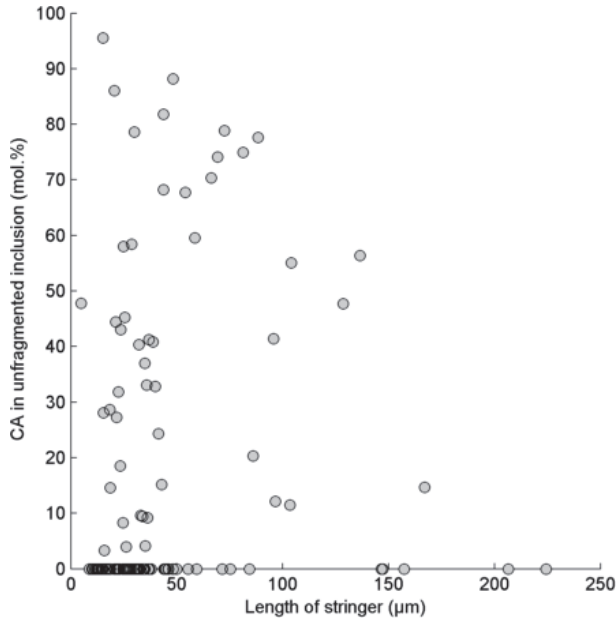


Fig. 83. CA content in an unfragmented inclusion vs. the stringer length.

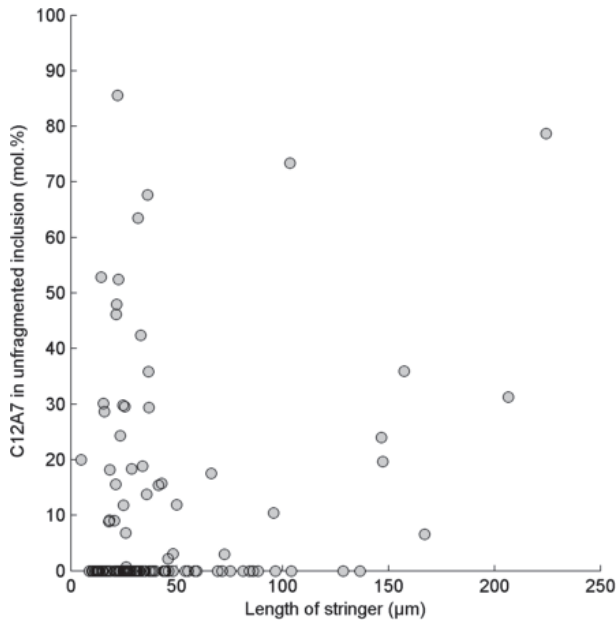


Fig. 84. C12A7 content in an unfragmented inclusion vs. the stringer length.

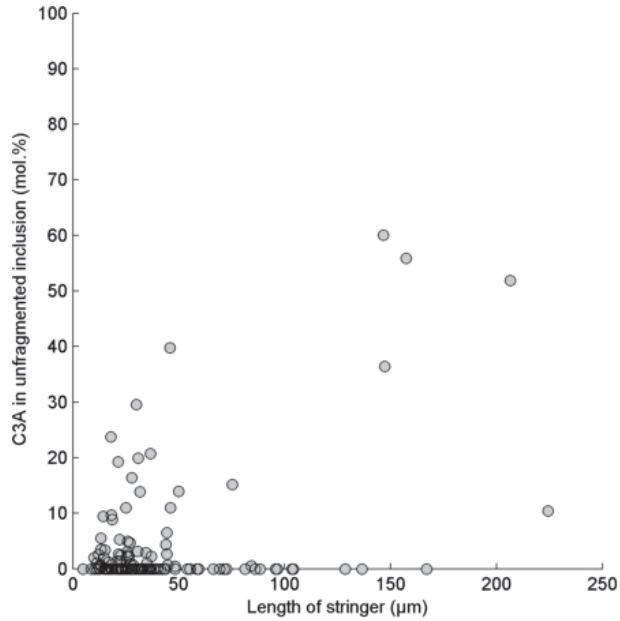


Fig. 85. C3A content in an unfragmented inclusion vs. the stringer length.

CaO containing stringers are typically not very long, as seen in Figure 86. Most of these are CaO–CaS stringers. Usually, stringers contain some amount of calcium sulphide phase. In Figure 87, it can be seen that high CaS contents were observed in various stringer lengths. However, the longest stringers with lengths over 200 µm contained negligible amounts of calcium sulphide phase, indicating their composition is completely formed of oxides.

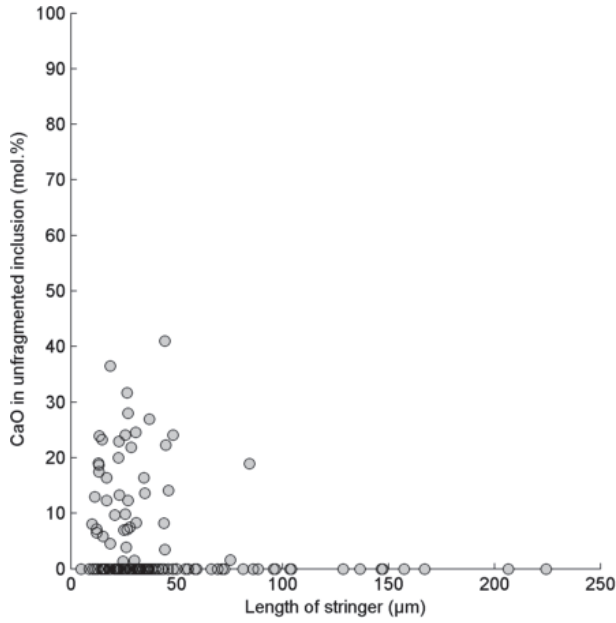


Fig. 86. CaO content in an unfragmented inclusion vs. the stringer length.

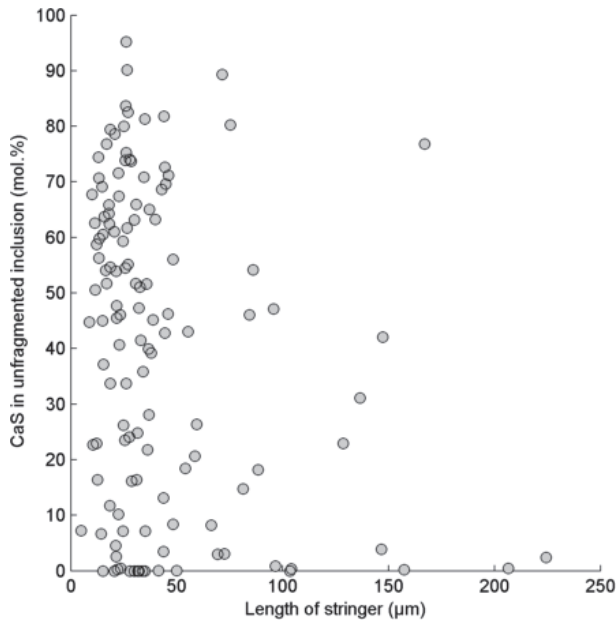


Fig. 87. CaS content in an unfragmented inclusion vs. the stringer length.

Inclusions belonging to stringers

Not only were the inclusions in the CaO–C3A–MgO triangle the most prone to elongate, they were also observed in stringers. In Figure 88, the aspect ratios of OX, OX CaS, and CaS classes are presented, with highlighted inclusions observed in stringers. In general, elongation and stringering complied with each other. It can also be seen that stringered inclusions often contain oxides without CaS. On the other hand, pure calcium sulphides were rarely observed in the stringers. The finding contradicts reports by Zhao et al. (2015), who stated that CaS formed by colliding with oxide broke into pieces easily during rolling.

With moderate calcium treatment, an optimal inclusion composition can be obtained, found within the C12A7–CA–MgO triangle. These liquid inclusions ensure good castability, while they do not easily deform into detrimental stringers after continuous casting. The CaS content of such inclusions has hardly any effect on the deformation behaviour. The result varies from the findings by Xu et al. (2016), who reported a protective role played by a CaS layer on the deformation of oxide phases.

A notable number of CaO–CaS inclusions were observed in the dataset. Such elongated stringers have not been reported in the literature. Instead, Wang et al. (2014) recommended the treatment of inclusions in the CaO–CaS system in order to prevent elongation of oxides.

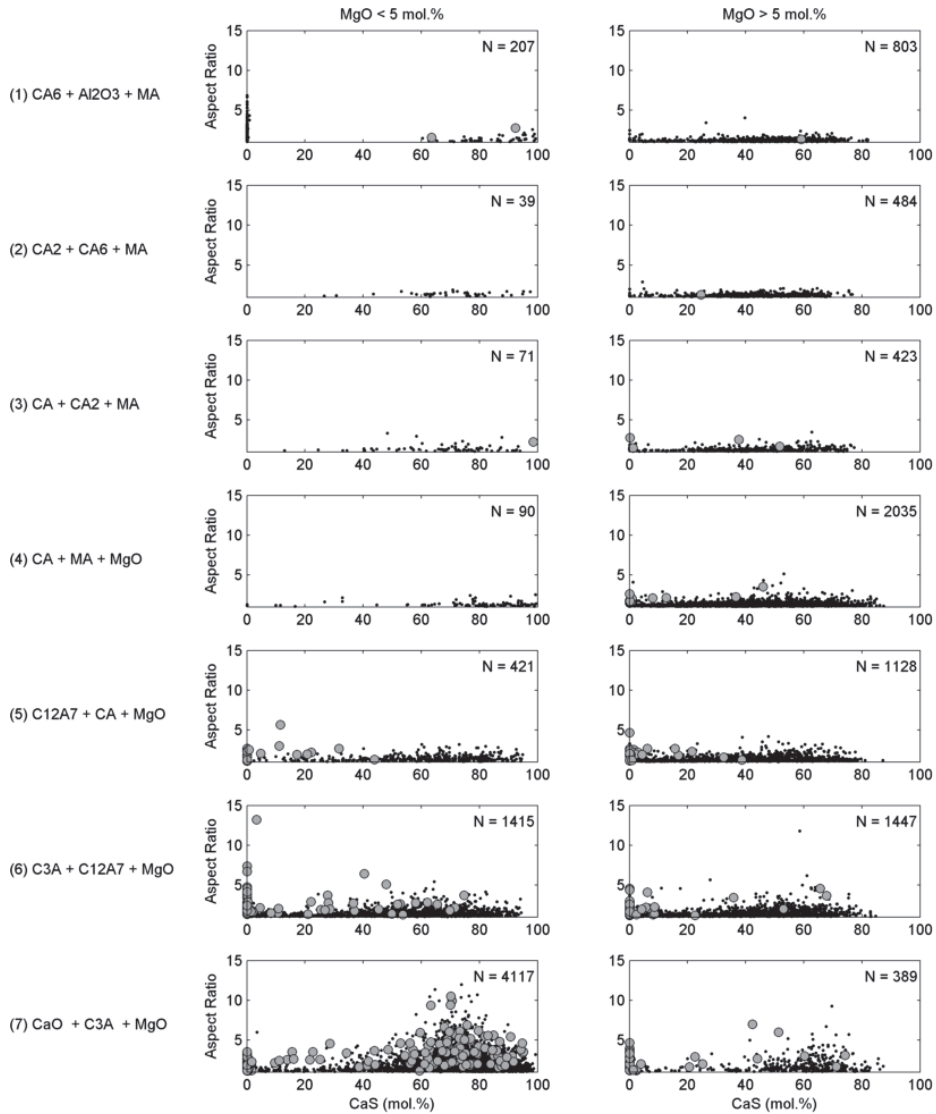


Fig. 88. Aspect ratios of OX, OX CaS, and CaS classes, divided into oxide phase triangles and MgO content. Inclusions in stringers are highlighted.

OX CaS MnS inclusions were typically not a part of stringers, as illustrated in Figure 89. On the other hand, the seventh triangle withholds a marked number of OX CaS MnS inclusions found in stringers. It should be pointed out that the

stringered inclusions found in the fourth triangle are not elongated, indicating a differing formation mechanism.

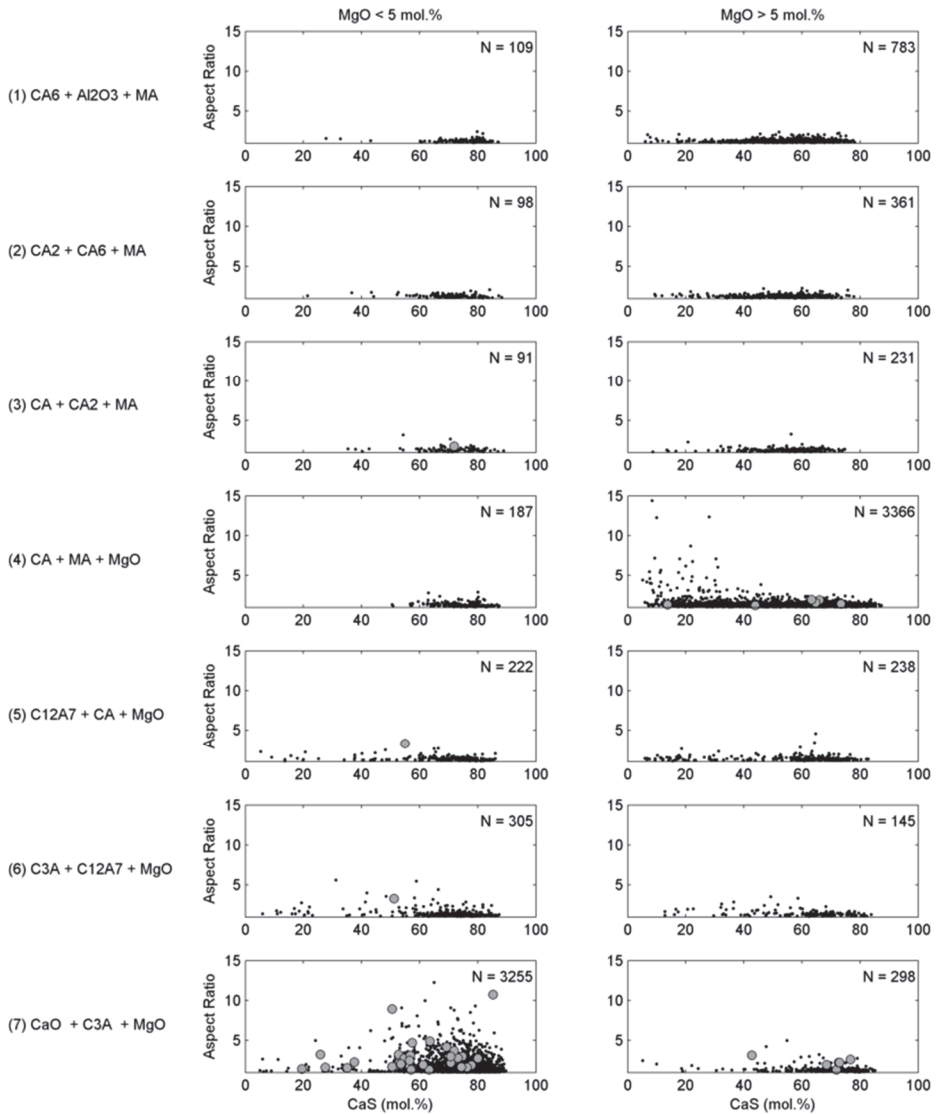


Fig. 89. Aspect ratios of the OX CaS MnS class, divided into oxide phase triangles and MgO content. Inclusions in stringers are highlighted.

OX CaS TiN inclusions are rarely observed in stringers, as depicted in Figure 90. In addition, the inclusions in the stringers are typically not very elongated. It can be concluded that the multiphase inclusions are not prone to elongate or to form stringers during hot rolling.

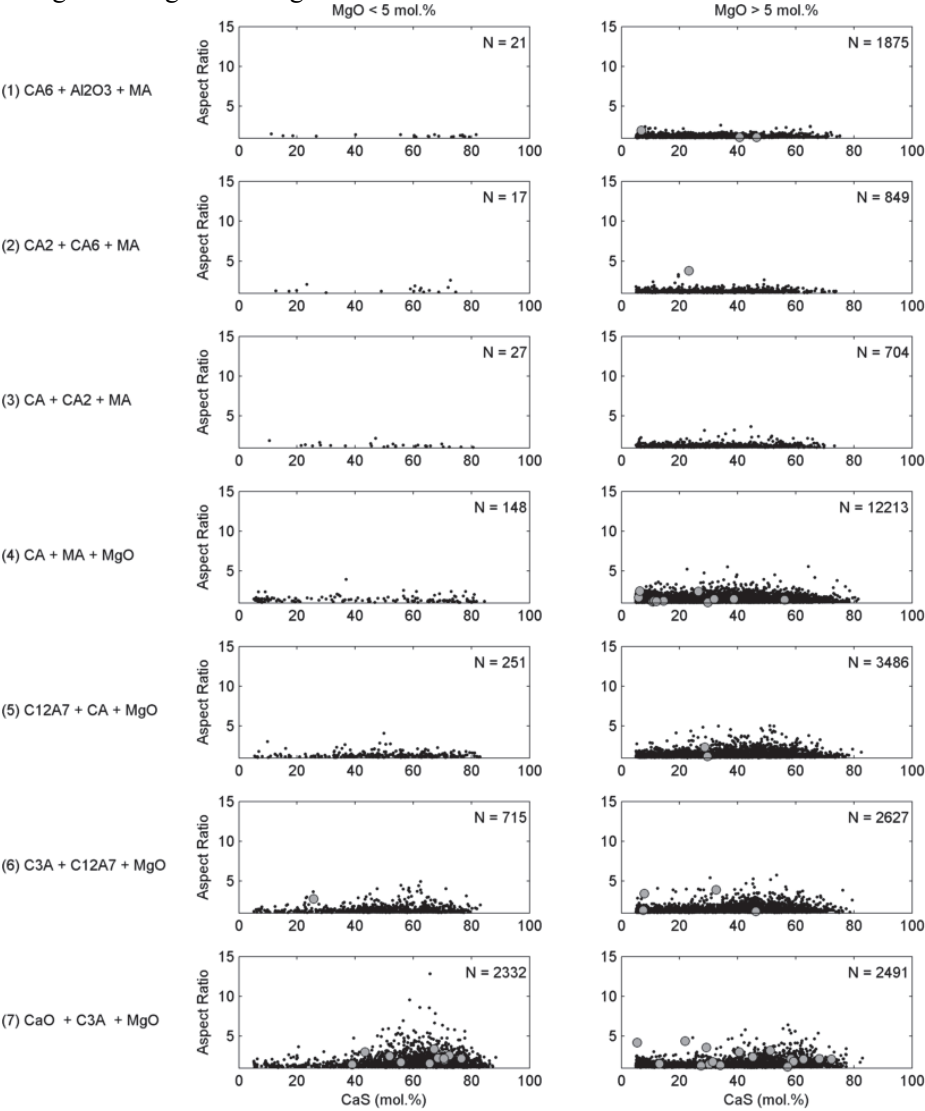


Fig. 90. Aspect ratios of the OX CaS TiN class, divided into oxide phase triangles and MgO content. Inclusions in stringers are highlighted.

It is revealed in Figure 91 that some stringered OX CaS MnS TiN inclusions were found in the seventh oxide compatibility triangle, similarly to other inclusion classes. However, the stringered inclusions in the fourth triangle are not elongated, in spite of the presence of MnS. This is in accord with the OX CaS MnS inclusions.

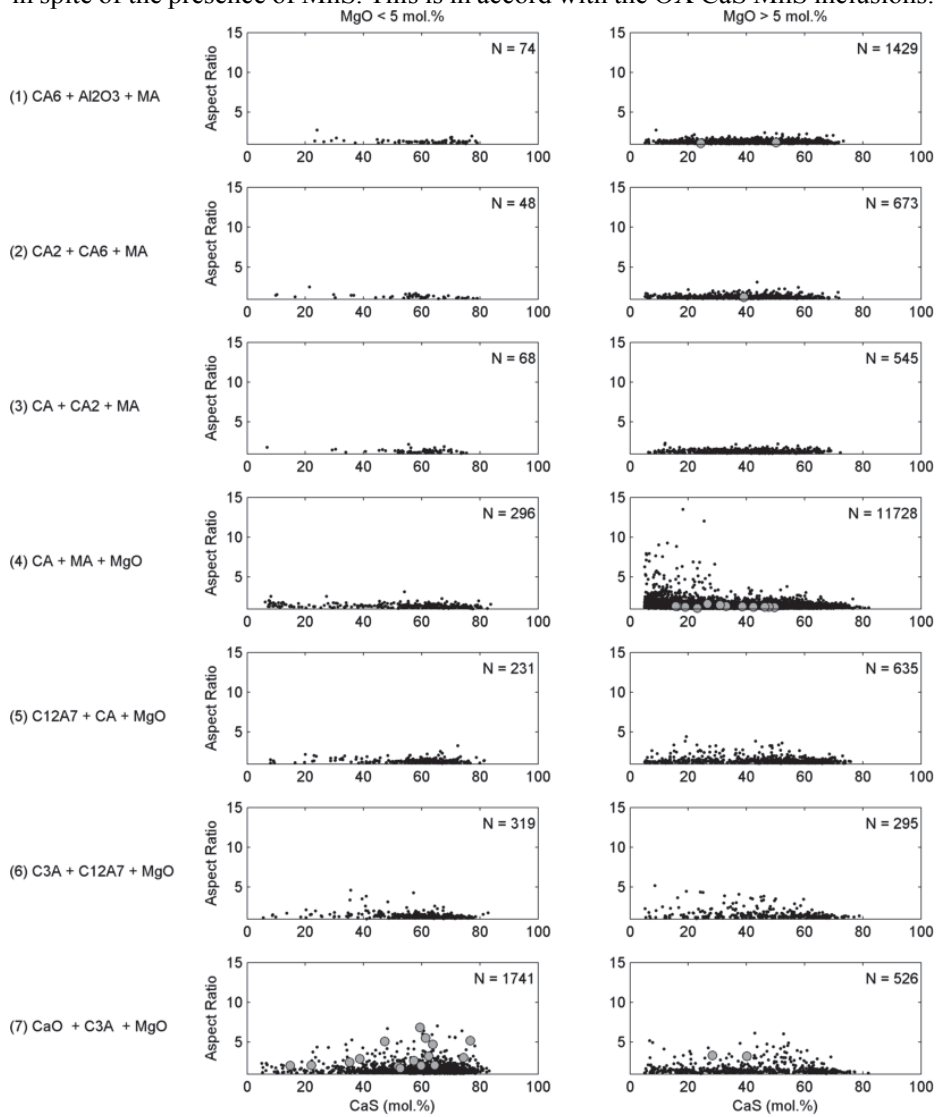


Fig. 91. Aspect ratios of the OX CaS MnS TiN class, divided into oxide phase triangles and MgO content. Inclusions in stringers are highlighted.

In Figure 92, the percentage of inclusions found in stringers of all the detected inclusions, by inclusion class and the composition of the oxide phase is illustrated. Among the oxide containing inclusion classes, the fraction of pure oxides found in stringers was the largest. Around ten percent of the OX class inclusions in compatibility triangles 3–6 were found as a part of stringers. For the seventh triangle in the OX class, more than 50% of the inclusions belonged to stringers. In the other OX triangles 3–6, the fraction was essentially larger than in other inclusion classes, not taking into account the OX MnS inclusions with oxide composition in triangles 6 & 7.

Some of the OX MnS inclusions, especially in the sixth triangle, belong to stringers. However, the number of inclusions in the class is relatively low. For the other inclusion classes, the percentage of stringered inclusions was very low, in the order of one percent. In the figure, it can be seen that $OX > CaS$ inclusions with almost all compositions were observed in stringers, whereas for $OX < CaS$ inclusions this was the case only for some compositions. In both of these classes, inclusions with a high CaO content, i.e., with an oxide composition in the seventh triangle, were slightly more prone to occur in stringers.

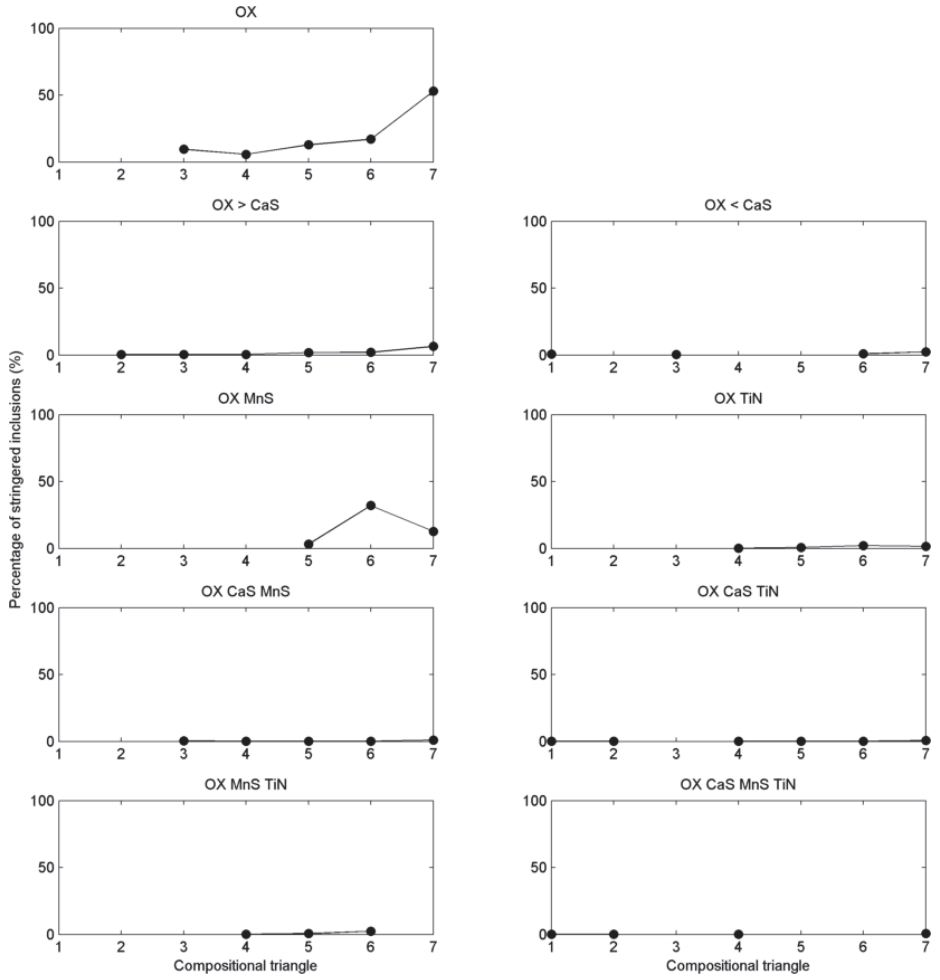


Fig. 92. Percentage of inclusions found in stringers, by inclusion class and oxide compositional triangle.

8 Summary

8.1 Development of a new inclusion classification method

The presented inclusion phase identification and classification method (IPIM) offers valuable information on the phases of inclusions. This data is often buried within simple inclusion classification criteria. The method offers the best approximation of the phases in each inclusion detected with minimal time, if no time-consuming elemental map analyses are available.

The IPIM method offers a comprehensible classification, based on the typical phases encountered in aluminium-killed, calcium treated steels. In addition to oxide phases in the $\text{Al}_2\text{O}_3\text{--CaO--MgO}$ system, calcium sulphides, manganese sulphides and titanium nitrides are taken into account in the classification. The combinations of OX, CaS, MnS, and TiN make a total of 15 inclusion classes, substantially less than the criteria presented in the literature.

For each inclusion, the oxide phase calculation procedure presented here provides fractions of thermodynamically stable oxide combinations. For example, spinel phase ($\text{MgO}\cdot\text{Al}_2\text{O}_3$) cannot exist in equilibrium with calcium aluminates with compositions of C12A7 and C3A. In practice, the phases are calculated with an assumption of equilibrium solidification, revealing the phases present in a given compatibility triangle using the lever rule.

8.2 New information obtained with the inclusion classification and data treatment

By identifying the actual oxide phases in inclusions in hot rolled steels, comprehensible classification is possible. For instance, pure oxides can be distinguished, and in addition, the oxide phase composition for each inclusion.

As an example, the dispersion of inclusions in lollipop samples was investigated using the classification method. Clear differences were found in the magnesium content and size distributions of pure oxide inclusions.

Furthermore, the elongation tendency of varying oxide phases during hot rolling can be assessed. Similarly, the effect of calcium sulphide amount is revealed. As a result, elongation tendencies, i.e., aspect ratios, for inclusions in each compatibility triangle in the $\text{Al}_2\text{O}_3\text{--CaO--MgO}$ system are presented, as a function of the CaS content. On top of this, aspect ratio ternary contours for each inclusion

class on the $\text{Al}_2\text{O}_3\text{--CaO--MgO}$ system for aspect ratios are illustrated, showing elongation tendencies on comprehensible diagrams.

As a case study, an in-depth investigation on the characterisation of oxide–sulphide stringers in hot rolled products was presented. The following properties were presented for each stringer: the number of inclusions and length of stringer, phase fractions and compositions, and the composition of the unfragmented inclusion in the slab before hot rolling.

8.3 Dispersion of inclusions in lollipop samples

Not only does the inclusion size differ within sections of lollipop samples, but the composition also varies. Therefore, the inclusions in the lollipop sample do not represent the inclusions in the liquid steel as such. In order to estimate primary inclusions, the most suitable section is near the surface of the sample, where the MgO content is lower. The higher MgO content of inclusions in the centre parts of the samples implies that the MgO phase is abundantly precipitated during solidification. The MgO contents in the oxides were markedly higher than the solubility of MgO in the liquid inclusions, indicating abundant MgO precipitation from the steel melt during solidification of the samples. On top of this, titanium nitrides are mostly found in the centre parts of the samples. However, the number of pure calcium sulphides is low, even in the centre parts of the lollipop sample.

The results indicate that the majority of secondary inclusion phases precipitate on existing inclusions, rather than as singular inclusions. For the assessment of primary inclusions in liquid steel, e.g. with online applications such as OES-PDA, the surface parts of the samples are recommended.

8.4 Assessment of inclusion evolution during steel melt shop processing with the developed method

The oxide composition of inclusions may vary greatly from the mould sample to hot-rolled product. In assessing the inclusion composition, the use of Al–Ca–S ternary diagrams can be misleading, mainly because they do not differentiate between Al_2O_3 and spinel inclusions. The presence of Al_2O_3 or spinel phases in the product samples is not necessarily a sign of reoxidation. Rather, the reverse reaction direction of $(\text{Al}_2\text{O}_3)+3\text{CaS}=3(\text{CaO})+2[\text{Al}]+3[\text{S}]$ is dominated by the total sulphur concentration in the steel. The results for the investigated steels show that with sulphur contents higher than 10 ppm, calcium aluminates were back-modified to

alumina and spinel inclusions during casting. However, with decreasing sulphur contents, and simultaneous adequate calcium treatment of oxides, Al_2O_3 and spinel formation was hindered or even avoided.

8.5 Assessment of inclusion evolution during liquid steel sampling with the developed method

According to the thermodynamic calculations of the steel compositions in question, aluminium oxides are not a stable phase at steelmaking temperatures. Still, they were analysed in the samples. This indicates that the inclusions in the mould had not reached the equilibrium state, i.e., calcium modification was still on-going. In the heats with sulphur contents up to 10 ppm, virtually all sulphur was found dissolved in the molten steel. Keeping in mind that pure oxide inclusions are relatively rare in lollipop samples even in low-sulphur heats, it is reasonable to state that a marked portion of sulphides precipitate during sampling of the liquid steel.

Some TiN phases which had precipitated during sampling were found in all samples. In the inclusions observed in the solidified samples, MgO and CaS were not found dissolved in the calcium aluminates. Presumably, any MgO and CaS components in the liquid inclusions had precipitated during the sampling. MgO was often found on the outer surface of inclusions analysed in the lollipop samples, indicating precipitation from the liquid steel. However, CaS was observed in various forms, indicating formation either by chemical reactions or collision of inclusions.

8.6 Elongation of inclusions during hot rolling

The most prone inclusion types found to elongate in this study were CaO–CaS inclusions, which was obviously a result of excess calcium treatment. The most elongated were ~70 mol.% CaS–CaO inclusions with MgO less than 5 mol.%, in some instances with aspect ratios over 10. This finding contradicts the investigations of Wang et al. (2014), who proposed that the occurrence of CaO–CaS inclusions would decrease the severity rating of the samples, according to the ASTM E45 standard.

According to the current results, low melting Al_2O_3 –CaO(–MgO) inclusions were not the most elongated oxide inclusions in the hot rolled product. With moderate calcium treatment, an optimal oxide composition is obtained, which is found within the C12A7–CA–MgO triangle. These liquid inclusions ensure good

castability, while they do not easily fragment into detrimental stringers after continuous casting. The CaS content of such inclusions has hardly any effect on the deformation behaviour.

For other inclusion types, the aspect ratios of $OX < CaS$ inclusions were found to be slightly larger than those for the $OX > CaS$ inclusions. In other words, increased CaS content often resulted in more elongated inclusions. However, the effect of the CaS content on the elongation of oxide–sulphide inclusions was not linear. In addition, the results showed that the effect of MgO content on the elongation of oxide–sulphide inclusions was also not linear.

In each inclusion class, inclusions with oxide phases located in the CaO–C3A–MgO and C3A–C12A7–MgO compatibility triangles were the most elongated. This leads to the conclusion that excess calcium treatment must be avoided.

The thickness location of inclusions did not markedly affect the elongation of inclusions. This was established by dividing the hot rolled product into three same-sized thickness sections, and comparing the aspect ratios within each inclusion class, according to the oxide compositions.

Inclusions enclosing a spinel phase, i.e., those inclusions in which the oxide composition lies above the CA–MgO line, strongly resisted deformation during hot rolling. Spinel inclusions are hard and nondeformable, and may act as cavity nucleation sites during hot rolling, even when accompanied with some sulphides.

8.7 Oxide–sulphide stringers

According to the calculations, the original sizes of stringer-forming inclusions in the slabs were below 20 μm . This is in accordance with the estimations by Fuhr et al. (2007) and Kanbe et al. (2011).

Pure CaS inclusions were rarely found in the oxide-sulphide stringers. It can be concluded that when complex oxide–sulphide inclusions were broken into stringers, the fragmentation did not strictly follow the oxide–sulphide phase boundaries.

Typically, the compositions of oxide inclusions in a single stringer varied. This indicates that the stringers might have formed from agglomerated inclusions instead of singular inclusions with constant oxide compositions.

The most elongated inclusions were often also found in stringers. The typical inclusions observed during this study in stringers were a) oxides in C3A–C12A7–MgO and CaO–C3A–MgO triangles without CaS, and b) CaO–CaS inclusions with 60–80 mol.% CaS.

OX CaS TiN multiphase inclusions were the most abundant in the hot rolled products. Still, these inclusions were relatively rarely observed in stringers. Unlike the OX & OX CaS classes, the most elongated OX CaS TiN inclusions were usually not part of stringers, and not prone to form stringers. It can be concluded that the TiN including multiphase inclusions resist deformation, and do not elongate or form stringers during hot rolling.

The fraction of stringered inclusions was essentially largest in the OX inclusion class, compared to the other inclusion classes. Over 50% of inclusions in the CaO–C3A–MgO triangle were included in stringers.

8.8 Theoretical implications

In order to maintain the achieved steel cleanliness, the prevention of reoxidation in the tundish is essential. If reoxidation in the tundish should occur, it could lead to the formation of spinel inclusions, which are notably detrimental to the steel properties. On the other hand, the removal of large liquid inclusions before casting will minimise the number of oxide stringers in the hot rolled product.

According to the thermodynamic calculations used in this study, the dissolved calcium content was almost constant in the liquid steel and was around 3 ppm in the heats investigated. Consequently, it is clear that excess calcium additions cannot act as a buffer for the prevention of manganese sulphide formation during continuous casting of steel. Instead, calcium additions should be moderate and well controlled according to the total oxygen and sulphur contents in the steel melt.

8.9 Practical implications

It should be well noted that the optimal oxide composition perspectives of casting and elongation are not the same. It is often stated that liquid inclusions during casting will prevent the clogging of the submerged entry nozzle. According to the results of this study, there is a clear difference between the elongation tendency of inclusions in the CA–C12A7–MgO and C12A7–C3A–MgO triangles, which are both considered liquids at steelmaking temperatures. In regard to both casting successfulness and moderate elongation of inclusions during hot rolling, the former composition is recommended, and this is achievable with moderate calcium additions.

With high sulphur contents, the risk of back-modification of calcium aluminates into aluminium oxides or spinel inclusions during the solidification of

the steel is evident. Therefore, low sulphur contents below 10 ppm should be achieved in order to conserve the calcium aluminate phases in the inclusions.

8.10 Reliability and validity

The inclusion classification method can be modified according to the inclusion characteristics for other steel grades as well. In this case, calcium is the only element which forms both oxides and sulphides. Consequently, oxygen was not taken as an input in the calculation. Instead, oxygen contents could be used to assess the goodness of the composition calculation.

The inclusion dispersion in lollipop samples is affected by various factors, such as the geometry of the samplers, the sampling depth, and the sampling temperature. The results confirm that even with relatively small samples, variance in inclusion size and composition exist in different sections of the samples.

In this study, aluminium killed and calcium treated steels were investigated. The dispersion of non-metallic inclusions in the slabs and consequently on hot rolled products can be considered caster dependent to some extent. The investigation of oxide–sulphide stringers is a case study of steels produced by SSAB Europe Raahe steelworks.

8.11 Recommendations for further research

By utilising the inclusion classification method, the effect of the inclusion phase composition on inclusion and steel properties could be depicted. For instance, slab samples could be investigated to assess stringer-forming inclusions before their fragmentation during hot rolling. In addition, the dispersion of inclusions in the continuously cast slabs could be studied. The trajectories of inclusions in dendritic solidification are affected by the composition of the inclusions and solidification type, among other aspects.

After hot rolling, the optimal inclusion composition in regard to the steel properties could be investigated. For the optimisation of the mechanical properties of steel, the effect of various oxide phases, combined with varying sulphide amounts in inclusions should be studied.

References

- Abdelaziz, S., Megahed, G., El-Mahallawi, I., & Ahmed, H. (2009). Control of Ca addition for improved cleanness of low C, Al killed steel. *Ironmaking and Steelmaking*, 36(6), 432-441.
- Abraham, S., Raines, J., & Bodnar, R. (2013). Development of an inclusion characterization methodology for improving steel product cleanliness. Paper presented at the AISTech 2013 Iron and Steel Technology Conference, Pittsburgh, PA., 1 1069-1084.
- Ahlborg, K., Fruehan, R. J., Potter, M. S., Badger, S. R., & Casuccio, G. S. (2003). Inclusions in aluminium-killed steel with varying calcium additions. *ISSTech Proceedings*, 1, pp. 177-194. April 27-30, 2003, Indianapolis, Indiana.
- Andersson, J.-O., Helander, T., Höglund, L., Shi, P., & Sundman, B. (2002). Thermo-Calc & DICTRA, computational tools for materials science. *Calphad: Computer Coupling of Phase Diagrams and Thermochemistry*, 26(2), 273-312.
- ASTM E45 (2005) Standard Test Methods for Determining the Inclusion Content of Steel. ASTM International.
- ASTM E2142 (2008) Standard Test Methods for Rating and Classifying Inclusions in Steel Using the Scanning Electron Microscope. ASTM International.
- Atkinson, H. V., & Shi, G. (2003). Characterization of inclusions in clean steels: A review including the statistics of extremes methods. *Progress in Materials Science*, 48(5), 457-520.
- Bale, C. W., Chartrand, P., Degterov, S. A., Eriksson, G., Hack, K., Ben Mahfoud, R., . . . Petersen, S. (2002). FactSage thermochemical software and databases. *Calphad: Computer Coupling of Phase Diagrams and Thermochemistry*, 26(2), 189-228.
- Bartosiaki, B. G., Pereira, J. A. M., Bielefeldt, W. V., & Vilela, A. C. F. (2015). Assessment of inclusion analysis via manual and automated SEM and total oxygen content of steel. *Journal of Materials Research and Technology*, 4(3), 235-240.
- Bernard, G., Riboud, P. V., & Urbain, G. (1981). Étude de la plasticité d'inclusions d'oxydes. *Cahiers D'Informations Techniques - Revue De Metallurgie*, 78(5), 421-433.
- Bielefeldt, W. V., & Vilela, A. C. F. (2015). Study of inclusions in high sulphur, Al-killed Ca-treated steel via experiments and thermodynamic calculations. *Steel Research International*, 86(4), 375-385.
- Cappel, J., Flender, R., Hoffken, R., Kemper, G., & Wunnenberg, K. (2005). Centre segregation, soft reduction and oxide cleanness for large diameter line pipe with highest demands on HIC. *Steel Research International*, 76(8), 588-594.
- Castro, F., Herrera, M., Mendez, J., Castro, M., Solis, H., Barbaro, M., & Castella, A. (2005). Evaluation of cleanness in steel slabs. Paper presented at the 15th IAS Steelmaking conference, San Nicolas, Argentina.
- Choudhary, S. K. (2011). Influence of modified casting practice on steel cleanliness. *ISIJ International*, 51(4), 557-565.
- Choudhary, S. K., & Ghosh, A. (2008). Thermodynamic evaluation of formation of oxide-sulphide duplex inclusions in steel. *ISIJ International*, 48(11), 1552-1559.

- Choudhary, S. K., & Ghosh, A. (2009). Mathematical model for prediction of composition of inclusions formed during solidification of liquid steel. *ISIJ International*, 49(12), 1819-1827.
- Cicutti, C. E., Madías, J., & González, J. C. (1997). Control of microinclusions in calcium treated aluminium killed steels. *Ironmaking and Steelmaking*, 24(2), 155-159.
- De Santis, M., Poli, A., Tscheuschner, C., Koitzsch, R., Jung, H. P., & Leuvenink, D. (Eds.). (2010). *Innovative tundish management for final steel thermal and chemical adjustment (Tundjust)*. European Commission. Luxembourg.
- Dekkers, R., Blanpain, B., & Wollants, P. (2003). Steel sampling to study inclusions. Paper presented at the ISSTech Conference Proceedings, 1007-1019.
- Deng, Z., & Zhu, M. (2013). Evolution mechanism of non-metallic inclusions in Al-killed alloyed steel during secondary refining process. *ISIJ International*, 53(3), 450-458.
- Deutsches Institut für Normung (1985) DIN 50602, *Metallographische Prüfverfahren; Mikroskopische Prüfung von Edelstählen Auf Nichtmetallische Einschlüsse Mit Bildreihen*. Beuth Verlag GmbH, Berlin.
- Deutsches Institut für Normung (2007) DIN EN 10247, *Metallographische Prüfung des Gehaltes Nichtmetallischer Einschlüsse in Stählen mit Bildreihen*. Beuth Verlag GmbH, Berlin.
- Ericsson, O. T. (2010). An experimental study of a liquid steel sampling process. Doctoral dissertation, KTH, Sweden.
- Faraji, M., Wilcox, D. P., Thackray, R., Howe, A. A., Todd, I., & Tsakiroopoulos, P. (2015). Quantitative characterization of inclusions in continuously cast high-carbon steel. *Metallurgical and Materials Transactions B: Process Metallurgy and Materials Processing Science*, 46(6), 2490-2502.
- Faulring, G. M. (1999). Inclusion modification in semi-killed steels. *Iron and Steelmaker (I and SM)*, 26(7), 29-36.
- Fuchs, A., Wagner, K., Jacobi, H., & Wunnenberg, J. (1993). Determination of macroscopic cleanliness in C.C. slabs using off-line ultrasonic testing of 42 kg rolled specimens. Paper presented at the ECSC on Steelmaking Proceedings.
- Fuhr, F., Cicutti, G., Walter, G., & Torga, G. (2003). Relationship between nozzle deposits and inclusion composition in the continuous casting of steels. *Iron and Steelmaker (I and SM)*, 30(12), 53-58.
- Fuhr, F., Torga, G., Medina, F., & Cicutti, C. (2007). Application of slag tracers to investigate source of non-metallic inclusions. *Ironmaking and Steelmaking*, 34(6), 463-470.
- Gagné, M., & Thibault, E. (1998). Behaviour of inclusions during rolling of continuously cast billets. *CIM Bulletin*, 91(1021), 98-103.
- Geldenhuis, J. M. A., & Pistorius, P. C. (2000). Minimisation of calcium additions to low carbon steel grades. *Ironmaking and Steelmaking*, 27(6), 442-449.
- Goldstein, J. I., Newbury, D. E., Echlin, P., Joy, D. C., Lyman, C.E., Lifshin, E., Sawyer, L., & Michael, J. R. (2007). *Scanning electron microscopy and X-ray microanalysis*. Third Edition. Springer New York.

- Guo, J., Cheng, S., Cheng, Z., & Xin, L. (2013). Thermodynamics for precipitation of CaS bearing inclusion and their deformation during rolling process for Al-killed Ca-treated steel. *Steel Research International*, 84(6), 545-553.
- Harris, M., Adaba, O., Lekakh, S., O'Malley, R., & Von Richards, L. (2015). Improved methodology for automated SEM/EDS non-metallic inclusion analysis of mini-mill and foundry steels. Paper presented at the AISTech 2015 Iron and Steel Technology Conference and 7th International Conference on the Science and Technology of Ironmaking, ICSTI 2015, 3 3315-3325.
- Holappa, L. (2001). Inclusion control for castability of resulphurized steels. Paper presented at the 84th Steelmaking Conference. Baltimore, Maryland, March 25-28.
- Holappa, L. (2010). On physico-chemical and technical limits in clean steel production. *Steel Research International*, 81(10), 869-874.
- Holappa, L. E. K., & Helle, A. S. (1995). Inclusion control in high-performance steels. *Journal of Materials Processing Tech.*, 53(1-2), 177-186.
- Holappa, L., Hämäläinen, M., Liukkonen, M., & Lind, M. (2003). Thermodynamic examination of inclusion modification and precipitation from calcium treatment to solidified steel. *Ironmaking and Steelmaking*, 30(2), 111-115.
- Holappa, L., Kekkonen, M., Louhenkilpi, S., Hagemann, R., Schröder, C., & Scheller, P. (2013). Active tundish slag. *Steel Research International*, 84(7), 638-648.
- Holappa, L., & Wijk, O. (2014). Inclusion engineering. In S. Seetharaman, A. McLean, R. Guthrie & S. Sridhar (Eds.), *Treatise on process metallurgy* (pp. 347-372) Elsevier.
- Huet, L., Jönsson, P., & Reinholdsson, F. (1997). The effect of deoxidation practise on inclusion characteristics in bearing steel production. *Steel Times International*, 21(6), 47-50.
- International Organization of Standardization (1998) ISO 4967, Steel - Determination of Content of Nonmetallic Inclusions - Micrographic Method Using Standard Diagrams.
- Ito, Y.-i., Suda, M., Kato, Y., Nakato, H., & Sorimachi, K.-i. (1996). Kinetics of shape control of alumina inclusions with calcium treatment in line pipe steel for sour service. *ISIJ International*, 36(SUPPL.), S148-150.
- Janis, J., Nakajima, K., Karasev, A., Jonsson, S., Inoue, R., & Jönsson, P. G. (2013). Effects of primary oxide and oxide-nitride particles on the solidification structure in a Fe-20 mass%Cr alloy deoxidised with Ti and M (M = Zr or Ce). *ISIJ International*, 53(2), 221-229.
- Janke, D., Ma, Z., Valentin, P., & Heinen, A. (2000). Improvement of castability and quality of continuously cast steel. *ISIJ International*, 40(1), 31-39.
- Japanese Standards Association (2003) JIS G0555 Microscopic Testing Method of the Nonmetallic Inclusion in Steel.
- Jung, I.-H., Deckerov, S. A., & Pelton, A. D. (2004). Computer applications of thermodynamic databases to inclusion engineering. *ISIJ International*, 44(3), 527-536.
- Juretzko, F. R., Dhindaw, B. K., Stefanescu, D. M., Sen, S., & Curreri, P. A. (1998). Particle engulfment and pushing by solidifying interfaces: Part I. ground experiments. *Metallurgical and Materials Transactions A: Physical Metallurgy and Materials Science*, 29(6), 1691-1696.

- Kanbe, Y., Karasev, A., Todoroki, H., & Jönsson, P. G. (2011). Application of statistics of extreme values for inclusions in stainless steel on different stages of steel making process. *ISIJ International*, 51(12), 2056-2063.
- Karasev, A. V., Jafari, K., & Jönsson, P. G. (2015). Assessment of sulphide inclusions in deformed steels and their effect on steel quality. Paper presented at the 9th International Conference on Clean Steel, Budapest, Hungary.
- Kaushik, P., Pielet, H., & Yin, H. (2009). Inclusion characterisation - tool for measurement of steel cleanliness and process control: Part 1. *Ironmaking and Steelmaking*, 36(8), 561-571.
- Kaushik, P., & Yin, H. (2012). Thermodynamics, engineering and characterization of inclusions in advanced high strength steels. Paper presented at the 8th International Conference on Clean Steel, Budapest, Hungary.
- Kawahara, J., Tanabe, K., Banno, T., & Yoshida, M. (1992). Advance of valve spring steel. *Wire Journal International*, 55-61.
- Kekkonen, M., Leuverink, D., & Holappa, L. (2017). Improving cleanliness of 16MnCrS5 case hardening steels by optimized active tundish flux. *Steel Research International*, 88(7).
- Keskinkilic, E. (2011). Sulphide-type inclusion morphologies of a Ca-treated hot-rolled wheel steel. *Journal of the Southern African Institute of Mining and Metallurgy*, 111(6), 417-422.
- Kiessling, R., & Lange, N. (1978). *Non-metallic inclusions in steel* (2nd ed.). London: Metals Society.
- Li, J. Z., Jiang, M., He, X.-F., Sun, W., & Wang, X.-H. (2016). Investigation on nonmetallic inclusions in ultra-low-oxygen special steels. *Metallurgical and Materials Transactions B: Process Metallurgy and Materials Processing Science*, 47(4), 2386-2399.
- Liao, H., Yang, S., Li, J., & Feng, J. (2017). Characteristics of non-metallic inclusions in steel obtained from different-sized samplers. *Metallurgical and Materials Transactions B: Process Metallurgy and Materials Processing Science*, 48(6), 3101-3108.
- Lind, M., & Holappa, L. (2010). Transformation of alumina inclusions by calcium treatment. *Metallurgical and Materials Transactions B: Process Metallurgy and Materials Processing Science*, 41(2), 359-366.
- Lu, D.-Z., Irons, G. A., & Lu, W.-K. (1994). Kinetics and mechanisms of calcium dissolution and modification of oxide and sulphide inclusions in steel. *Ironmaking and Steelmaking*, 21(5), 362-371.
- Maiti, R., & Hawbolt, E. B. (1985). The effect of hot rolling on the inclusion morphology of a semi-killed and a calcium treated X-70 pipeline steel. *Journal of Materials for Energy Systems*, 6(4), 251-262.
- Malkiewicz, T., & Rudnik, S. (1963). Deformation of non-metallic inclusions during rolling of steel. *Journal of the Iron and Steel Institute*, 201(1), 33-38.
- Martinez R., E. (1995). Formation of CaS during secondary metallurgy and solidification of steel. *Iron and Steelmaker (I and SM)*, 22(6), 19-23.

- Miettinen, J., Louhenkilpi, S., Kytönen, H., & Laine, J. (2010). IDS: Thermodynamic-kinetic-empirical tool for modelling of solidification, microstructure and material properties. *Mathematics and Computers in Simulation*, 80(7), 1536-1550.
- Nurmi, S., Louhenkilpi, S., & Holappa, L. (2009). Thermodynamic evaluation of inclusions formation and behaviour in steels during casting and solidification. *Steel Research International*, 80(6), 436-440.
- Nuspl, M., Wegscheider, W., Angeli, J., Posch, W., & Mayr, M. (2004). Qualitative and quantitative determination of micro-inclusions by automated SEM/EDX analysis. *Analytical and Bioanalytical Chemistry*, 379(4), 640-645.
- Ohta, H., & Suito, H. (2006). Dispersion behaviour of MgO, ZrO₂, Al₂O₃, CaO-Al₂O₃ and MnO-SiO₂ deoxidation particles during solidification of Fe-10mass%Ni alloy. *ISIJ International*, 46(1), 22-28.
- Ototani, T. (1986). *Calcium clean steel*. Springer-Verlag, Berlin.
- Pandey, J. C., Choubey, P. N., & Raj, M. (2008). Study of inclusion bands in continuously cast steel billets for rolling thermomechanically treated rebars. *Metallurgical and Materials Transactions A: Physical Metallurgy and Materials Science*, 39(7), 1727-1737.
- Pickering, F. B. (1958). Some effects of mechanical working on the deformation of non-metallic inclusions. *Journal of the Iron and Steel Institute*, 189, 148-159.
- Pistorius, P. C., & Patadia, A. (2012). The steel matrix affects microanalysis of CaO-Al₂O₃-CaS inclusions. Paper presented at the 8th International Conference on Clean Steel, Budapest, Hungary.
- Pistorius, P. C., Presoly, P., & Tshilombo, K. G. (2006). Magnesium: Origin and role in calcium-treated inclusions. Paper presented at the 2006 TMS Fall Extraction and Processing Division: Sohn International Symposium, San Diego, CA., 2 373-378.
- Pistorius, P. C., Roy, D., & Verma, N. (2013). Examples of how fundamental knowledge can improve steelmaking: Desulphurisation kinetics calcium and modification. *Transactions of the Indian Institute of Metals*, 66(5-6), 519-523.
- Pretorius, E. B., Oltmann, H. G., & Cash, T. (2010). The effective modification of spinel inclusions by Ca treatment in LCAK steel. *Iron and Steel Technology*, 7(7), 31-44.
- Ren, Y., Zhang, L., & Li, S. (2014). Transient evolution of inclusions during calcium modification in linepipe steels. *ISIJ International*, 54(12), 2772-2779.
- Ren, Y., Zhang, L., Ling, H., Wang, Y., Pan, D., Ren, Q., & Wang, X. (2017). A reaction model for prediction of inclusion evolution during reoxidation of Ca-treated Al-killed steels in tundish. *Metallurgical and Materials Transactions B: Process Metallurgy and Materials Processing Science*, 48(3), 1433-1438.
- Ren, Y., Zhang, Y., & Zhang, L. (2017). A kinetic model for Ca treatment of Al-killed steels using FactSage macro processing. *Ironmaking and Steelmaking*, 44(7), 497-504.
- Ruby-Meyer, F., Evrard, S., Vergauwens, M., & Balland, P. (2011). Improvement of the sampling for cleanliness measurement at liquid steel stage. Paper presented at the 8th International Workshop on Progress in Analytical Chemistry & Materials Characterisation in the Steel and Metal Industries (CETAS 2011). Luxembourg. 294-301.

- Ruby-Meyer, F., Evrard, S., Vergauwens, M., & Balland, P. (2013). Improvement of the sampling methodology for the cleanliness measurement in the liquid steel stage. Paper presented at the AISTech - Iron and Steel Technology Conference Proceedings; AISTech 2013 Iron and Steel Technology Conference, Pittsburgh, PA., 1 1051-1059.
- Sahai, Y., & Emi, T. (2007). Tundish technology for clean steel production. World Scientific Publishing, Singapore.
- Sancho, L. F., Colla, V., Cateni, S., Fera, S., Laine, J., Mapelli, C., . . . (Eds.). (2011). Prediction of inclusions in the slabs from the process characteristics (PREDINC) European Commission. Luxembourg.
- Saxena, S. K. (1982). Improving inclusion morphology, cleanness, and mechanical properties of aluminium-killed steel by injection of lime-based powder. *Ironmaking and Steelmaking*, 9(2), 50-57.
- Sjökvist, T. (2001). Influence of ferrochromium and ferromanganese additions on inclusion characteristics in steel. Doctoral dissertation, KTH, Sweden.
- SSAB Europe (2012) Steel Production. Presentation material.
- Story, S. R. (2001). Analysis of the influence of slag, metal and inclusion chemistry on the cleanliness and castability of steel. Paper presented at the 84th Steelmaking Conference, Baltimore, Maryland, March 25-28.
- Story, S. R., Liu, Q. E., Cathcart, C. R., & Molnar, M. (2015). Effect of process route on inclusion modification by calcium treatment. Paper presented at the 9th International conference on Clean Steel, Budapest, Hungary.
- Story, S. R., Piccone, T. J., Fruehan, R. J., & Potter, M. (2003). Inclusion analysis to predict casting behaviour. Paper presented at the ISSTech 2003 Conference Proceedings.
- Sugimura, T., Deura, T., Sakamoto, K., Sukenaga, S., Saito, N., & Nakashima, K. (2011). Effect of Li₂O addition on crystallization behaviour of CaO-Al₂O₃-MgO based inclusions. *ISIJ International*, 51(12), 1982-1986.
- Tervo, H., Kaijalainen, A., Pikkarainen, T., Mehtonen, S., & Porter, D. (2017). Effect of impurity level and inclusions on the ductility and toughness of an ultra-high-strength steel. *Materials Science and Engineering A*, 697, 184-193.
- Thunman, M., & Sichen, D. (2008). Origins of non-metallic inclusions and their chemical development during ladle treatment. *Steel Research International*, 79(2), 124-132.
- Tiekink, W., Santillana, B., Kooter, R., Mensonides, F., Deo, B., & Boom, R. (2006). Calcium: Toy, tool or trouble? Paper presented at the AISTech 2006 - Iron and Steel Technology Conference, Cleveland, OH., 2 395-403.
- Van Ende, M.-A., & Jung, I.-H. (2017). A kinetic ladle furnace process simulation model: Effective equilibrium reaction zone model using FactSage macro processing. *Metallurgical and Materials Transactions B: Process Metallurgy and Materials Processing Science*, 48(1), 28-36.
- Verma, N., Lind, M., Pistorius, P. C., & Fruehan, R. J. (2010). Modification of spinel inclusions by calcium in liquid steel. *AIST Transactions*, 7, 189-197.

- Verma, N., Pistorius, P. C., Fruehan, R. J., Potter, M. S., Oltmann, H. G., & Pretorius, E. B. (2012). Calcium modification of spinel inclusions in aluminium-killed steel: Reaction steps. *Metallurgical and Materials Transactions B: Process Metallurgy and Materials Processing Science*, 43(4), 830-840.
- Verma, N., Pistorius, P. C., Fruehan, R. J., Potter, M., Lind, M., & Story, S. (2011a). Transient inclusion evolution during modification of alumina inclusions by calcium in liquid steel: Part I background experimental techniques and analysis methods. *Metallurgical and Materials Transactions B: Process Metallurgy and Materials Processing Science*, 42(4), 711-719.
- Verma, N., Pistorius, P. C., Fruehan, R. J., Potter, M., Lind, M., & Story, S. R. (2011b). Transient inclusion evolution during modification of alumina inclusions by calcium in liquid steel: Part II results and discussion. *Metallurgical and Materials Transactions B: Process Metallurgy and Materials Processing Science*, 42(4), 720-729.
- Wang, X., Li, X., Li, Q., Huang, F., Li, H., & Yang, J. (2014). Control of stringer shaped non-metallic inclusions of CaO-Al₂O₃ system in API X80 linepipe steel plates. *Steel Research International*, 85(2), 155-163.
- Wang, Y., Valdez, M., & Sridhar, S. (2002). Formation of CaS on Al₂O₃-CaO inclusions during solidification of steels. *Metallurgical and Materials Transactions B: Process Metallurgy and Materials Processing Science*, 33(4), 625-632.
- Way, L. D. (2001). Cleanliness, castability, and surface quality of formable sheet steels. *Materials Science and Technology*, 17(10), 1175-1190.
- Wijk, O. (1995). Inclusion engineering. Paper presented at the SCANINJECT VII - 7th International Conference on Refining Processes, Luleå, Sweden., 1 35-67.
- Winkler, W., Angeli, J., & Mayr, M. (2007). Automated SEM-EDX cleanliness analysis and its application in metallurgy. *BHM Berg- Und Hüttenmännische Monatshefte*, 152(1), 4-9.
- Xu, G., Jiang, Z., & Li, Y. (2016). Formation mechanism of CaS-bearing inclusions and the rolling deformation in Al-killed, low-alloy steel with Ca treatment. *Metallurgical and Materials Transactions B: Process Metallurgy and Materials Processing Science*, 47(4), 2411-2420.
- Yang, D., Wang, X., Yang, G., Wei, P., & He, J. (2014). Inclusion evolution and estimation during secondary refining in calcium treated aluminium killed steels. *Steel Research International*, 85(11), 1517-1524.
- Yang, G., Wang, X., Huang, F., Wang, W., Yin, Y., & Tang, C. (2014). Influence of reoxidation in tundish on inclusion for Ca-treated Al-killed steel. *Steel Research International*, 85(5), 784-792.
- Yang, S.-f., Li, J.-s., Wang, Z.-f., Li, J., & Lin, L. (2011). Modification of MgO·Al₂O₃ spinel inclusions in Al-killed steel by Ca-treatment. *International Journal of Minerals, Metallurgy and Materials*, 18(1), 18-23.
- Yang, S., Wang, Q., Zhang, L., Li, J., & Peaslee, K. (2012). Formation and modification of MgO·Al₂O₃-based inclusions in alloy steels. *Metallurgical and Materials Transactions B: Process Metallurgy and Materials Processing Science*, 43(4), 731-750.

- Yang, W., Guo, C., Li, C., & Zhang, L. (2017). Transformation of inclusions in pipeline steels during solidification and cooling. *Metallurgical and Materials Transactions B: Process Metallurgy and Materials Processing Science*, 48(5), 2267-2273.
- Yang, W., Zhang, L., Wang, X., Ren, Y., Liu, X., & Shan, Q. (2013). Characteristics of inclusions in low carbon Al-killed steel during ladle furnace refining and calcium treatment. *ISIJ International*, 53(8), 1401–1410.
- Ye, G., Jönsson, P., & Lund, T. (1996). Thermodynamics and kinetics of the modification of Al₂O₃ inclusions. *ISIJ International*, 36(Supplement), S105-108.
- Zhang, L. (2006). State of the art in the control of inclusions in tire cord steels - A review. *Steel Research International*, 77(3), 158-169.
- Zhang, L.-f. (2006). Indirect methods of detecting and evaluating inclusions in steel – A review. *Journal of Iron and Steel Research International*, 13(4), 1-8.
- Zhang, L., & Thomas, B. G. (2003). State of the art in evaluation and control of steel cleanliness. *ISIJ International*, 43(3), 271-291.
- Zhang, L., Zhi, J., Mei, F., Zhu, L., Jiang, X., Shen, J., . . . Thomas, B. G. (2006). Basic oxygen furnace based steelmaking processes and cleanliness control at Baosteel. *Ironmaking and Steelmaking*, 33(2), 129-139.
- Zhang, Z., Tilliander, A., Karasev, A., & Jönsson, P. G. (2010). Simulation of the steel sampling process. *ISIJ International*, 50(12), 1746-1755.
- Zhang, X., Zhang, L., Yang, W., Wang, Y., Liu, Y., & Dong, Y. (2017). Characterization of the three-dimensional morphology and formation mechanism of inclusions in linepipe steels. *Metallurgical and Materials Transactions B: Process Metallurgy and Materials Processing Science*, 48(1), 701-712.
- Zhao, D., Li, H., Bao, C., & Yang, J. (2015). Inclusion evolution during modification of alumina inclusions by calcium in liquid steel and deformation during hot rolling process. *ISIJ International*, 55(10), 2115-2124.
- Ånmark, N., Karasev, A., & Jönsson, P. G. (2015). The effect of different non-metallic inclusions on the machinability of steels. *Materials*, 8(2), 751-783.

666. Kaleva, Jarkko (2018) Decentralized multiantenna transceiver optimization for heterogeneous networks
667. Hänninen, Tuomo (2018) Detection algorithms and FPGA implementations for SC-FDMA uplink receivers
668. Huotari, Joni (2018) Vanadium oxide nanostructures and thin films for gas sensor applications
669. Anttila, Severi (2018) Influence of minor elements on some weldability issues of intermediate purity stabilized ferritic stainless steels
670. Hartmann, Robert (2018) Flotation using cellulose-based chemicals
671. Porambage, Pawani (2018) Lightweight authentication and key management of wireless sensor networks for Internet of things
672. Bibikova, Olga (2018) Plasmon-resonant gold nanoparticles for bioimaging and sensing applications
673. Venkatraman, Ganesh (2018) Traffic aware resource allocation for multi-antenna OFDM systems
674. Isokangas, Elina (2018) Quantifying the groundwater dependence of boreal ecosystems using environmental tracers
675. Tervasmäki, Petri (2018) Reaction and mass transfer kinetics in multiphase bioreactors : experimental and modelling studies
676. Leinonen, Markus (2018) Distributed compressed data gathering in wireless sensor networks
677. He, Jiguang (2018) Performance of MIMO and non-orthogonal transmission in Lossy Forward relay networks
678. Matinmikko-Blue, Marja (2018) Stakeholder analysis for the development of sharing-based spectrum governance models for mobile communications
679. Paaso, Henna (2018) Direction of arrival estimation algorithms for leaky-wave antennas and antenna arrays
680. Pap, Nora (2018) Value-added processing of blackcurrants : Use of membrane technologies for clarification and concentration of blackcurrant juice and extraction of anthocyanins from blackcurrant marc
681. Tolvanen, Jarkko (2018) Novel sensor and switch applications for flexible and stretchable electronic materials

S E R I E S E D I T O R S

A
SCIENTIAE RERUM NATURALIUM
University Lecturer Tuomo Glumoff

B
HUMANIORA
University Lecturer Santeri Palviainen

C
TECHNICA
Postdoctoral research fellow Sanna Taskila

D
MEDICA
Professor Olli Vuolteenaho

E
SCIENTIAE RERUM SOCIALIUM
University Lecturer Veli-Matti Ulvinen

E
SCRIPTA ACADEMICA
Planning Director Pertti Tikkanen

G
OECONOMICA
Professor Jari Juga

H
ARCHITECTONICA
University Lecturer Anu Soikkeli

EDITOR IN CHIEF
Professor Olli Vuolteenaho

PUBLICATIONS EDITOR
Publications Editor Kirsti Nurkkala

